The Thesis Committee for William Salter Betts
Certifies that this is the approved version of the following thesis:

Compressibility and Permeability of Gulf of Mexico Mudrocks, Resedimented and In-Situ.

APPROVED BY
SUPERVISING COMMITTEE:

Supervisor:

Peter B. Flemings

M. Bayani Cardenas

Julia Schneider Reece

Compressibility and Permeability of Gulf of Mexico Mudrocks, Resedimented and In-Situ.

by

William Salter Betts, BS

Thesis

Presented to the Faculty of the Graduate School of

The University of Texas at Austin

in Partial Fulfillment

of the Requirements

for the Degree of

Master of Science in Geological Sciences

The University of Texas at Austin

May 2014

Acknowledgements

I would like to thank Peter Flemings for serving as my advisor, and for supporting and directing my research. I would also like to thank Julia Reece and Bayani Cardenas for serving on my thesis committee. I also wish to thank the current and past members of the UT Geofluids team, particularly Jack Germaine, Julia Reece, Amy Adams, Brendan Casey, Aiden Horan and Brian Fahy, who contributed much to this thesis including guidance with experiment design and methodology, advice and help with data interpretation, and providing supplemental data for comparison and context.

I also thank Peter Polito, Donnie Brooks, Mark Andrews and Carmen Atkins for their valuable assistance in the laboratory, and Tessa Green for keeping everything organized and on-track. I also thank the sponsors of the UT Geofluids consortium and the Jackson School of Geosciences for the financial support which made this thesis possible.

Abstract

Compressibility and Permeability of Gulf of Mexico Mudrocks, Resedimented and In-Situ.

William Salter Betts, MSGeoSci

The University of Texas at Austin, 2014

Supervisor: Peter B. Flemings

Uniaxial consolidation tests of resedimented mudrocks from the offshore Gulf of Mexico reveal compression and permeability behavior that is in many ways similar to those of intact core specimens and field measurements. Porosity (n) of the resedimented mudrock also falls between field porosity estimates obtained from sonic and bulk density well logs at comparable effective stresses.

Laboratory-prepared mudrocks are used as testing analogs because accurate in-situ measurements and intact cores are difficult to obtain. However, few direct comparisons between laboratory-prepared mudrocks, field behavior, and intact core behavior have been made. In this thesis, I compare permeability and compressibility of laboratory-prepared specimens from Gulf of Mexico material to intact core and field analysis of this material.

I resediment high plasticity silty claystone obtained from Plio-Pleistocene-aged mudrocks in the Eugene Island Block 330 oilfield, offshore Louisiana, and characterize its compression and permeability behavior through constant rate of strain consolidation

tests. The resedimented mudrocks decrease in void ratio (e) from 1.4 (61% porosity) at 100 kPa of effective stress to 0.34 (26% porosity) at 20.4 MPa. I model the compression behavior using a power function between specific volume (v=1+e) and effective stress (σ'_v):

$$v=1.85\sigma'^{-0.108}_{v}$$

Vertical permeability (k) decreases from $2.5\bullet10^{-16}$ m^2 to $4.5\bullet10^{-20}$ m^2 over this range, and I model the permeability as a log-linear function of porosity (n):

$$\log_{10} k = 10.83n - 23.21$$

Field porosity estimates are calculated from well logs using two approaches; an empirical correlation based on sonic velocities, and a calculation using the bulk density. Porosity of the resedimented mudrock falls above the sonic-derived porosity and below the density porosity at all effective stresses. Measurements on intact core specimens display similar compression and permeability behavior to the resedimented specimens. Similar compression behavior is also observed in Ursa Basin mudrocks. Based on these similarities, resedimented Gulf of Mexico mudrock is a reasonable analog for field behavior.

Table of Contents

List of Tables

List of Figures

Chapter 1: Overview

1.1 Introduction

When sediments are buried, they are compressed by overlying sediments, resulting in a decrease in volume as fluids are driven out and porosity is lost. The loss of porosity reduces the permeability, and the coupled process of volume change (compression) and fluid flow is called consolidation. During consolidation, the physical properties of the mudrock, including density, strength, permeability, and acoustic velocity, change affecting applications such as subsurface drilling and seismic imaging. Additionally, fluid flow is affected (Schowalter, 1979) and overpressure may develop when sediments are buried faster than the pore fluid can escape. Overpressure creates conditions in which submarine slope failure and tsunami generation can occur (Dugan and Flemings, 2000; Prior and Coleman, 1982), and contributes to the initiation and activation of faults and fractures (Rubey and Hubbert, 1959). Overpressure also represents a hazard to drilling and other seafloor and subsurface operations (Fertl, 1976).

1.2 Approaches to Measure compressibility and permeability during burial

The evolution of compression and consequently the decline in permeability with burial is studied through a variety of techniques. One approach to study compression behavior is to make measurements on natural sedimentary deposits. For example, we measure in the field the porosity (or void ratio) and density either directly (through core) or indirectly (through geophysical logging) at different burial depths where the fluid pressure is known. From these measurements, a compression curve can be constructed which describes the porosity (or void ratio) at any particular effective stress (Skempton and Jones, 1944). One challenge to this approach is that lithologic variation generally results in large scatter in the compression behavior.

A second approach to determine compression behavior is to perform laboratory consolidation tests upon intact samples. In this approach, a single sample is subjected to a range of effective stresses to interpret the compression behavior. The compression curve obtained from consolidating an intact core specimen in the laboratory has been used to predict field compression behavior (Long et al., 2011).

It is more difficult to measure permeability in-situ in low permeability rocks and the most common approach is to extract samples and measure the permeability at the in-situ effective stress (Bryant et al., 1975). Further information can be gained if a sample is subjected to increasing effective stress under uniaxial strain and the permeability is measured.

All of the above approaches attempt to test intact material in some manner. An alternative approach is to prepare in the laboratory sedimentary rocks of known composition and then subject these sediments to increasing effective stress. This approach generally involves mixing the sediment with added water. These specimens are sometimes called reconstituted (Burland, 1990), remoulded (Leroueil et al., 1985; Skempton and Jones, 1944), disaggregated (Karig and Ask, 2003), or resedimented specimens (Bensari, 1984; Schneider et al., 2011). I use the term Resedimentation in this thesis unless presenting work of previous authors, in which case I follow their terminology. The resedimentation process includes combining a powder made by crushing or grinding natural mudrocks with water to form a slurry and then uniaxially consolidating the slurry to form a specimen with a known stress history (Schneider et al., 2011).

Resedimentation was pioneered using Boston Blue Clay, a well-studied mudrock from the Boston area, and in recent years has been used to study other mudrocks of different compositions from around the world, including Kaolinite deposits from the US

and Europe (Gao, 2013), shallow mudstones from the Ursa basin in the Gulf of Mexico (Mazzei, 2008), and Nankai mudstone from offshore Japan (Schneider et al., 2011).

Resedimented specimens have been used for systematic studies showing the effects of grain size distribution (Schneider et al., 2011) and pore fluid salinity (Horan, 2012) on mudrock compression and permeability. They have also been used to study the anisotropy of mudrocks (Adams et al., 2013; Seah, 1990), and mudrock shearing behavior (Ahmed, 1990; Bensari, 1984; Casey and Germaine, 2013; Cauble, 1993).

1.3 RESEDIMENTATION VS. INTACT MEASUREMENTS

The analysis of material behavior from resedimented material has numerous advantages. There is little sample disturbance (the damage done during the coring and handling process of a sample), the composition and stress history are known, and the process is repeatable. Finally, it does not require intact core samples, which are difficult and expensive to obtain.

However, there are justifiable concerns with the approach. Resedimentation removes the in-situ fabric that was created in the rock during the initial deposition, so as this rock is experimentally compressed it may not accurately reflect the fabric of the original rocks (Skempton and Jones, 1944). If the fabric is not correctly reproduced then it is unlikely that the permeability and compression behavior will be analogous to that occurring in the field. A second concern is the effect of strain rate: in the laboratory, loading and strain occur over a period of days to weeks, whereas in the field the same amount of strain may occur over millions of years. At least two effects of strain rate have been proposed. First, that the inter-particle bonding imparts strength to an open-fabric of clay that resists low strain rates but is overcome by high strain rates (Burland, 1990; Skempton and Jones, 1944; Terzaghi, 1941), and second, that very low strain rates allow

secondary consolidation or creep (Taylor, 1942) to occur along with primary consolidation (Karig and Ask, 2003) which may result in lower porosities (and greater strains) for the intact material relative to resedimented material at a given effective stress. Finally, cementation and diagenesis are processes that increase the strength of sediments if they occur.

Only a few studies have compared field and laboratory mudrock behavior, and consensus on how permeability and compressibility may differ has not been reached. Burland (1990) found that laboratory-prepared specimens had lower porosities at a given effective stress than field specimens, and attributed the enhanced strength of the field specimens to the development of structure in the natural sediments. Structure refers to the combined effects of fabric and bonding (Mitchell, 1976). Santagata and Kang (2007) also found that resedimented Boston Blue Clay had lower porosities than field specimens at the same effective stress. In contrast, Karig and Ask (2003) laboratory-derived specimens had higher porosities than intact samples at the same stress; they attributed this to secondary consolidation occurring over a long term of burial. Figure 1.1 shows a conceptual comparison of the relationships between field and laboratory-prepared specimens found by Burland (1990) and by Karig and Ask (2003), demonstrating the wide range of behaviors described in the literature.

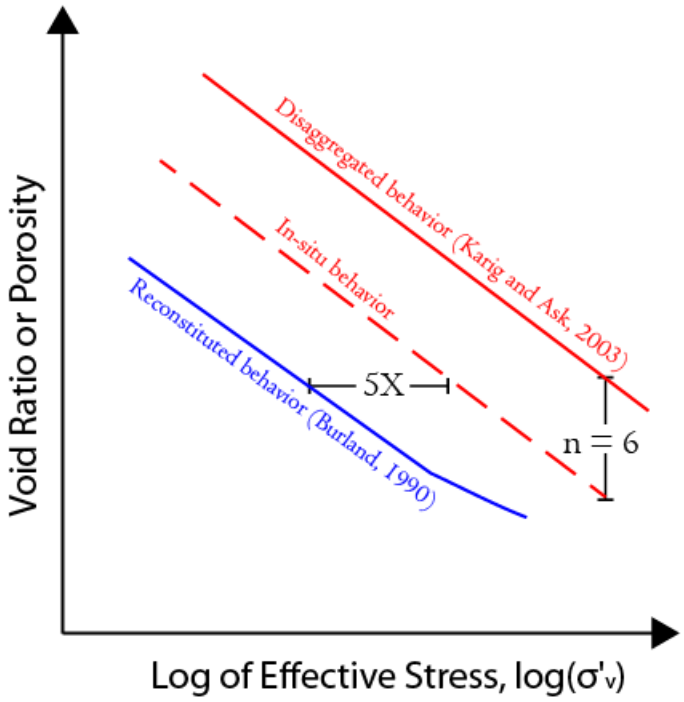

Figure 1.1: Comparison of in-situ or field porosity-effective stress behavior and resedimentation-like experiments. Burland (1990) found that for many natural clays, field sediments tended to support about five times as much effective stress as reconstituted specimens at the same porosity. At high effective stresses (above 10 MPa) the two curves begin to converge. Karig and Ask (2003) found that disaggregated Eugene Island clay produced a compression curve with the same slope as the intact material but about 6 porosity units higher.

1.4. GOAL OF THIS THESIS

In this thesis, I analyze the evolution of compressibility and permeability of a single material: resedimented mudrock from the Eugene Island Block 330 Oilfield (EI330). I then compare these results to a range of measurements made on intact samples in this oilfield. My goal is to address whether resedimentation accurately reproduces the field behavior or if there is some systematic difference between the two approaches.

1.5 STRUCTURE OF THE THESIS.

In this chapter (Chapter 1), I present an overview of the motivation and structure of this thesis. My key findings are presented in Chapter 2, in which I present my resedimentation experiments and characterize the compression and permeability properties. I also describe the origin and review the geologic setting of the sediment obtained from the Eugene Island Block 330 Oilfield of offshore Louisiana, and summarize its composition and physical properties. I call this sediment RGoM-EI. I then compare the compression and permeability behavior of RGoM-EI, obtained from Constant Rate of Strain Consolidation (CRS) tests, with in-situ observations from core and well logs and with tests of intact core.

Chapter 2 is based upon an extensive program of laboratory experiments, of which the approaches and detailed results I document in Appendices A through D. Appendix A presents a thorough geotechnical characterization of the RGoM-EI powder, including mineralogical composition, grain size distribution, and Atterberg Limits. Appendix B contains additional notes regarding the resedimentation of RGoM-EI. Appendix C presents the complete results for the suite of CRS tests. Appendix D contains SEM images of RGoM-EI at maximum past vertical effective stresses of 0.1, 8 and 20 MPa, as well as of intact core from well A20ST2 from Eugene Island Block 330, allowing comparisons of microstructure.

RGoM-EI posed special challenges for resedimentation and CRS testing. It has high plasticity and low permeability relative to previously tested materials such as Boston Blue Clay (BBC) and Kaolinite, and resedimentation and constant rate of strain testing required adaptations to existing procedures. Appendix E contains experimental procedure instructions I developed for the laboratory as an improvement to the preexisting document.

1.6 SUMMARY OF RESULTS

I find that permeability vs. porosity behavior of RGoM-EI material duplicates that obtained from intact core measurements. The permeability vs. porosity behavior of RGoM-EI falls along the low end of previously reported marine mudrock permeabilities, and is comparable to London Clay and some Ursa Basin mudrocks.

I compare the laboratory compression behavior of two intact core tests from Eugene Island with the compression behavior of RGoM-EI material: in one case the porosity of the intact material at a given effective stress is slightly above that of RGoM-EI, while in the second case, it is slightly below. C_c, the slope of the compression curve, is similar for both RGoM-EI and the intact measurements. I also found that the laboratory compression behavior of RGoM-EI is very similar to the observed compression behavior of an intact core from 51.14 meters below the seafloor in the Ursa Basin (Long et al., 2011). Intact porosity estimated from wireline sonic in the Eugene Island fields are lower by an average of 2.7% than the porosities interpreted from CRS of RGoM-EI material at the same vertical effective stress. In contrast, porosities predicted from wireline density are higher than CRS porosities at the same effective stress by up to 7 porosity units. Overall, these results suggest that the behavior and structure of the natural sediment is

largely captured in the resedimented material. These results support the use of resedimented mudrocks as analogs for in-situ mudrock behavior.

1.7 LIMITATIONS

The major limitation of this study is that it is difficult to constrain the field behavior. Only a few core plug porosities were available. Field porosities were derived from sonic velocity and bulk density well logs, but constants used in calculations could not be independently verified. Furthermore, the results of the two methods were substantially different from one another. More core porosity measurements would reduce the uncertainty in the field porosity estimates. Porosity measurements near the surface in particular are entirely lacking in the Eugene Island field data. The use of water-based mud may also have introduced a bias into the bulk-density log measurements. A more accurate density profile might be obtained from wells drilled with oil-based mud (Allen et al., 1993; Braunsdorf and Kittridge, 2003).

A related difficulty is accurately estimating the overburden. Bulk density logs began at 630 feet below sea level (192 mbsl) for well 331-SH-1, which had the shallowest logs in the studied area. I estimated the overburden by extrapolating bulk density up to the seafloor using an exponential function which was not constrained by any real data.

Similarly, only two intact core tests were available for these Eugene Island wells from Stump and Flemings (2002), and both had relatively high preconsolidation stresses. Thus, direct comparison of the intact core to the resedimentation could only be made above 7.1 MPa where post-yield consolidation data for the core was available. Likewise, the single permeability specimen tested by Stump and Flemings (Stump and Flemings, 2002a) matched the permeability of the resedimented specimen, but testing permeability

of intact cores at multiple porosities could confirm or disprove the trend established by the resedimented material.

Another limitation of this study is the uncertainty that is introduced into porosity and void ratio values of the resedimented material. The variation in calculated values of initial saturation (Chapter 2, Table 2.3) including some initial saturations above 100% is a symptom of some inaccuracy in the initial void ratio.

Although I believe the variation in void ratio to be small and constrained by the repeatability of the tests, the void ratio is computed based on a single measurement taken at the end of each CRS test and extrapolated back throughout the test based on volume changes. Several factors can cause problems in this approach: volume calculations during resedimentation depended on initial measurements taken with a ruler on the side of the tube, and their accuracy cannot be counted upon. The final measurement itself is affected by a small amount of material lost during the test. Additionally, specimen void ratios are calculated assuming that the salinity of the pore fluid remains constant throughout the resedimentation process, but that assumption has not been proven. Finally, the mudrock powder is not oven-dried, and exists in equilibrium with the air, thus, some amount of additional water is included in the initial dry mass measurements. I measured 3.5% water included in the powder during its initial characterization and calculated void ratios assuming this percentage, but that percentage may not be constant. Thus, reported void ratios and porosities may be slightly off of real values, particularly at low stresses, and the values reported for resedimentation should be considered approximate.

1.8 RECOMMENDATIONS AND FUTURE WORK

Based on my work, resedimented mudrocks show considerable promise as an analogue for field and intact core behavior. Obtaining more field data, such as shallow

geophysical logs and geotechnical cores, and testing the compression and permeability from cores at other depths in the Eugene Island Block 330 oilfield than already tested here will help constrain the relationships between field, intact, and resedimented behavior in the Gulf of Mexico. An alternative is to conduct a program of testing on resedimented material from another Gulf of Mexico sub-basin, where shallow sediment behavior has already been well documented. The Ursa Basin fits this description. Integrated Ocean Drilling Program (IODP) cores are available along with extensive moisture and density data in the shallow section, and numerous tests on intact cores have already been performed to characterize the compression (Long et al., 2011; Long et al., 2008) and permeability behavior of the sediments (Reece et al., 2012). In-situ pressure measurements have been taken (Long et al., 2007) and grain size distribution of the sediments has been measured (Sawyer et al., 2008). With so much field data available for comparison, we would be able to get a much better idea of the relationship between field data and resedimentation. Some experiments with resedimented Ursa Basin material performed by Mazzei (2008) could serve as a starting point for further investigation.

Additionally, modifications to the resedimentation apparatus could be made to facilitate resedimentation. Reducing the length of the consolidometer tube would make it easier to fill without incorporating air bubbles or getting sediment smeared on the inside of the upper portion of the tube (which results in loss of material and additional friction and makes it difficult to measure specimen height accurately). Also, a system where the tube is immersed in a water bath would make it easier to regulate salinity fluctuations that occur with evaporation from the small reservoir at the top of the current apparatus and the one to which the apparatus drains at the base. These salinity fluctuations may result in variable diffusion gradients and affect the concentration of salt in the pore fluids. These

modifications could result in more reliable measurements during the resedimentation, leading to more accurate void ratio values for this stage of compression.

References

Adams, A.L., Germaine, J.T., Flemings, P.B., Day, S.J., 2013. Stress Induced Permeability Anisotropy of Resedimented Boston Blue Clay. Water Resour. Res.

Ahmed, I., 1990. Investigation of normalized behavior of resedimented Boston Blue Clay using Geonor direct simple shear apparatus, Department of Civil Engineering. Massachusetts Institute of Technology, Cambridge, p. 225.

Bensari, J.E., 1984. Stress-strain characteristics from undrained and drained triaxial tests on resedimented Boston blue clay, Department of Civil and Environmental Engineering. Massachusetts Institute of Technology, Cambridge, p. 193.

Bryant, W.R., Hottman, W., Trabant, P., 1975. Permeability of Unconsolidated and Consolidated Marine Sediments, Gulf of Mexico. Marine Geotechnology 1, 1-14.

Burland, J.B., 1990. On the compressibility and shear strength of natural clays. Geotechnique 40, 329-378.

Casey, B., Germaine, J.T., 2013. The stress-dependence of shear strength in fine-grained soils and correlations with liquid limit. Journal of Geotechnical and Geoenvironmental Engineering 139, 1709-1717.

Cauble, D.F., 1993. The behavior of resedimented Boston blue clay at OCR4 in cyclic and post-cyclic undrained direct simple shear, Department of Civil and Environmental Engineering. Massachusetts Institute of Technology, Cambridge, p. 819.

Dugan, B., Flemings, P.B., 2000. Overpressure and Fluid Flow in the New Jersey Continental Slope: Implications for Slope Failure and Cold Seeps. Science 289, 288-291.

Fertl, W.H., 1976. Abnormal Formation Pressures: Implications to Exploration, Drilling, and Production of Oil and Gas Resources. Elsevier, Amsterdam.

Gao, B., 2013. Pore pressure within dipping reservoirs in overpressure basins. The University of Texas, Austin, TX.

Horan, A.J., 2012. The Mechanical Behavior of Normally Consolidated Soils as a Function of Pore Fluid Salinity, Department of Civil and Environmental Engineering. MIT, Cambridge, MA, p. 354.

Karig, D.E., Ask, M.V.S., 2003. Geological perspectives on consolidation of clay-rich marine sediments. J. Geophs. Res. 108, 2197.

Leroueil, S., Tavenas, F., Locat, J., 1985. Discussion: Correlations between index tests and the properties of remoulded clays. Geotechnique 35, 223-226.

Long, H., Flemings, P.B., Germaine, J., Dugan, B., Sawyer, D., 2007. In Situ Pore Pressure at IODP Site U1324, Ursa Basin, Gulf of Mexico. Proceedings of the Offshore Technology Conference, Houston, Texas.

Long, H., Flemings, P.B., Germaine, J.T., Saffer, D.M., 2011. Consolidation and Overpressure near the seafloor in the Ursa Basin, Deepwater Gulf of Mexico. Earth and Planetary Science Letters 305, 11-20.

Long, H., Flemings, P.B., Germaine, J.T., Saffer, D.M., Dugan, B., 2008. Data report: consolidation characteristics of sediments from IODP Expedition 308, Ursa Basin, Gulf of Mexico, in: Flemings, P.B., Behrmann, J.H., John, C.M. (Eds.), Proc. IODP. Proc. IODP, Sci. Results, College Station, TX, p. 47.

Mazzei, D.P.C., 2008. Normalized Mechanical Properties of Resedimented Gulf of Mexico Clay from Integrated Ocean Drilling Program Expedition Leg 308, Department of Civil and Environmental Engineering. Massachusetts Institute of Technology, Cambridge, p. 137.

Mitchell, J.K., 1976. Fundamentals of Soil Behavior. Wiley, New York.

Reece, J.S., Flemings, P.B., Dugan, B., Long, H., Germaine, J.T., 2012. Permeability-porosity relationships of shallow mudstones in the Ursa Basin, northern deepwater Gulf of Mexico. J. Geophs. Res. 117.

Rubey, W.W., Hubbert, M.K., 1959. Overthrust belt in geosynclinal area of western Wyoming in light of fluid-pressure hypothesis, 2: Role of fluid pressure in mechanics of overthrust faulting. GSA Bulletin 70, 167-205.

Santagata, M.C., Kang, Y.I., 2007. Effects of geologic time on the initial stiffness of clays. Engineering Geology 89, 98-111.

Sawyer, D.E., Jacoby, R., Flemings, P.B., Germaine, J.T., 2008. Data report: particle size analysis of sediments in the Ursa Basin, IODP Expedition 308 Sites U1324 and U1322, northern Gulf of Mexico, in: Flemings, P.B., Behrmann, J.H., John, C.M. (Eds.), Proc. IODP, College Station, TX, p. 20.

Schneider, J., Flemings, P.B., Day-Stirrat, R.J., Germaine, J.T., 2011. Insights into pore-scale controls on mudstone permeability through resedimentation experiments. Geology 39, 1011-1014.

Seah, T.H., 1990. Anisotropy of resedimented Boston Blue Clay, Department of Civil Engineering. Massachusetts Institute of Technology, Cambridge, p. 627.

Skempton, A.W., Jones, O.T., 1944. Notes on the compressibility of clays. Quarterly Journal of the Geological Society of London 100, 119-135.

Stump, B., Flemings, P.B., 2002. Consolidation State, Permeability, and Stress Ratio as Determined from Uniaxial Strain Experiments on Mud Samples from the Eugene Island 330 Area, Offshore Louisiana,, in: Huffman, A.R., Bowers, G.L. (Ed.), Pressure Regimes in Sedimentary Basins and Their Prediction, pp. 131-144.

Taylor, D.W., 1942. Research on Consolidation of Clays. M.I.T. Department of Civil and Sanitary engineering, Cambridge, MA.

Terzaghi, K., 1941. Undisturbed clay samples and undisturbed clays. Journ. Boston Soc. C.E. 28, 211.

Chapter 2: Compressibility and permeability of mudrocks from the Eugene Island Block 330 Oil Field, Resedimented and In-Situ.

ABSTRACT

Uniaxial consolidation tests of resedimented mudrocks from the offshore Gulf of Mexico reveal compression and permeability behavior that is in many ways similar to those of intact core specimens and field measurements. Porosity (n) of the resedimented mudrock also falls between field porosity estimates obtained from sonic and bulk density well logs at comparable effective stresses.

Laboratory-prepared mudrocks are used as testing analogs because accurate in-situ measurements and intact cores are difficult to obtain. However, few direct comparisons between laboratory-prepared mudrocks, field behavior, and intact core behavior have been made. In this thesis, I compare permeability and compressibility of laboratory-prepared specimens from Gulf of Mexico material to intact core and field analysis of this material.

I resediment high plasticity silty claystone obtained from Plio-Pleistocene-aged mudrocks in the Eugene Island Block 330 oilfield, offshore Louisiana, and characterize its compression and permeability behavior through constant rate of strain consolidation tests. The resedimented mudrocks decrease in void ratio (e) from 1.4 (61% porosity) at 100 kPa of effective stress to 0.34 (26% porosity) at 20.4 MPa. I model the compression behavior using a power function between specific volume (v=1+e) and effective stress (σ'_v):

$$v=1.85\sigma'^{-0.108}_{v}$$

Vertical permeability (k) decreases from $2.5\cdot10^{-16}$ m^2 to $4.5\cdot10^{-20}$ m^2 over this range, and I model the permeability as a log-linear function of porosity (n):

$$\log_{10} k = 10.83n - 23.21$$

Field porosity estimates are calculated from well logs using two approaches; an empirical correlation based on sonic velocities, and a calculation using the bulk density. Porosity of the resedimented mudrock falls above the sonic-derived porosity and below the density porosity at all effective stresses. Measurements on intact core specimens display similar compression and permeability behavior to the resedimented specimens. Similar compression behavior is also observed in Ursa Basin mudrocks. These similarities suggest that resedimentation can replicate the structure formed in natural deposits, and that resedimented Gulf of Mexico mudrock is a reasonable analog for field behavior in the Gulf of Mexico.

NOMENCLATURE

Symbol	Meaning	Dimensions
C	Butterfield (1979) coefficient	
C_c	Compression index	
e	Void ratio	
e_i	Initial void ratio	
ε	Volumetric strain	
ε_i	Initial strain	
G_s	Grain density	M/L^3
h	Specimen height	L
k	Permeability	L^2
m_v	Compressibility	LT^2/M
n	Porosity	
r	Pore pressure ratio	
S_i	Initial saturation	
σ'_v	Effective Vertical Stress	M/LT^2
σ'_{iv}	Effective stress at start of the test	M/LT^2
Δt	Travel time	T
Δt_{ma}	Matrix travel time	T
u	Pressure	M/LT^2
u_b	Chamber pressure	M/LT^2
v	Specific volume	
v_0	Reference specific volume at 1 MPa	
w_c	Water content from trimmings	
w_n	Water content from specimen	
x	Issler (1992) coefficient	

Table 2.1: Nomenclature

INTRODUCTION

Mudrocks (fine-grained sediments and their sedimentary rock equivalents) comprise about 60-70% of the fill of sedimentary basins around the world (Aplin et al., 1995; Dewhurst et al., 1998). During burial, mudrocks decrease in volume as fluids are driven out and pores collapse. This thesis uses the term compression for this process, which is termed compaction or gravitational compaction in geologic literature (Skempton, 1970). Marine mudrocks, when deposited at the seafloor often have initial porosities (n) of 75-80% or greater (Bryant et al., 1975; Bryant et al., 1986a). Compression can reduce the porosity to less than 15% after 5 km of burial (Aplin et al., 2006). This porosity reduction is accompanied by a decrease in permeability of several orders of magnitude (Bryant et al., 1975; Neuzil, 1994).

The evolution of mechanical and transport properties during burial affects a wide range of processes such as the migration and trapping of hydrocarbons and other fluids (Flemings et al., 2002; Schowalter, 1979), the generation of overpressure (Rubey and Hubbert, 1959), the development of structures such as faults and fractures (Rubey and Hubbert, 1959), and slope stability (Dugan and Flemings, 2000; Flemings et al., 2002). Thus, understanding the compression and permeability behavior of mudrocks is necessary in order to understand the hydrology and structure development in sedimentary basins. Additionally, applications such as drilling for oil and gas or seismic imaging of the subsurface are affected by the changes in physical properties that occur during compression.

The volume change that occurs during uniaxial compression is described by its compression curve (Skemption, 1970): a plot of void ratio (e) vs. vertical effective stress (σ'_v). The void ratio is the ratio of the porosity (n) to the solid volume (1-n), and vertical effective stress is the total vertical stress (σ_v) less the pore pressure (u).

$$e = \frac{n}{1-n}, \quad (1)$$

$$\sigma'_v = \sigma_v - u. \quad (2)$$

During uniaxial compression, void ratio varies directly with strain, and the coefficient of compressibility (m_v) is described by the ratio of incremental strain (ε) to incremental stress:

$$m_v = \frac{\Delta\varepsilon}{\Delta\sigma'} \quad . \quad (3)$$

Mudrock compressibility (m_v) varies depending on the composition (Mondol et al., 2007) and the structure or fabric (Burland, 1990) and the stress state. Permeability is also controlled by the compression behavior as it is controlled by the effective porosity, pore throat sizes, and the tortuosity of the path which fluids must take through the mudrock (Carman, 1937). At a given porosity, permeability varies between mudrocks by as much as three orders of magnitude (Neuzil, 1994) due to variations in lithology including the amount and type of clay minerals and the size and shape of grains.

Mudrock compressibility and permeability have been studied in the laboratory and in the field. The field approach typically involves comparing porosities (or void ratios) of mudrocks at different depths. Using known or assumed overburden and pore pressure gradients, a relationship between porosity and effective stress, called a sedimentation compression curve, is then found (Burland, 1990; Skempton and Jones, 1944; Terzaghi, 1941). A second approach is to subject intact samples of natural mudrocks to compression in the laboratory, where the volume change and pressures can be monitored, to obtain the compression curves (Bryant et al., 1986a; Bryant et al., 1986b; Dewhurst et al., 1999; Dewhurst et al., 1998; Dugan et al., 2003; Long et al., 2008; Yang and Aplin, 2007).

The variability of natural mudrocks presents a challenge in both of these approaches, as often more than one variable is changing and consequently, there is large scatter in any permeability or compressibility relationship.

A third approach is to study material behavior in laboratory-prepared mudstone samples. In this approach, composition is controlled and the behavior that results from changing only one parameter can be studied. This technique has been used to explore the relationships between permeability and other petrophysical properties in smectite–kaolinite mixtures (Mondol et al., 2008), the impact of composition on permeability and compressibility (Mondol et al., 2007; Schneider, 2011; Schneider et al., 2011), and the relationship between vertical and lateral stresses in mudrocks (Karig and Ask, 2003; Karig and Hou, 1992).

The last approach described above allows control of sample variability and sample disturbance is minimized. However, it is not well understood whether the laboratory-derived compression reasonably reproduces the natural process of sediment burial that occurs over much longer time scales than compression tests in the laboratory. A few studies have directly compared the two. When compared, natural mudrocks have often shown enhanced resistance to compression relative to laboratory-prepared specimens (Skempton and Jones, 1944; Terzaghi, 1941). For instance, Burland (1990) showed that the field behavior of a variety of natural mudrocks differed from their laboratory-prepared counterparts, with the field material being able to support approximately five times as much vertical stress at a given void ratio as the laboratory equivalent. At the high end of the stress range represented in the dataset, the field-derived and laboratory-prepared datasets begin to converge (Burland, 1990). The enhanced resistance is attributed to “structure” in the natural deposits not replicated in the laboratory (Burland, 1990; Terzaghi, 1941). Structure is defined as the combined

influence of fabric, which is the arrangement of particles, and bonding, which is the effects of interparticle forces (Burland, 1990; Mitchell, 1976). Natural clays are often deposited with a highly open fabric controlled by intermolecular bonding between the edges and faces of the clay particles (Terzaghi, 1941). This structure has been theorized to impart strength to the natural sediment, which is partially overcome by the high rate of strain and loading incurred in laboratory testing (Skempton and Jones, 1944; Terzaghi, 1941). It has been suggested that the disaggregation and slurrying of samples removes this structure completely (Skempton and Jones, 1944). To what extent the resedimentation procedure replicates the initial structure of the natural deposits is not fully understood, but similar structures are expected to be reflected in similar behaviors between field and laboratory specimens.

Karig and Ask (2003) found lower void ratios in the field and intact cores than in their laboratory-prepared specimens. They argued that at greater depths and higher stresses, different behavior could be expected than that described by Terzaghi (1941), Skempton and Jones (1944), Burland (1990), and others. They attributed this difference to secondary compression or “creep”, a time-dependent process occurring during and after the primary consolidation which occurs due to excess pressure dissipation (Taylor, 1942). The slow rate of loading and strain in the field and the age of the sediments allows secondary compression to proceed to completion.

I used the resedimentation method (Adams, 2011; Mazzei, 2008; Santagata and Kang, 2007; Schneider, 2011; Sheahan, 1991) and constant rate of strain (CRS) compression tests (ASTM, 2006b; Sheahan and Watters, 1997; Wissa et al., 1971) to study the compression and permeability evolution of Plio-Pleistocene-aged mudrock from the Eugene Island Block 330 oilfield, offshore Louisiana, over a range of 10 kPa to 20.5 MPa. I then compare the results to previous in-situ data derived from well logs

(Audet, 1996; Hart et al., 1995) and to previous tests of intact core (Long et al., 2011; Stump and Flemings, 2002a). I find similarities and a lack of systematic differences between the field data, intact core and the resedimented material. While field and intact data are limited, these results support the use of resedimented Gulf of Mexico mudrocks as field analogues.

Geologic Setting

I study mudrocks from the Eugene Island (EI) Block 330 oilfield, located on the outer continental shelf of offshore Louisiana, about 270 km southwest of New Orleans (Figure 2.1). The EI 330 field is located on the hanging wall of a downdropped shelf minibasin of Plio-Pleistocene age (Alexander and Flemings, 1995). The basin began to form prior to 2.8 Ma, as bathyal and prodelta shales, turbidites, and distal deltaic sands loaded and mobilized the underlying salt sheet. These distal deposits are overlain by a thick section dominated by proximal deltaic sediments, deposited when lowstand shelf-margin deltas reached the minibasin and stalled there as rapid salt withdrawal created accommodation space. The final phase of deposition is marked by fluvial deposition that filled incised valleys.

Whole core from Well A-12, located in Block 316, and Well A-20ST2, located in Block 330 (Figure 2.1), were used as source material for my resedimentation experiments. The mudrock in the cored intervals was deposited in an outer neritic environment during the prodelta phase early in the evolution of the minibasin (Alexander and Flemings, 1995). Well A-20ST2 penetrates the basin-bounding regional growth fault (Figure 2.2), and we use core material taken from the footwall. Cored material was taken between the 1.8 million-year-old *Robulus 64* horizon and the 2.2 Million year old *Globorotalia Miocenica* horizon, and was described as “silty shale with minor sand beds”

(Losh et al., 1994). Well A-12 is located on the upthrown block to the north of the basin-bounding growth fault (Figure 2.2) and the cored interval begins below the upper Lentic-1 sand (Stump, 1998), which is about 2.2 million years old (Alexander and Flemings, 1995).

Hart et al. (1995) described the pore pressure and overburden stress for wells 331-SH-1 and A-20ST2. The upper 1500 m are hydrostatically pressured, followed by a moderately overpressured transition zone of 500 m, and then severe overpressures, equaling up to 95% of the total overburden pressure occurring below 2000 m. Other wells in the Eugene Island Block 330 field show similar pressure profiles, though the depth at which the overpressure is encountered varies with the basin structure (Gordon and Flemings, 1998).

The cores used in this study are taken from the severely overpressured zone. In-situ effective stresses in the cored interval are estimated using the yield stress from consolidation experiments on the intact core, which corresponds to the maximum past effective stress in uncemented and undisturbed mudrocks (Casagrande, 1936; Karig and Morgan, 1994). Subsamples taken from the A-12 core at 2039 MBSF and from the A-20ST2 core at 2240 MBSF had experimental yield stresses of 7.2 MPa and 8.6 MPa, respectively (Stump and Flemings, 2002a). The same samples had estimated in-situ effective stresses of 7.1 and 7.3 MPa calculated by Stump and Flemings (2002a) using the porosity-effective stress method of Hart et al. (1995). Hydrodynamic modeling (Gordon and Flemings, 1998), mud weight data, and in-situ reservoir pressure measurements (Gordon and Flemings, 1998; Hart et al., 1995) predict generally similar effective stress conditions throughout the severely overpressured zone.

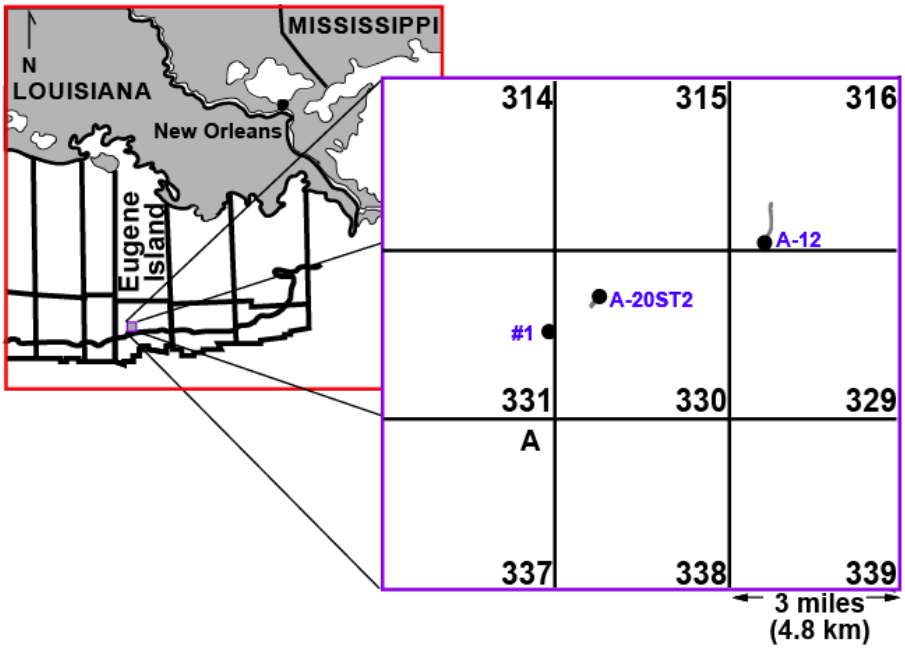

Figure 2.1: Index map showing Eugene Island Block 330 oilfield, consisting of block 330 and the surrounding blocks, and the locations of wells used in this study.

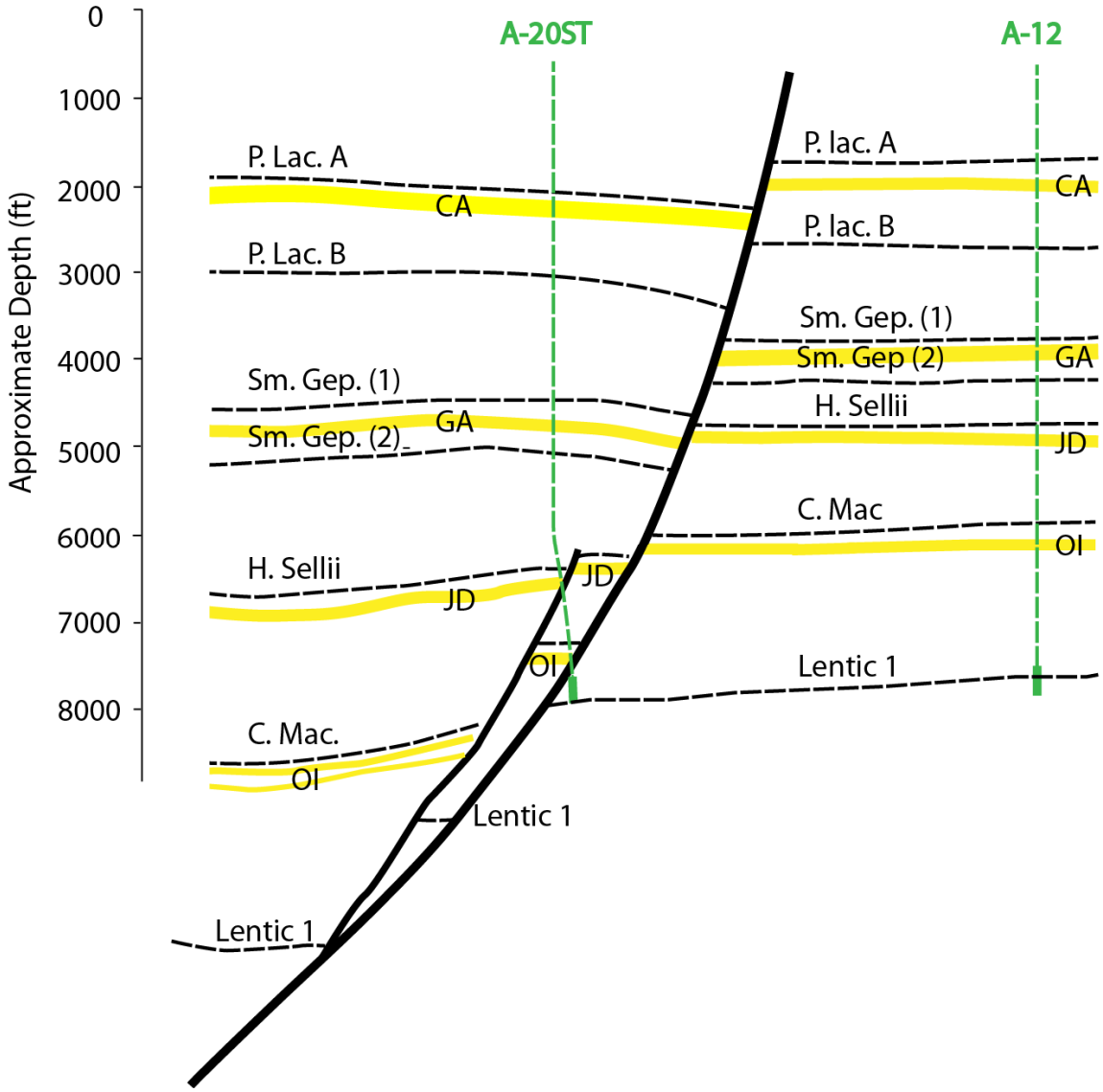

Figure 2.2: Cartoon cross-section of EI330 minibasin. Cores from wells A-12 and A-20ST2 were used in resedimentation experiments. Approximate locations of cored intervals are denoted with solid green lines. Adapted from Alexander and Flemings (1995).

LABORATORY METHODS

Core Processing

Material was removed from core tubing using hand tools and sandy intervals were discarded. The material was sledgehammer-crushed to fist-sized pieces. It was then spread on plastic sheeting in a layer less than 2 in (51 mm) thick and allowed to air-dry for 18 days. It was then shipped to an industrial processing service, where it was crushed to the specification that 99% should pass through a #100 mesh sieve (150 microns), and homogenized. This material, termed RGoM-EI was then used for resedimentation experiments.

Physical characterization

The processed powdered core was subjected to grain size analysis using the hydrometer method (ASTM, 2007). Atterberg limits were measured using the multipoint method for liquid limit and the hand method for plastic limit (Appendix A) (ASTM, 2005b). Grain density was measured using the water submersion method (ASTM, 2006c). Mineralogy was analyzed by X-ray powder diffraction (XRPD) at Macaulay Scientific Consulting LTD in Aberdeen, Scotland (Phillips, 2011). Water content of the air-dried powder was measured by oven-drying (ASTM, 2005a). Methods of physical characterization tests are further detailed in Appendix A.

Resedimentation

Samples were prepared from the powder using the resedimentation method (Adams, 2011; Mazzei, 2008; Santagata and Kang, 2007; Schneider, 2011; Sheahan, 1991). The homogenized powder was mixed with de-ionized water at a ratio of 1:1.12. I found that this ratio produced a stable slurry after mixing several small batches at different water contents in test tubes. Before mixing, sea salt was added to the water to

create a concentration of 74 to 80 g/l, which fell within the range of in-situ pore fluid salinities found in the Eugene Island block 330 field area (Losh and Wood, 1995). The resultant mixture was manually blended with a spatula for at least ½ hour until it reached a uniform, lumpless consistency. It was then allowed to sit, covered, overnight to ensure that all clay particles were fully hydrated. Finally, it was re-blended with the spatula and subjected to a vacuum for ½ to 1 hour to remove air bubbles. The slurry was then poured into a 3 in diameter tube-shaped consolidometer which allows top and bottom drainage through porous stones and a filter membrane. Load was then applied in increasing increments to the top of the specimen in a manner similar to the traditional oedometer test, allowing the specimen to consolidate. Eleven load increments were used, with loads increasing from 60 grams to 38 kilograms, which resulted in a final stress of 100 kPa. The final load increment was left on for at least 10 times the time required to reach end of primary consolidation, allowing secondary compression to occur, before being unloaded to 25 kPa. A displacement transducer was added on the fifth increment, at approximately 10 kPa, and used to monitor axial displacement thereafter. Void ratios for the end of each increment were later computed from the changes in specimen height and a constant mass of solids determined at the end of the CRS test. The resedimented material was then extruded from the consolidometer tube, packed in cellophane wrap, and stored in plastic containers chilled at 2 °C. Each resedimentation batch yielded two test specimens.

Constant Rate of Strain Consolidation Testing

We used constant rate of strain consolidation tests (ASTM, 2006b) to measure the compression and permeability behavior of the resedimented Gulf of Mexico mudrock (Appendix C). We used a computer-controlled pump and a 10,000 lb capacity load frame with 10,000 lb capacity load cell and pressure transducers rated to 300 PSI. The specimen

sat laterally confined in a steel ring, within a chamber filled with a mixture of de-ionized water and 80 g/l sea salt, and was left under 56 PSI backpressure for a minimum of 20 hours in order to saturate the specimen and drive any gas into solution. Strain was applied via a piston at rates which varied from 0.35 to 0.075 percent per hour. Strain rates were reduced periodically during the test in order to keep the pore pressure ratio (ASTM, 2006b) between 2% and 15% and to keep the absolute pressure at the base of the specimen less than 140 PSI (0.97 MPa), which prevented development of leaks in the system. The base was undrained and the top of the specimen was open to the chamber pressure. Specimen height, axial load, base pressure, and cell pressure were monitored. The Linear CRS consolidation theory (Sheahan and Watters, 1997; Wissa et al., 1971) was used to directly calculate hydraulic conductivity, and hence permeability, of the specimens from the measured volume change and pressure gradient across the specimen. Void ratio and porosity were calculated from the specimen volume and the dry solid mass of the specimen, taken after the end of the test, and using a grain density of 2.775 g/cm^3.obtained by measurement of the RGoM-EI powder (Appendix A).

Tests were conducted in general accordance with ASTM D 4186 (2006b) and in accordance with established UT Geomechanics laboratory procedures. There were some adaptations made to the existing procedures because they were developed and optimized for materials with a lower plasticity, higher permeability, and lower pore fluid salinity than the RGoM-EI. The specimen initial heights used in this study were 12 to 17 mm, which is less than the minimum height of 20 mm specified by ASTM D 4186. The specimen heights were reduced in order to limit the consolidation time and minimize the effects of friction with the confining ring. The specimen heights satisfied the condition given by Germaine and Germaine (2009) that the height be greater than 10 times the maximum particle diameter and that the diameter to height ratio of the specimen be

between 2.5 and 4. The water chemistry is not dictated by ASTM D 4186. I used water with a salinity similar to that used in the Resedimentation batching in order to reduce diffusion effects such as those described by Van Paassen and Gareau (2004). In CRS107, a small amount of oil was added to the tubing between the pump and the cell to prevent saline chamber fluid from diffusing into the pump. A reservoir was connected to the tubing between the pump and the chamber to allow the introduction of saline fluid to the chamber. For a detailed step-by-step enumeration of the CRS procedures, refer to Appendix E.

RESULTS

Characterization of powder

Key results of the grain size, mineralogy, and Atterberg limits are presented here. For complete results of tests characterizing the RGoM-EI powder, refer to Appendix A.

Four hydrometer test results on RGoM-EI powder are shown in Figure 2.3. The four tests are from specimens taken from different parts of the large bag shipped to us from the processing service, so variation between analyses is likely a result of particle segregation during shipping. The average of the four tests shows that the RGoM-EI material is composed of 62.4% clay-size particles (<2 microns) and 37.6% silt-size particles (Figure 2.3), making it a silty claystone (Shepard, 1954).

The overall mineralogy of the RGoM-EI material is dominated by illite + illite/smectite (44.4 wt. %), quartz (27.8 wt. %), and kaolinite (9.1 wt. %). plagioclase, k-feldspar, barite, muscovite, calcite, and siderite were also detected at concentrations ranging from 6 wt. % to 1 wt. % (Table 2.2, Figure 2.4). Trace minerals identified included dolomite, pyrite, anatase, halite, and chlorite. Identification of the trace mineral phases is subject to some uncertainty, and some of the trace phases identified may not

actually be present (Phillips, 2011). The barite most likely is from the drilling fluid used when the core was extracted.

A separate analysis, performed only on the clay-size particle fraction, shows that it consists primarily of illite+smectite (87 wt. %) of 70-80% expandability. Illite (8 wt. %), kaolinite (4 wt. %) and chlorite (1 wt. %) are also present. Expandability of mixed-layer clays is often correlated with the proportion of smectite present (Ransom and Helgeson, 1989); the high expandability of the illite+smectite suggests that smectite is the dominant component.

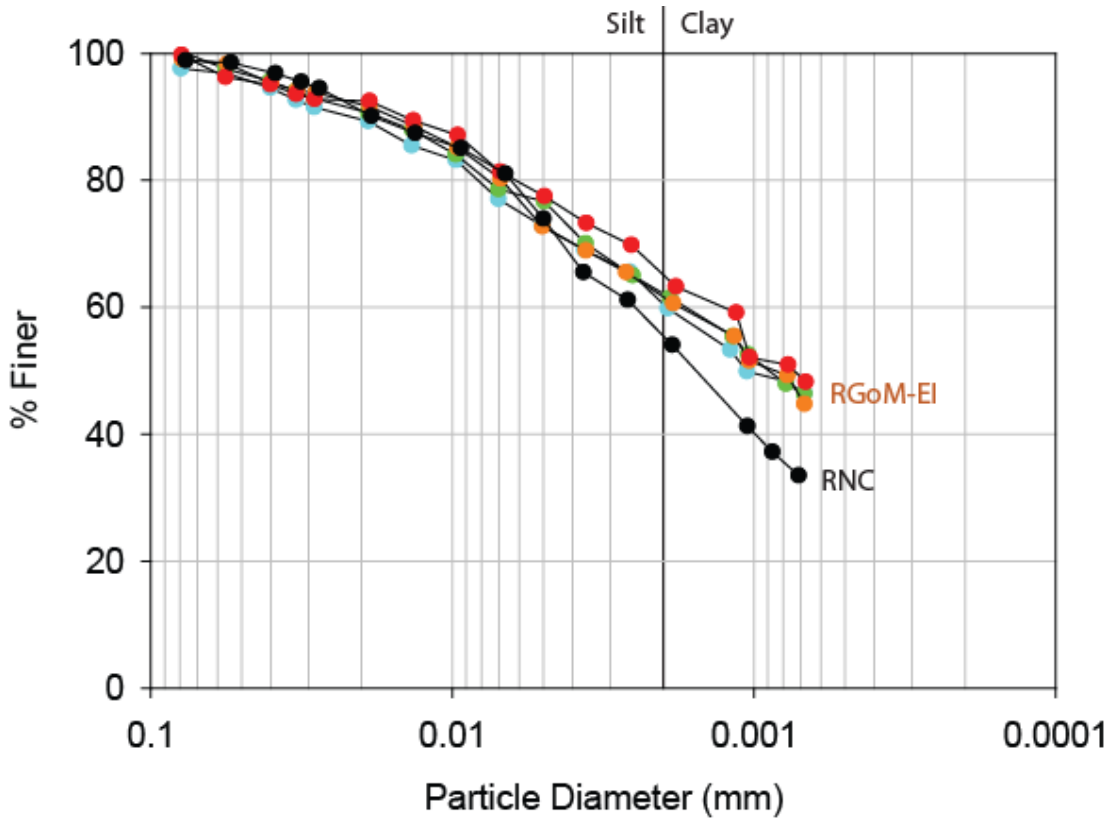

Figure 2.3: Grain size distributions of RGoM-EI from four hydrometer sedimentation analyses. 2.4% of particles are clay-size (under 2 micrometer) from the average of the four analyses. Nankai clay (Schneider, 2011) is also included for comparison (black circles labeled RNC).

RGoM-EI Overall Mineralogy		Clay-size fraction mineralogy	
Quartz	27.8	Kaolinite	4
Plagioclase	5.3	Illite	8
K-Feldspar	4.0	Illite+Smectite	87
Calcite	1.2	Chlorite	1
Dolomite	0.8	Total	100
Siderite	1.0		
Pyrite	0.7	% Expandability	70-80
Anatase	0.2		
Barite	3.2		
Halite	0.2		
Muscovite	1.9		
Illite + I/S	44.4		
Kaolinite	9.1		
Chlorite	0.4		
Total	100.2		

Table 2.2: The mineralogical makeup of a specimen of RGoM-EI determined by X-Ray Powder diffraction using the reference intensity ratio (RIR) method (Hillier, 2000).

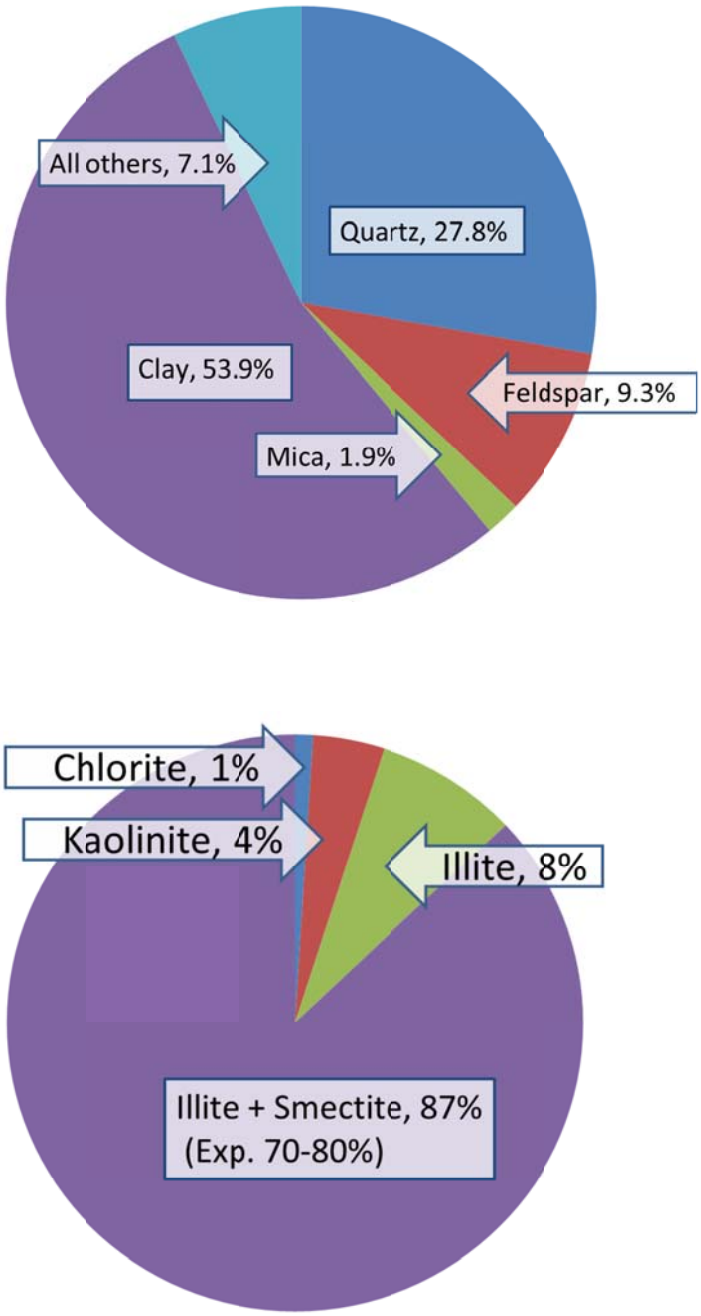

Figure 2.4: Bulk (top) and clay-size fraction (bottom) mineralogical makeup of RGoM-EI from X-Ray Powder Diffraction analysis. For complete XRD results refer to Appendix A.

Compression Behavior

The RGoM-EI slurry has an initial void ratio of 3.4 (n = 77%). Eleven incremental loading steps are added to compress the material to a stress of 0.1 MPa. As these loads are applied, the material is compressed. Specimen heights at prescribed effective stresses are converted into void ratio and plotted as yellow circles on Figure 2.5. Void ratio declines to a minimum of 1.4 (n = 58%) (Figure 2.5) resulting in a volumetric strain of 59%. After resedimentation, the material is unloaded and a small amount of swelling is observed (red circle, at 0.1 MPa.).

I performed four constant rate of strain tests (CRS) on the RGoM-EI material (Table 2.3, Figure 2.6). CRS 110 is plotted on figure 2.5 along with the resedimentation increments from which it was derived, and I describe its compression behavior in detail. During resedimentation, the material was preloaded to 0.1 MPa. Thus, at the start of CRS 110, the material is overconsolidated (the current effective stress is less than the maximum past effective stress). During initial loading, void ratio decreases only a small amount, from 1.6 to 1.5 (n = 62% to 61%) (Figure 2.5). At 0.1 MPa, there is a sharp break in the compression curve: at greater stresses, the void ratio declines from 1.5 to 0.5 at 8 MPa. The break in slope corresponds to the maximum loading which occurred during resedimentation, thus the yield stress is the pre-consolidation stress and marks the boundary from elastic to elastoplastic deformation (Casagrande, 1936). During compression, the compression curve has a convex up profile in this semi-log plot (Figure 2.5). Ultimately, from the initial mixture (0 MPa) to the final CRS stress (8.4 MPa), void ratio declines from 3.4 to 0.5 (porosity from 77% to 33%) with a bulk strain of 65.9%. Void ratios as low as 0.35 (26% porosity) were achieved by the higher-stress CRS tests, resulting in a bulk strain of 69.3 %.

I use Butterfield's (1979) empirical compression model to capture this compression behavior:

$$v = v_0 {\sigma'_v}^C, \quad (4)$$

where v is specific volume with $v = e/(1+e)$, v_0 is the specific volume at an effective stress of 1 MPa, and C is an empirical constant. I use linear regressions of a log-log plot of specific volume vs. vertical effective stress to constrain v_0 and C following the approach of Long et al. (2011), regressing the datasets between 0.1 MPa and the end of the test. In CRS 110, I find that v_0 is 1.85 and C is -0.112 (Table 2.3).

In four different CRS tests on the RGoM-EI material, the compression behavior was very similar (Figure 2.6). Three of the tests (CRS 107, 110, 111) nearly overlie each other. CRS 109 slightly underlies the other three tests. This may be because some material was lost due to extrusion through the end cap during the CRS test resulting in a higher calculated void ratio than was actually present. Starting with CRS109, I compensated for this by collecting extruded material and adjusting the void ratios. Some salt water was collected with the extruded material in CRS109, resulting in a low calculated void ratio.

To determine the characteristic compression behavior of RGoM-EI material, I did the following: I regressed all four CRS tests (Figure 2.6) from the preconsolidation stress of 0.1 MPa to the maximum value of the test and determined the values of C and v_0 for each. I found that v_0 ranged from 1.80 to 1.88 and C from -0.107 to -0.112 (Table 2.3). I then averaged the values of v_0 and the values of C to get an average v_0 of 1.85 and an average C of -0.110. In fact, these parameters are similar to CRS 110 and CRS 111 curves to two decimal places. CRS 111 has a greater stress range, so I consider it representative and use CRS 111 to interpret the virgin compression behavior of the RGoM-EI material as:

$$v = 1.85{\sigma'_v}^{-0.108}, \quad (5)$$

where the effective stress (σ'_v) is expressed in MPa.

Permeability Behavior

Permeability was continuously measured over the course of all four tests. A linear relationship between porosity and the log of permeability was observed in all four tests (Figure 2.7) as has been seen in previous studies (Bryant et al., 1975; Neuzil, 1994). The four datasets cluster together in a band ranging from $2.0 \cdot 10^{-17}$ m^2 at 60% porosity (e = 1.5) to $4.5 \cdot 10^{-20}$ m^2 at 27% porosity (e = 0.37), a change of nearly four orders of magnitude. The visible linear relationship between porosity and the logarithm of permeability is characterized using the following expression (Neuzil, 1994; Nelson, 1994; Saffer and Bekins, 2006):

$$\log_{10}(k) = \gamma \cdot n + \log_{10}(k_0), \quad (6)$$

where γ is the permeability index and $\log(k_0)$ is the logarithm of the permeability at a porosity of zero (Schneider, 2011). Values of γ and k_0 for each test are constrained by a linear regression and provided in Table 2.3. A regression of the combined datasets of the four tests yields the following expression:

$$\log_{10} k = 10.83n - 23.21 \quad (7)$$

Equation 7 is represented as a dashed red line in Figure 2.7.

Test Number	Index test			Specimen Data				
	w_c (%)	SD	N	w_n (%)	e_i	S_i (%)	Gs (g/cm^3)	H (mm)
CRS107	51.6	1.1	4	44.6	1.55	95.59	2.775	12.9
CRS109	49.3	3.2	4	58.02	1.55	103.7	2.775	23.6
CRS110	47.2	3.7	4	55.44	1.52	99.1	2.775	23.6
CRS111	51.6	1.1	4	61.31	1.56	109	2.775	12.9

	Test Conditions						Test Results			
Test # Origin	u_b (kPa)	σ'_{iv} (kPa)	ε_i	$d\varepsilon/dt$ (s^{-1})	$\sigma'v_{max}$ (Mpa)	r at σ'_{vmax}	V_0	C	γ	log(k_0)
CRS107 Resed075	386	25	-0.003	0.35-0.15	20.9	1.47	1.88	-0.107	10.82	-23.19
CRS109 Resed066	386	14.8	0.062	0.15-0.10	8.7	1.44	1.80	-0.112	10.39	-22.90
CRS110 Resed065A	386	14.9	0.019	0.15-0.075	8.6	8	1.85	-0.112	11.05	-23.45
CRS111 Resed075	386	19.5	-0.1	0.10-0.075	20.4	0.8	1.85	-0.108	11.75	-23.55
Average	-	-	-	-	-	-	1.85	-0.110	-	-
Combined	-	-	-	-	-	-	-	-	10.83	23.21

Table 2.3: Specimen properties, test conditions, and results for CRS testing of RGoM-EI. SD and N represent the standard deviation and number of measurements of water content from trimmings.

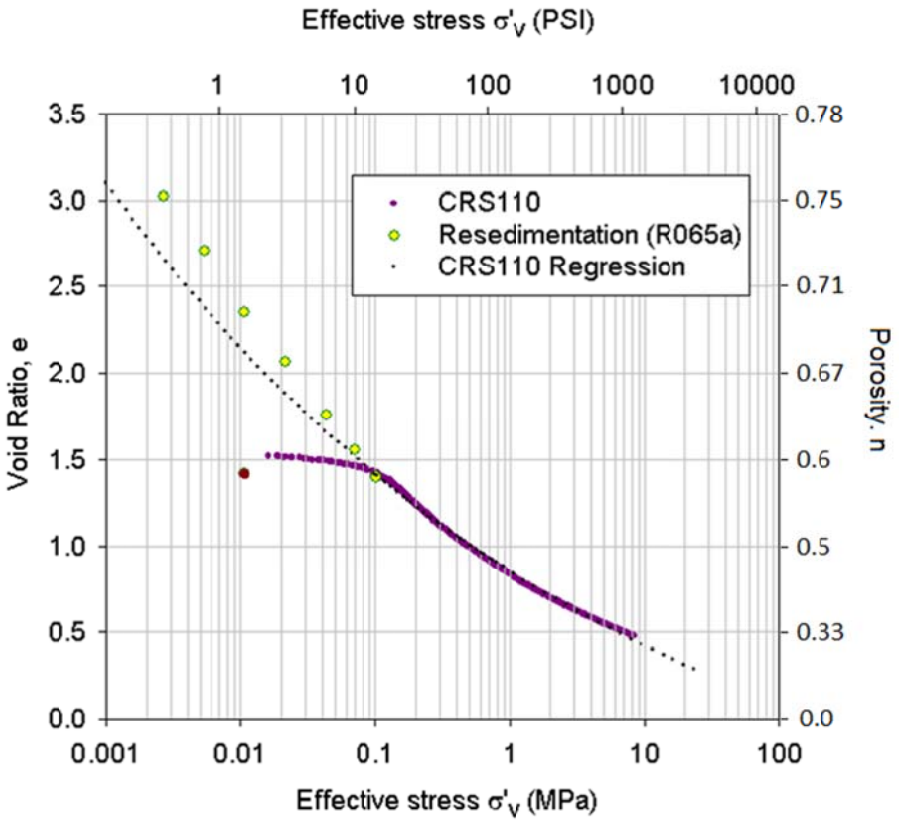

Figure 2.5: Compression curve for RGoM-EI material. Yellow circles represent void ratio at successive load increments during resedimentation of sample R065a. Purple dots record void ratio during the constant rate of strain test performed on R065a (CRS 110). The black dotted line is a regression of CRS 110 data between 0.1 MPa and the end of the test. The initial void ratio, prior to re-sedimentation was 3.4 which is in agreement with the trend produced by the other data points.

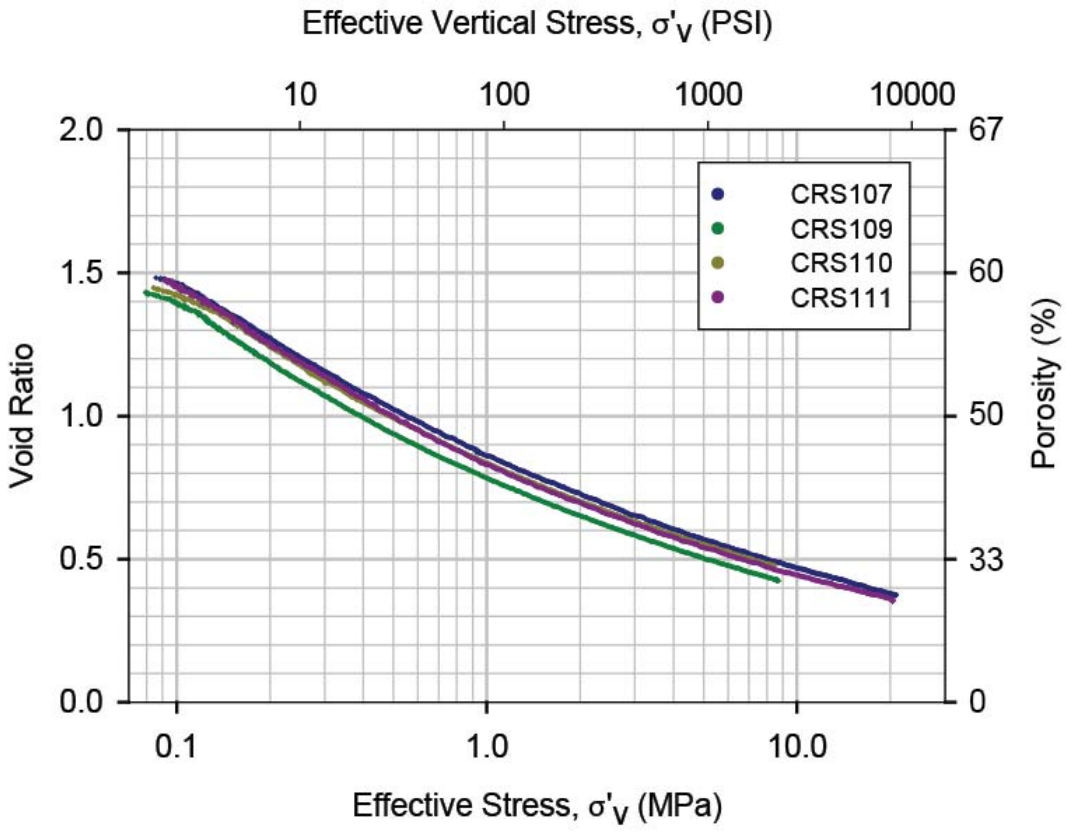

Figure 2.6: Compression curves resulting from four CRS tests of RGoM-EI. Data are only plotted during the virgin compression part of the CRS test, for effective stresses greater than the pre-consolidation stress of 0.1 MPa and to the maximum value in the test. CRS 109 has slightly lower porosity than the others, probably due to excess salt included while accounting for a dry mass of extruded material.

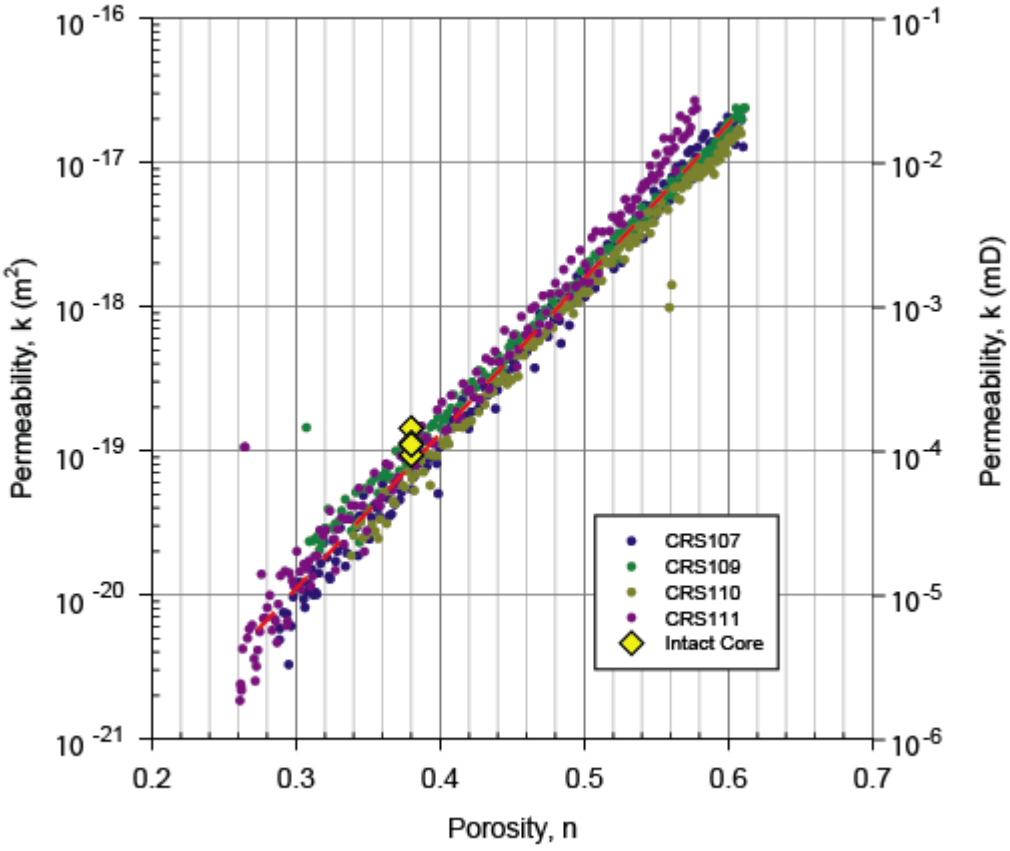

Figure 2.7: Porosity-permeability relationship derived from four CRS tests and comparison with intact core permeability from Stump & Flemings (2002). Only three intact core data points are visible, the fourth is obscured behind another. The red dashed line shows the relationship $\log_{10} k = 10.83n - 23.21$ obtained from a regression of the four combined datasets.

DISCUSSION

Experimental and field compression curves

In order to define the field compression behavior, I estimate porosity and effective stress based on geophysical logs from well 331-SH-1. I use two approaches to define the field porosity. In the first approach, following Hart et al. (1995), I estimate mudstone porosity in the Eugene Island 330 oil field using a sonic velocity log of well #331-SH-1 and the empirical relationship suggested by Issler (1992).

$$n = 1 - \left(\frac{\Delta t_{ma}}{\Delta t}\right)^{1/x}, \qquad (8)$$

where Δt is log-derived travel time, Δt_{ma} is matrix travel time, and x is a constant. I assumed Δt_{ma} = 220 μs/m and x = 2.19, which were proposed for low organic carbon, non-calcareous shales by Issler (1992).

In the second approach, I calculate the porosity from the bulk density log from well 331-SH-1 using values of 2775 kg/m^3 for grain density and 1050 kg/m^3 for pore fluid density. The grain density value used is the measured grain density of RGoM-EI, while the water density value is assumed. In both approaches, the total vertical stress (σ_v) at any depth was estimated by integrating the bulk density log. An exponential function fit to the density porosity was extrapolated to the surface, with porosity fixed at 90% at 0.5 feet below seafloor (Figure 2.8). In the shallow section, where pore pressures were known to be hydrostatic (Hart et al., 1995), I subtract a hydrostatic pore pressure gradient of 10.5 MPa/km from the integrated bulk density to calculate effective stress.

The resulting porosity-effective stress relationships are plotted in Figure 2.9. The CRS porosities at a given effective stress are on average 2.7 porosity units higher than the in-situ estimates from velocity data; although the two porosity types do converge at

higher stresses (Figure 2.9). When only data points above 5 MPa are considered, the average difference shrinks to 1.3 porosity units. Porosities measured from the bulk density log (blue dots, Figure 2.9) are 2-7 porosity units higher than the CRS data at a given vertical effective stress.

Both the velocity based and the density based approaches have challenges. Porosities derived from velocity (Eq. 8) should be viewed with caution because they are not a direct measurement of velocity, but rather are based on empirical correlation. This relationship was also observed by Karig and Ask (2003) for a disaggregated Eugene Island mudrock sample that had a compression curve above the field curve obtained from the Hart dataset, and they proposed that the constants used in the empirical correlation were causing an underestimate.

Bulk-density based measurements are challenging for two reasons. First, this is a padded tool and to measure the formation accurately, it needs to be in contact with the formation. If it is not in contact, for example due to borehole washout, then the observed porosity may be too low. Second, these holes were drilled with water-based mud. It has been shown that in smectite-rich material, swelling can occur due to the interaction of fresher water with the shale. This results in an arbitrarily lower bulk density and hence higher porosity measured by the log (Allen et al., 1993; Braunsdorf and Kittridge, 2003). Reduction in density of between 0.03 to 0.08 g/cm^3 has been observed in Gulf of Mexico wells drilled with water-based mud (Braunsdorf and Kittridge, 2003). This would result in overreporting of density porosities, for instance, applying a correction of 0.08 g/cm^3 to the bulk density log would reduce a density porosity of 40% to 34%. This correction would also affect the lithostatic gradient and the effective stress.

The velocity-based approach and the density based approach are compared to actual measurements of porosity in the A-20ST2, the Pathfinder well (Figure 2.10). Here,

I use depth instead of effective stress to avoid introducing uncertainties related to estimating the overburden and pore pressure. The limited number of directly measured core porosities (green squares, Figure 2.10) show that at a given depth, the core porosity is equal to or slightly less than the velocity-derived porosity in well A-20ST2. In contrast, the bulk density porosity is found to be about 10 porosity units higher than the sonic porosity in the overpressured zone. The in-situ porosity of T77 (Stump and Flemings, 2002a) is also shown and is intermediate to the two well-log derived porosity datasets. Thus, the velocity based sedimentation compression curve for Eugene Island lies an average of 3.2 porosity units below the laboratory curve and converges at higher stresses, whereas the density-based curve lies above it by 2-7 porosity units.

Intact core compression behavior

Stump and Flemings (2002) performed uniaxial consolidation tests on two intact core specimens from the Eugene Island Block 330 oilfield. These samples are from within the cored depth range of the same wells which provided core for RGoM-EI. T96 was taken from 2039 mbsl on well A-12 and T77 was taken from 2240 mbsl on well A-20ST2. The portion of the compression curve for T96 that is greater in stress than the pre-consolidation stress converges with that of the resedimented material, whereas T77 supports approximately twice the effective stress of RGoM-EI at a given void ratio (Figure 2.9). C_c values (a measure of the slope of the compression curve in e-log σ'_v space) were 0.27 for T96 and 0.29 for T77 (Stump, 1998). Visual inspection of Figure 2.9 suggests that the resedimented material has slightly higher C_c values (i.e. a slightly steeper negative slope), though CRS 111 yields a calculated C_c of 0.29 for stresses between 7 and 14 MPa, matching that of T77.

Intact core data, like well data, is lacking for the uppermost section at EI330. The Ursa basin provides a possible analogue. Long et al. (2011) used the Butterfield equation (Eq. 4) to obtain a compression curve from intact core in the shallow (0-500 mbsf) Ursa Basin. They found $v = 1.89\sigma'^{-0.979}_{v}$. Long et al. (2011) showed that this experimentally derived compression curve successfully predicted the observed porosity vs. effective stress behavior in the field. It is striking how similar the compression behavior derived from resedimented Eugene Island material (RGoM-EI) is to the Long et al. (2011) compression curve (Figure 2.9), including at low stresses.

Field and lab compression in literature

As previously mentioned, stiffer behavior (higher porosities at a given effective stress) has commonly been observed in the field relative to the laboratory-prepared specimens (Burland, 1990; Skempton and Jones, 1944; Terzaghi, 1941). The difference is attributed to the structure or fabric created by the intergranular contacts during deposition, which tends to be highly open (Burland, 1990; Skempton and Jones, 1944; Terzaghi, 1941). The high rates of loading in laboratory tests relative to the field tends to cause a partial breakdown of this structure (Terzaghi, 1941) and mixing clay with water to form a slurry must completely break down this structure, according to Skempton (Skempton and Jones, 1944). Thus, the expected pattern for the laboratory-prepared specimen has the lowest porosity at a given effective stress, followed by the laboratory compression curve of intact specimens, and the sedimentation compression curve, made from field porosity measurements, would have the highest porosities at a given effective stress.

An alternative interpretation was presented by Karig and Ask (2003). In this model, secondary compression or creep plays a significant role over longer timescales

and this results in lower porosity at a given effective stress for intact data relative to resedimented results, where the strain rate is much higher (Figure 2.11). Karig and Ask (2003) found that a disaggregated sample from Eugene Island had porosity about six units higher than the velocity-derived porosities. They attributed the difference to secondary compression and to possible underestimates of field porosity from the sonic log.

My density porosity dataset has higher porosities than the resedimentation dataset, consistent with the results of Burland (1990) and others. Like Karig and Ask (2003), I found that the velocity-derived porosity was lower than that of the resedimented experiment, although the sonic porosities do tend to converge with the CRS dataset at higher stresses. Neither one of these well-log derived datasets can be considered definitive, since the sonic log may underestimate porosity as Karig and Ask believed and the density porosity could be an overestimate incorporating clay altered by interaction with water-based mud (Braunsdorf and Kittridge, 2003). Thus, the actual porosity may be closer to the CRS data then either dataset appears. Based on these data, I cannot say how much effect structure and secondary compression have relative to each other, but the CRS data is effectively bracketed by the well-log porosity estimates, showing that it is a reasonable interpretation of the in-situ porosity.

SEM imaging

An open, highly porous sedimentary structure is formed by natural deposition of clay-rich sediments (Terzaghi 1941). Scanning electron microscope (SEM) photomicrographs were taken on intact core and on resedimented specimens, which had been compressed to a comparable effective stress (8.7 MPa), as well as resedimented

specimens at a low effective stress of 100 kPa and a higher effective stress (20.4 MPa), allowing qualitative analysis of the microstructure and its evolution during consolidation.

The structure of intact and resedimented specimens after compression to about 8 MPa can be seen in Figure 2.12. Photomicrographs are oriented perpendicular to bedding, and while the uniaxial consolidation might be expected to develop a strongly preferred orientation, both specimens include nearly-vertical large grains, associated with vertically elongated large pores. This suggests that the original open structure has not been broken down by the compression, and the general similarities between the structures of each suggest that their initial structures may also have been similar. The 100 kPa specimen shows an open, highly isotropic structure, while the 20.4 MPa specimen has lost most of its porosity and developed a preferred orientation (Figure 2.13).

Intact core vs. Resedimented Permeability

Stump and Flemings (2002a) measured the permeability of an intact specimen from the well A-12 core with 38% porosity. Four analyses, run using different pressure gradients, yielded closely grouped results with an average permeability value of 1.15 x 10^{-19} m^2 (1.17 x 10^{-4} mD). The permeability measured on the resedimented specimens at 38% porosity closely matches this result (Figure 2.7). Unfortunately, measurements of core at other porosities were not available.

Previously published permeability measurements and models for marine mudrocks provide an additional constraint on field behavior, and are compiled in Figure 2.14 (Stump and Flemings, 2002b). For a given porosity, RGoM-EI has permeabilities near the low end of the range of previously reported permeabilities for marine mudrocks, comparable to some Ursa Basin mudrocks and to London Clay. The slope of the porosity-permeability relationship is similar to that displayed by Nankai mudstone (Schneider,

2011), though the values are lower by approximately 1/3 of a log cycle of permeability. Nankai mudstone has a similar percentage of smectite to RGoM-EI, and the grain size distribution is also similar, although it seems that RGoM-EI has a greater fraction of ultra-fine particles (Figure 2.3) which may disproportionately impede the fluid transport.

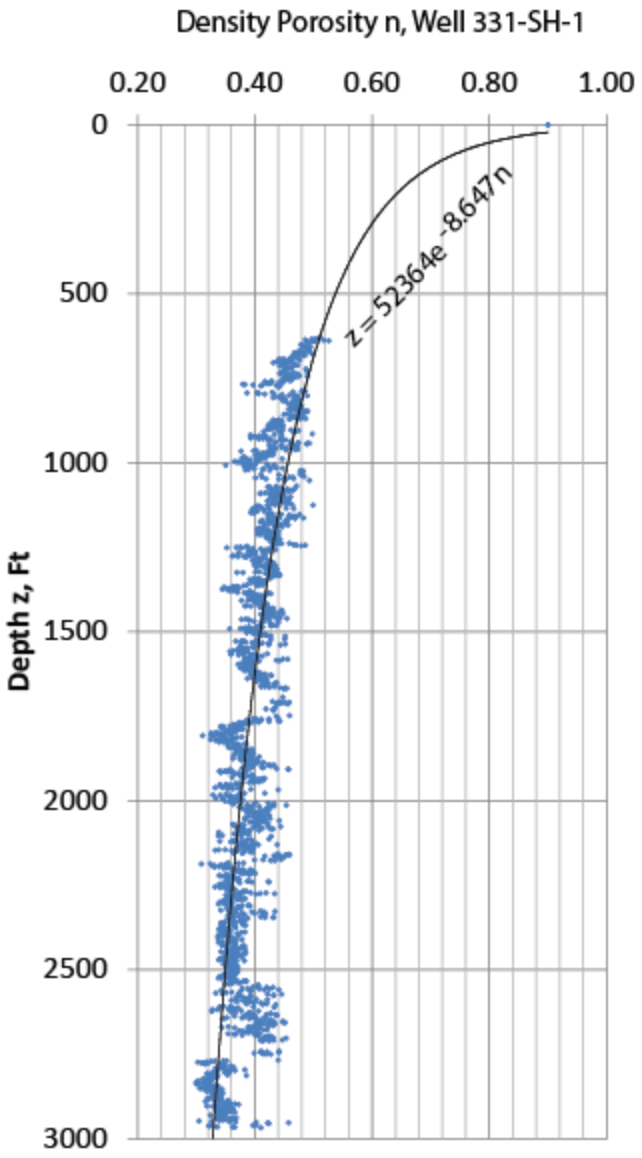

Figure 2.8: Bulk density log-derived porosity in well 331-SH-1. In order to estimate the overburden, Bulk densities in the first 630 feet below the seafloor were extrapolated using an exponential porosity-depth function, fit to the dataset with a fixed point of 90% porosity at 0.5 ft below seafloor.

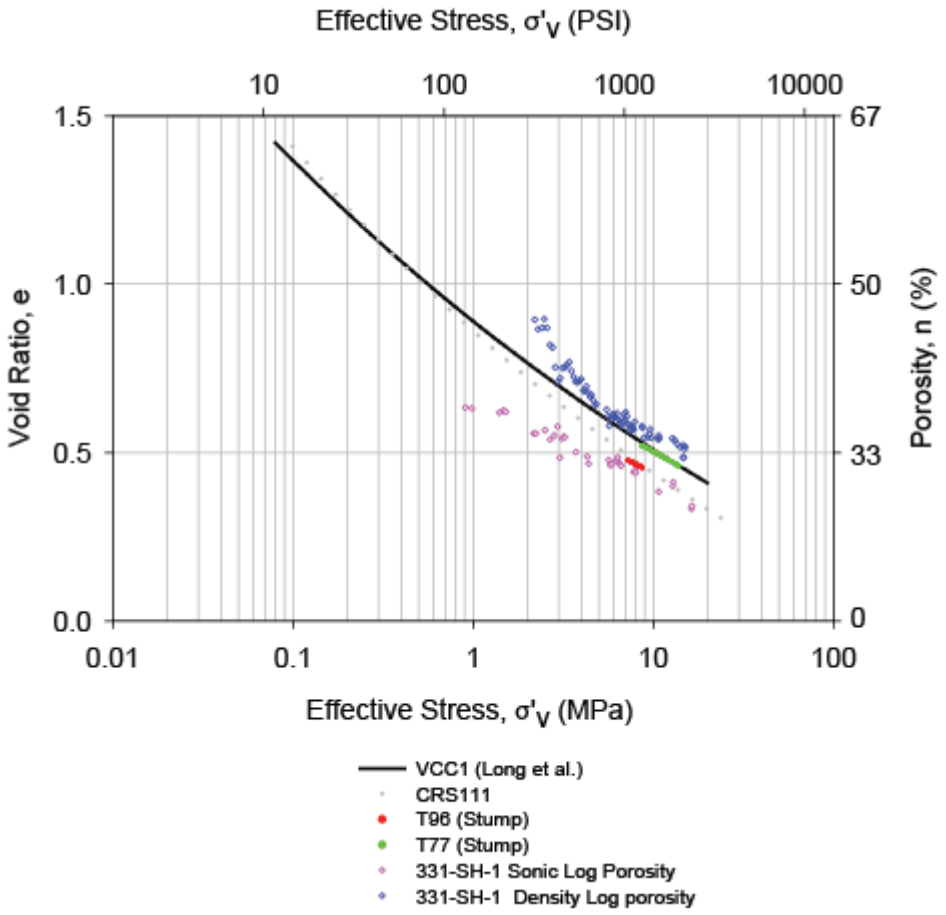

Figure 2.9: CRS 111 compared with intact core specimens tested by Stump & Flemings (2002). T77 was from the A-20 well at 2240 mbsf, and T96, a test performed on core taken from Block 316 well A-12 at 2039 mbsf. T96 has an experimentally derived preconsolidation pressure of 7.2 MPa. T77 has an experimentally derived preconsolidation pressure of 8.6 MPa. At a given void ratio, T77 supports approximately twice the effective stress of RGoM-EI (Figure 2.11).

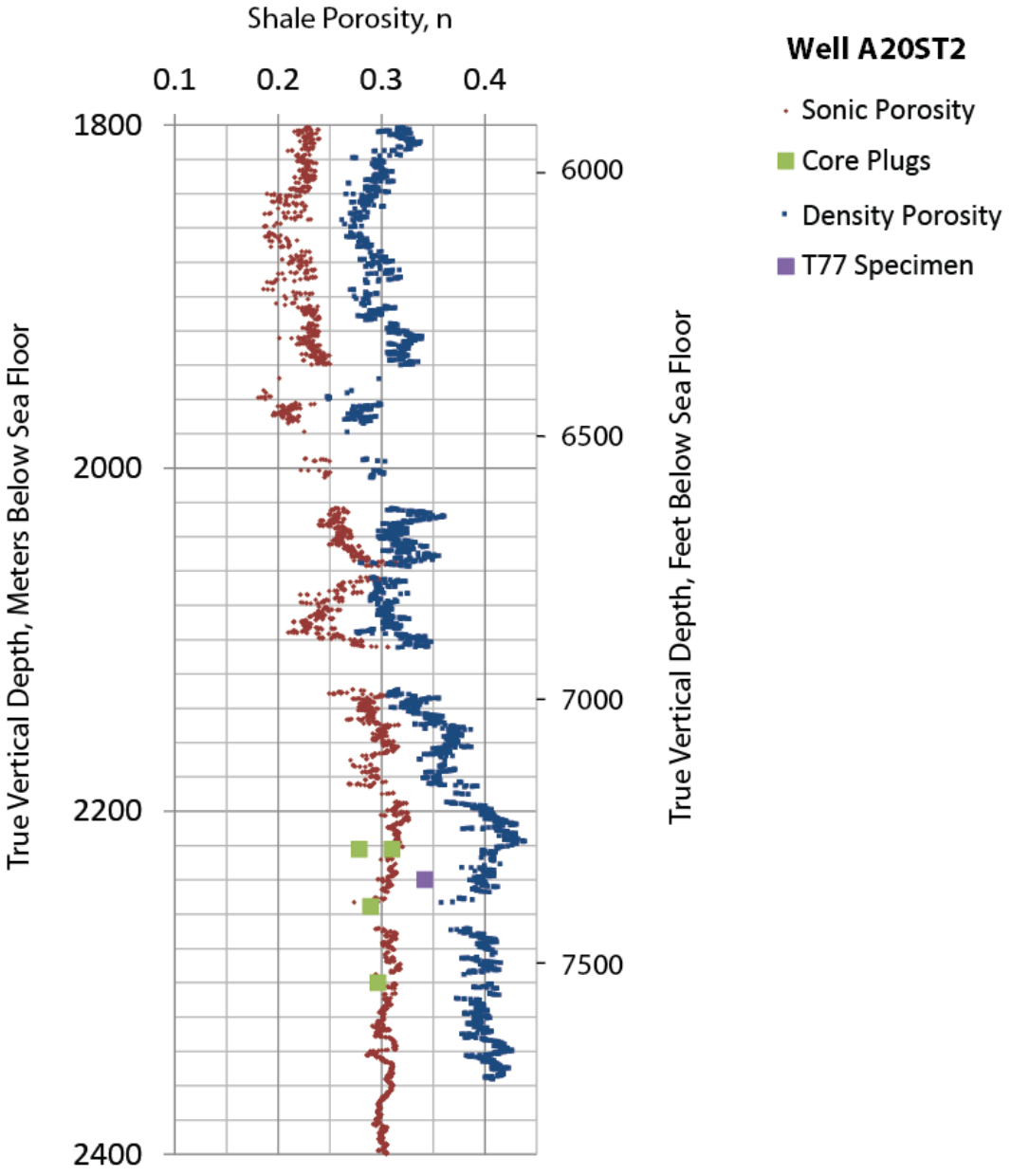

Figure 2.10: Porosity derived from velocity log (red) and bulk density log (blue) of the A-20ST2 well is compared with core plug porosities (green) and the porosity from intact core test T77 at its pre-consolidation stress. Density-derived porosities are approximately 10 units higher than sonic porosities in the overpressured zone.

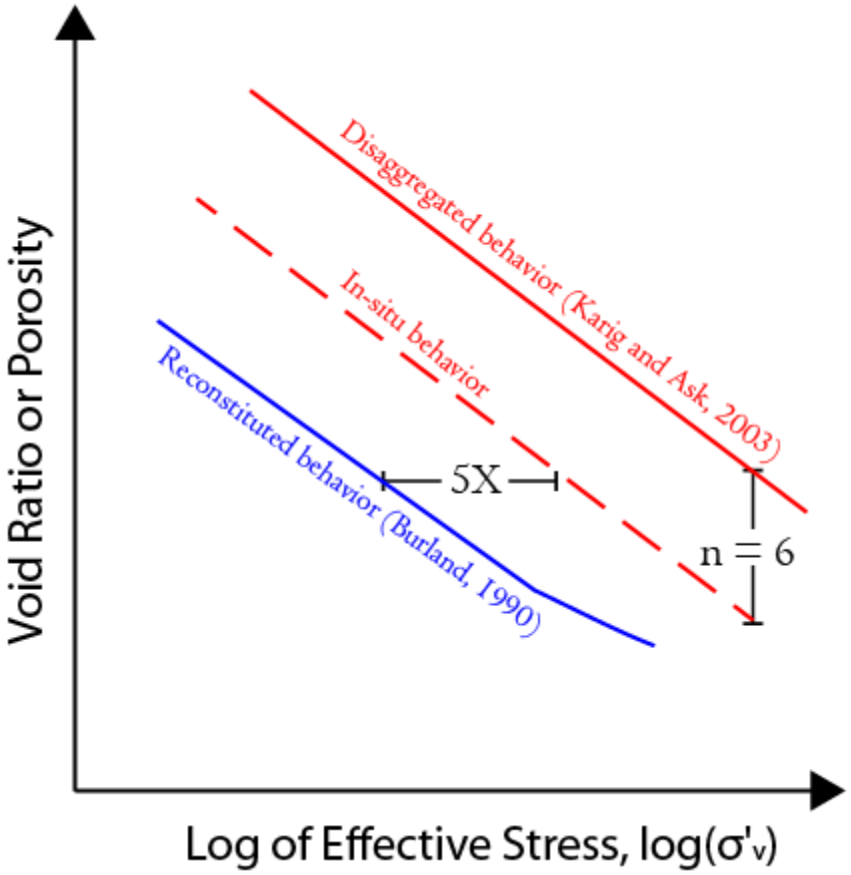

Figure 2.11: Conceptual relationship between in-situ clay behavior and that of laboratory-prepared (resedimented) specimens, showing range of possible behaviors for resedimented specimens compared to in-situ behavior.

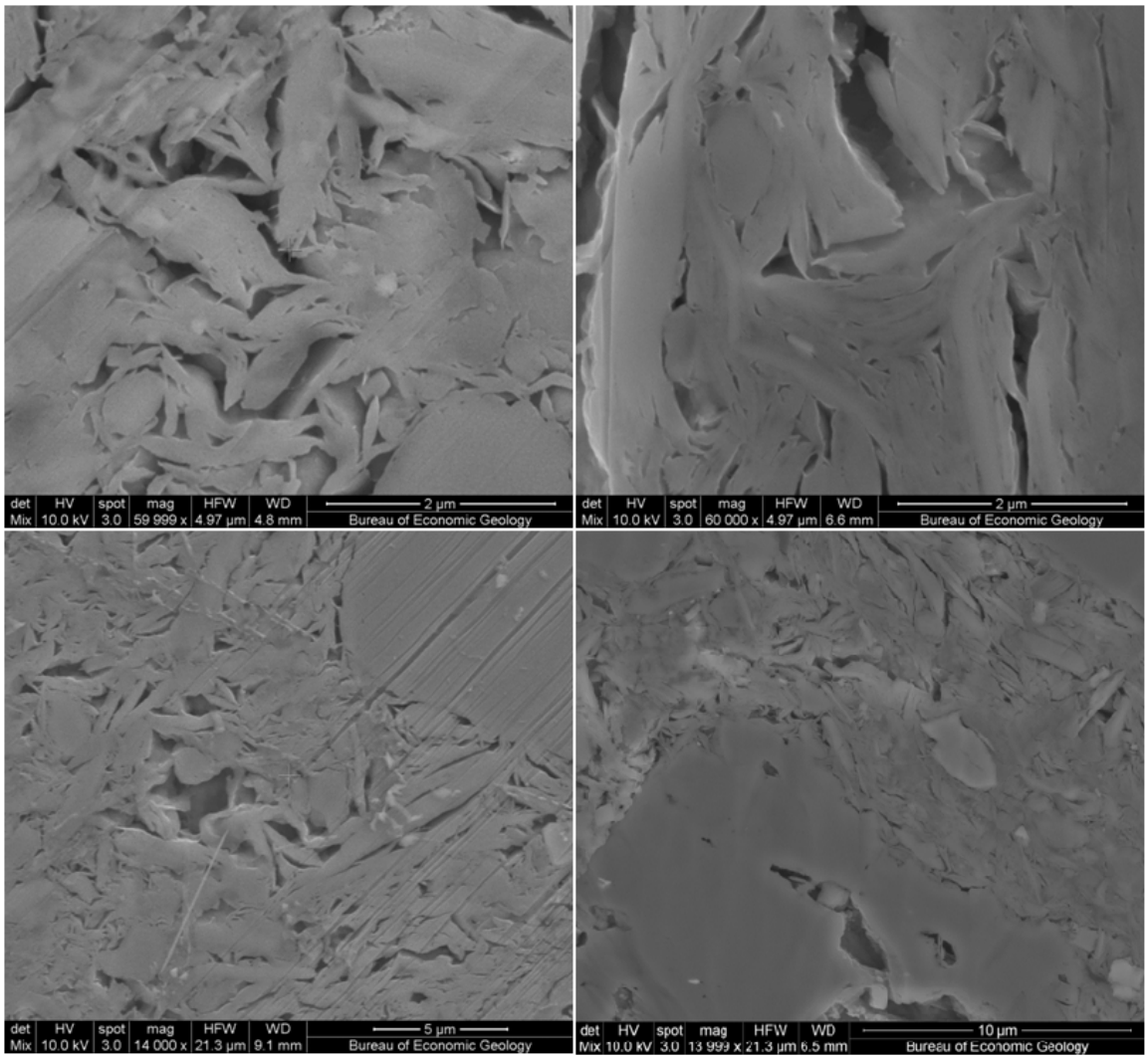

Figure 2.12: Scanning electron photomicrographs of intact pathfinder core and resedimented pathfinder core at a comparable stress (8.7 MPa). Left images are intact core, right images are resedimented specimen after CRS test. All images taken using mix of SE and BSE detectors.

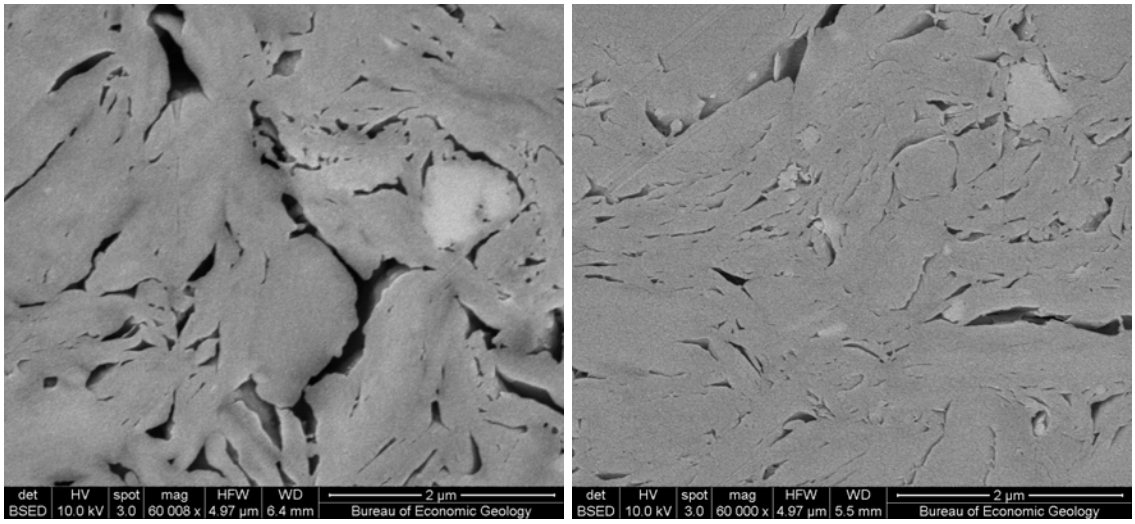

Figure 2.13: SEM Photomicrographs of RGoM-EI after compression to 100 kPa (left) and 20.4 MPa (right).

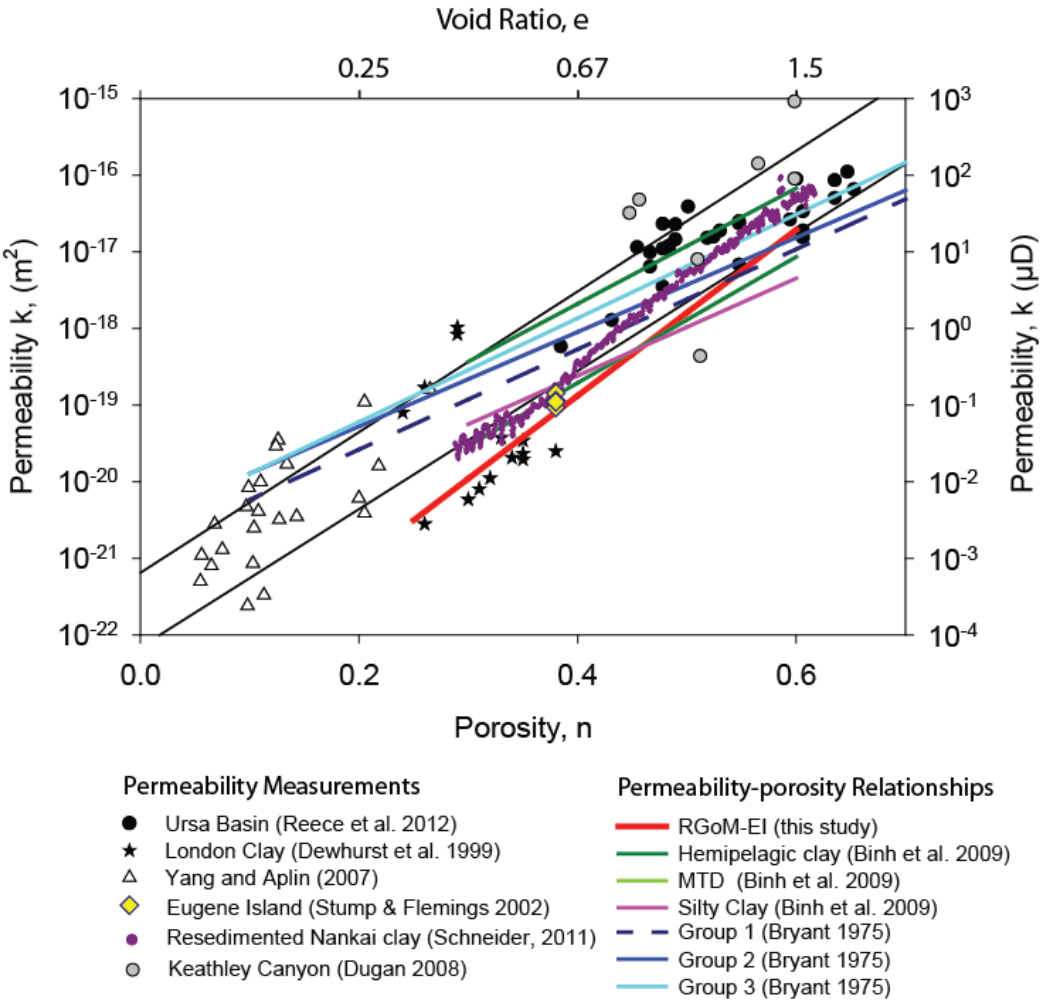

Figure 2.14: Permeability of RGoM-EI (red line) is compared with published measurements and permeability-porosity relationships for other marine mudrocks.

CONCLUSIONS

RGoM-EI, a homogenous bulk material made from mudrock from the Eugene Island Block 330 oilfield, exhibits properties similar to intact and in-situ Gulf of Mexico mudrocks when it is resedimented and used in consolidation experiments. The compression curves for resedimented Gulf of Mexico mudrock from the Eugene Island Block 330 oil field are obtained from CRS testing. Compression curves can be described with the expression $v = 1.85{\sigma'}_v^{-0.108}$. Field porosities derived from sonic velocity are lower than the resedimented material, while field porosities estimated from bulk density are higher. The well-log derived porosities bracket the CRS dataset, showing that it is a reasonable estimate of in-situ behavior. Likewise, the compression curves obtained from intact core samples resemble that of the resedimented material in both local slope (C_c) and absolute value, suggesting that compression behavior for RGoM-EI is similar to that occurring in the field. Additionally, a general agreement between the compression behavior of RGoM-EI and that of intact core from the Ursa basin suggests that RGoM-EI may be a useful analogue for other Gulf of Mexico mudrocks, even at relatively shallow depths and low stresses.

The permeability of the resedimented Gulf of Mexico mudrock can be described using the equation $\log_{10} k = 10.83n - 23.21$ for porosities between 62 and 27%. Permeability measured on resedimented specimens of Gulf of Mexico Mudrock at 38% porosity replicate the results of previous tests on the intact core of 1.15 x 10^{-19} m^2 (1.17 x 10^{-4} mD) at comparable porosity. Permeability also falls within, although near the low end of the range of previously published measurements and models of marine mudrock permeability. SEM photomicrographs of intact and resedimented mudrocks show fabric similarities including anisotropy and edge-to-face clay contacts.

The similarities between intact core and resedimented behavior suggest that resedimentation can replicate the structure formed in natural deposits, and show that resedimentation is a promising tool for understanding and predicting the compression and permeability of mudrocks in the Gulf of Mexico.

References

Adams, A.L., 2011, Laboratory evaluation of the constant rate of strain and constant head techniques for measurement of the hydraulic conductivity of fine grained soils Cambridge, MA, Massachusetts Institute of Technology.

Alexander, L.L., and Flemings, P.B., 1995, Geologic Evolution of a Pliocene-Pleistocene Salt-Withdrawal Minibasin: Eugene Island Block 330, Offshore Louisiana: AAPG Bulletin, v. 79, p. 1737-1756.

Allen, D.F., Best, D.L., Evans, M., and Holenka, J.M., 1993, The effect ot wellbore condition on wireline and MWD neutron density logs. : SPE Formation Evaluation, v. 8, p. 50-56.

Aplin, A.C., Matenaar, I.F., McCarty, D.K., and van der Pluijm, B.A., 2006, Influence of mechanical compaction and clay mineral diagenesis on the microfabric and pore-scale properties of deep-water Gulf of Mexico mudstones: Clays and Clay Minerals, v. 54, p. 500-514.

Aplin, A.C., Yang, Y.L., and Hansen, S., 1995, Assessment of beta, the compression coefficient of mudstones and its relationship with detailed lithology: Marine and Petroleum Geology, v. 12, p. 955-963.

ASTM, 2005a, Standard Test Methods for Laboratory Determination of Water (Moisture) Content of Soil and Rock by Mass, *in* International, A., ed., D 2216-05: West Conshohocken, PA, p. 7.

ASTM, 2005b, Standard Test Methods for Liquid Limit, Plastic Limit, and Plasticity Index of Soils, *in* International, A., ed., D 4318-05: West Conshohocken, PA, p. 16.

ASTM, 2006a, Standard test method for one-dimensional consolidation properties of saturated cohesive soils using controlled-strain loading (Standard D4186-06), *in* 04.08), A.B.o.A.S.V., ed., Soil and Rock (I): West Conshohocken, PA, American Society for Testing and Materials, p. 15.

ASTM, 2006b, Standard Test Methods for Specific Gravity of Soil Solids by Water Pycnometer, *in* International, A., ed., D 854-06: West Conshohocken, PA, p. 7.

ASTM, 2007, Standard D422, Standard Test Method for Particle-Size Analysis of Soils: West Conshohocken, PA.

Audet, D.M., 1996, Compaction and Overpressuring in Pleistocene Sediments on the Louisiana Shelf, Gulf of Mexico: Marine and Petroleum Geology, v. 13, p. 467-474.

Binh, N.T.T., Tokunaga, T., Nakamura, T., Kozumi, K., Nakajima, M., Kubota, M., Kameya, H., and Taniue, M., 2009, Physical properties of the shallow sediments in late Pleistocene formations, Ursa Basin, Gulf of Mexico, and their implications for generatino and preservation of shallow overpressures.: Marine and Petroleum Geology.

Braunsdorf, N., and Kittridge, M., 2003, Overburden pressure estimation in deepwater settings, PSU Geofluids consortium meeting,: Santa Cruz, CA.

Bryant, W.R., Hottman, W., and Trabant, P., 1975, Permeability of Unconsolidated and Consolidated Marine Sediments, Gulf of Mexico: Marine Geotechnology, v. 1, p. 1-14.

Bryant, W.R., Wetzel, A., and Sweet, W., 1986a, Geotechnical properties of intraslope basin sediments, Gulf of Mexico, Deep Sea Drilling Project leg 96, site 619, *in* Bouma, A.H., Coleman, J.M., and Meyer, A.W., eds., Init. Repts. DSDP, 96: Washington, U.S. Govt. Printing Office, p. 819-824.

Bryant, W.R., Wetzel, A., and Taylor, E., 1986b, Consolidation Characteristics and Permeability of Mississippi Fan Sediments, *in* Bouma, A.H., Coleman, J. M., Meyer, A. W., et al., , ed., Init. Repts. DSDP, 96: : Washington, DC U.S. Govt. Printing Office, p. 797-809.

Burland, J.B., 1990, On the compressibility and shear strength of natural clays: Geotechnique, v. 40, p. 329-378.

Butterfield, R., 1979, A natural compression law for soils (an advance on e-logp'): Geotechnique, v. 29, p. 469-480.

Carman, P.C., 1937, Flow through a granular bed: Trans. Inst. Chem. Eng. London, v. 15, p. 150-156.

Casagrande, A., 1936, The determination of the pre-consolidation load and its practical significance, *in* Casagrande, A., Rutledge, P.C., and Watson, J.D., eds., Proceedings of the 1st International Conference on Soil Mechanics and Foundation Engineering, Volume 3, American Society of Civil Engineers, p. 60-64.

Dewhurst, D.N., Aplin, A.C., and Sarda, J.P., 1999, Influence of clay fraction on pore-scale properties and hydraulic conductivity of experimentally compacted mudstones: Journal of Geophysical Research, v. 104, p. 29261-29274.

Dewhurst, D.N., Aplin, A.C., Sarda, J.P., and Yang, Y.L., 1998, Compaction-driven evolution of porosity and permeability in natural mudstones: An experimental study: Journal of Geophysical Research, v. 103, p. 651-661.

Dugan, B., 2008, Fluid flow in the Keathley Canyon 151 Mini-Basin, northern Gulf of Mexico: Marine and Petroleum Geology, v. 25, p. 919-923.

Dugan, B., and Flemings, P.B., 2000, Overpressure and Fluid Flow in the New Jersey Continental Slope: Implications for Slope Failure and Cold Seeps: Science, v. 289, p. 288-291.

Dugan, B., Flemings, P.B., Olgaard, D.L., and Gooch, M.J., 2003, Consolidation, effective stress, and fluid pressure of sediments from ODP Site 1073, US mid-Atlantic continental slope: Earth and Planetary Science Letters, v. 215, p. 13-26.

Flemings, P.B., Stump, B.B., Finkbeiner, T., and Zoback, M., 2002, Flow focusing in overpressured sandstones: theory, observations, and applications: American Journal of Science, v. 302, p. 827-855.

Gordon, D.S., and Flemings, P.B., 1998, Generation of overpressure and compaction-driven fluid flow in a Plio-Pleistocene growth-faulted basin, Eugene Island 330, offshore Louisiana: Basin Research, v. 10, p. 177-196.

Hart, B.S., Flemings, P.B., and Deshpande, A., 1995, Porosity and Pressure - Role of Compaction Disequilibrium in the Development of Geopressures in a Gulf-Coast Pleistocene Basin: Geology, v. 23, p. 45-48.

Issler, D.R., 1992, A new approach to shale compaction and stratigraphic restoration, Beaufort-Mackenzie Basin and Mackenzie Corridor, northern Canada: American Association of Petroleum Geologist Bulletin, v. 76, p. 1170-1189.

Karig, D.E., and Ask, M.V.S., 2003, Geological perspectives on consolidation of clay-rich marine sediments: J. Geophs. Res., v. 108, p. 2197.

Karig, D.E., and Hou, G., 1992, High-Stress Consolidation Experiments and Their Geologic Implications: J. Geophys. Res, v. 97, p. 289-300.

Karig, D.E., and Morgan, J., 1994, Tectonic deformation: stress paths and strain histories, *in* Maltman, A., ed., The geological deformation of sediments: New York, Chapman and Hall, p. 167-204.

Long, H., Flemings, P.B., Germaine, J.T., and Saffer, D.M., 2011, Consolidation and Overpressure near the seafloor in the Ursa Basin, Deepwater Gulf of Mexico: Earth and Planetary Science Letters, v. 305, p. 11-20.

Long, H., Flemings, P.B., Germaine, J.T., Saffer, D.M., and Dugan, B., 2008, Data report: consolidation characteristics of sediments from IODP Expedition 308, Ursa Basin, Gulf of Mexico, *in* Flemings, P.B., Behrmann, J.H., and John, C.M., eds., Proc. IODP, Volume 308: College Station, TX, Proc. IODP, Sci. Results, p. 47.

Losh, S., Eglinton, L., and Wood, J., 1994, Coring and Inorganic Geochemistry in the Pathfinder Well, Results of the Pathfinder drilling program into a major growth fault (CD-ROM): Palisades, NY, LDEO Press. Lamont Doherty Earth Observatory.

Losh, S., and Wood, J., 1995, Brine Chemistry, Blocks 330 and 316, Results of the Pathfinder drilling program into a major growth fault (CD-ROM): Palisades, NY, LDEO Press. Lamont Doherty Earth Observatory.

Mazzei, D.P.C., 2008, Normalized Mechanical Properties of Resedimented Gulf of Mexico Clay from Integrated Ocean Drilling Program Expedition Leg 308: Cambridge, Massachusetts Institute of Technology.

Mitchell, J.K., 1976, Fundamentals of Soil Behavior: New York, Wiley.

Mondol, N.H., Bjørlykke, K., and Jahren, J., 2008, Experimental compaction of clays: relationship between permeability and petrophysical properties in mudstones: Petroleum Geoscience, v. 14, p. 319-337.

Mondol, N.H., Bjorlykke, K., Jahren, J., and Hoeg, K., 2007, Experimental mechanical compaction of clay mineral aggregates - Changes in physical properties of mudstones during burial: Marine and Petroleum Geology, v. 24, p. 289-311.

Nelson, P. H. 1994, Permeability-porosity relationships in sedimentary rocks, Log Anal., 38– 62

Neuzil, C.E., 1994, How permeable are clays and shales?: Water Resources Research, v. 30, p. 145-150.

Phillips, I.M., 2011, Report on the Whole Rock and <2 Micron Clay Fraction Mineralogy of a Single Sample by X-Ray Powder Diffraction (XRPD): Craigiebuckler, Aberdeen, Scotland, Macaulay Scientific Consulting Ltd. .

Ransom, B., and Helgeson, H.C., 1989, On the correlation of expandability with mineralogy and layering in mixed-layer clays: Clays and Clay Minerals v. 37, p. 189-191.

Reece, J.S., Flemings, P.B., Dugan, B., Long, H., Germaine, J.T., 2012. Permeability-porosity relationships of shallow mudstones in the Ursa Basin, northern deepwater Gulf of Mexico. J. Geophs. Res. 117.

Rubey, W.W., and Hubbert, M.K., 1959, Overthrust belt in geosynclinal area of western Wyoming in light of fluid-pressure hypothesis, 2: Role of fluid pressure in mechanics of overthrust faulting: GSA Bulletin, v. 70, p. 167-205.

Saffer, D.M., and Bekins, B.A., 2006, An evaluation of factors influencing pore pressure in accretionary complexes: Implications for taper angle and wedge mechanics: Journal of Geophysical Research, v. 111.

Santagata, M.C., and Kang, Y.I., 2007, Effects of geologic time on the initial stiffness of clays: Engineering Geology, v. 89, p. 98-111.

Schneider, J., 2011, Compression and permeability behavior of natural mudstones: Thesis, The university of Texas at Austin, p. 302.

Schneider, J., Flemings, P.B., Day-Stirrat, R.J., and Germaine, J.T., 2011, Insights into pore-scale controls on mudstone permeability through resedimentation experiments: Geology, v. 39, p. 1011-1014.

Schowalter, T.T., 1979, Mechanics of secondary hydrocarbon migration and entrapment: AAPG Bulletin, v. 63, p. 723-760.

Sheahan, T.C., 1991, An experimental study of the time-dependent undrained shear behavior of resedimented clay using automated stress path triaxial equipment [Ph.D. thesis]: Cambridge, Massachusetts Institute of Technology.

Sheahan, T.C., and Watters, P.J., 1997, Experimental Verification of CRS Consolidation Theory: Journal of Geotechnical and Geoenvironmental Engineering, v. 123.

Skempton, A.W., 1970, The Consolidation of Clays by Gravitational Compaction: Quarterly Journal of the Geological Society of London, v. 125, p. 373-411.

Skempton, A.W., and Jones, O.T., 1944, Notes on the compressibility of clays: Quarterly Journal of the Geological Society of London, v. 100, p. 119-135.

Stump, B., and Flemings, P.B., 2002, Consolidation State, Permeability, and Stress Ratio as Determined from Uniaxial Strain Experiments on Mud Samples from the Eugene Island 330 Area, Offshore Louisiana,, *in* Huffman, A.R., Bowers, G.L. , ed., Pressure Regimes in Sedimentary Basins and Their Prediction, Volume AAPG Memoir 76, p. 131-144.

Stump, B.B., 1998, Illuminating basinal fluid flow in Eugene Island 330 (Gulf of Mexico) through in situ observations, deformation experiments, and hydrodynamic modeling [Masters Thesis thesis], The Pennsylvania State University.

Taylor, D.W., 1942, Research on Consolidation of Clays: Cambridge, MA, M.I.T. Department of Civil and Sanitary engineering, 143 p.

Terzaghi, K., 1941, Undisturbed clay samples and undisturbed clays: Journ. Boston Soc. C.E., v. 28, p. 211.

Van Paassen, L.A., and Gareau, L.F., 2004, Effect of Pore Fluid Salinity on Compressibility and Shear Strength Development of Clayey Soils Lecture Notes in Earth Sciences, v. 104, p. 327-340.

Wissa, A.E.Z., Christian, J.T., Davis, E.H., and Heiberg, S., 1971, Consolidation at constant rate of strain: Journal of the Soil Mechanics and Foundations Division, v. 97, p. 1393-1413.

Yang, Y.L., and Aplin, A.C., 2007, Permeability and petrophysical properties of 30 natural mudstones: Journal of Geophysical Research, v. 112.

Appendix A: Physical characterization of RGoM-EI, Resedimented Gulf of Mexico Mudrock from the Eugene Island Block 330 Oil Field.

MINERALOGY

A subsample of RGoM-EI was taken from an oven-dried CRS test specimen (CRS097) and sent to Macaulay Scientific Consulting, LTD in Craigiebuckler, Aberdeen, Scotland for X-Ray Powder Diffraction (XRPD) analysis. Procedure was as follows (Phillips, 2011):

> The bulk sample was wet ground (in ethanol) in a McCrone mill and spray dried to produce a random powder. The X-ray powder diffraction (XRPD) pattern was recorded from 2-75°2θ using Cobalt Kα radiation. Quantitative analysis was done by a normalised full pattern reference intensity ratio (RIR) method.
>
> A clay fraction of <2μm was obtained by timed sedimentation, prepared as an oriented mount using the filter peel transfer technique and scanned from 2-45°2θ in the air-dried state, after glycolation, and after heating to 300°C for one hour. Clay minerals identified were quantified using a mineral intensity factor approach based on calculated XRPD patterns.

XRPD results for bulk powder are given in Table A.1 and for clay minerals in the <2μm size fraction in Table A.2. The major components of the bulk sample were quartz (27.8%) and illite + illite/smectite (44.4%). Smaller amounts of kaolinite, plagioclase, K-feldspar, barite, muscovite calcite and siderite were also detected. Trace minerals identified included dolomite, pyrite, anatase, halite and chlorite. Identification of the trace mineral phases is subject to some uncertainty, and some of the trace phases identified may not actually be present (Phillips, 2011) The barite is believed to represent a contribution from drilling mud.

The clay-size fraction consisted primarily of Illite + Smectite of 70-80% expandability.

GRAIN SIZE

A sedimentation process (ASTM, 2007) was used to measure the size distribution of the particles. Four 50g samples were taken from the homogenized, processed powder prior to resedimentation. Material was blended in a mechanical stirring cup with water and 5 grams of sodium hexametaphosphate, a dispersing agent, to separate the particles. The slurry was then placed in a graduated cylinder, and a hydrometer was used to periodically measure the density of the suspension. The percent of mass remaining in suspension after each reading was determined from the density of the slurry, and effective particle diameters were calculated based on the settling times according to Stokes' law. Results of the grain size analysis for each of four repeat trials are shown in Figure A.3. Fractions of silt-size particles (greater than 2 μm) and clay-size particles (less than 2 μm) are given in Table A.3. Sedimentation experiments were conducted by Julia S. Reece.

ATTERBERG LIMITS

The physical behavior of a soil varies with its water content. The Atterberg limits measure the variance of the behavior of a soil over a range of water contents, from solid to fluid, using simple empirical tests which were developed by Atterberg (1911) and refined by Casagrande (1932). In contemporary geotechnical engineering practice, the most important of the Atterberg limits are the liquid limit and the plastic limit, which are index values used in the classification of soils (Germaine and Germaine, 2009). The liquid limit represents the water content at the transition between plastic and fluid behavior and the plastic limit represents the water content at the transition between solid and plastic behavior. The difference between these two values is known as the Plasticity Index, which along with the liquid limit itself and the grain size distribution, are used to classify soils for engineering purposes (ASTM, 2006a).

The liquid limit was measured using a Casagrande cup and with a grooving tool and the multipoint method (ASTM, 2006a). The test is designed to simulate a slope failing and measure how much energy is required to cause the slope to fail. The Casagrande cup is a device calibrated to deliver a certain amount of force to the soil each time a crank is turned. A slope of specified dimensions is created by placing a pat of soil mixed with distilled water in the cup and then using the grooving tool to carve a groove in it. The liquid limit is the water content at which the slope fails and the groove closes by 13 mm (1/2 in) after delivering 25 blows to the cup. The multipoint method which was used requires counting the number of blows required to close the groove at several different consistencies, graphing the results in water content/number of blows space, and then using the linear relationship obtained to predict the water content at 25 blows.

The plastic limit is defined as the water content in percent, rounded to the nearest whole number, at which a thread of the soil-water mixture crumbles at a diameter of 3.2 mm (1/8 in). It was obtained by pressing and rolling a thread of moist soil against a glass plate. As the soil dries out, it reaches a point where it can no longer be rolled to less than the specified diameter without crumbling. The water content of the material is then taken.

Values for liquid limit and plastic limit were found to be 87 and 24, respectively, resulting in a plasticity index of 63. Figure A.4 shows a Casagrande Plasticity chart as used in the Unified Soil Classification (ASTM, 2006a). RGoM-EI is classified in the category designated CH, called a high-plasticity clay or “Fat Clay”, based on the position at which it plots on the chart.

Labcode	**1079708**
Sample ID	**CRS-097-B**
Quartz	27.8
Plagioclase	5.3
K-Feldspar	4.0
Calcite	1.2
Dolomite	0.8
Siderite	1.0
Pyrite	0.7
Anatase	0.2
Barite	3.2
Halite	0.2
Muscovite	1.9
Illite + I/S	44.4
Kaolinite	9.1
Chlorite	0.4
Total	100.2

Table A.1: Bulk mineralogy (weight %) by RIR method, from Phillips (2011).

Labcode	**1079708**
Sample ID	**CRS-097-B**
Chlorite	1
Kaolinite	4
Illite	8
Illite-Smectite	87
% exp	70-80

Table A.2: Relative percentage of clay minerals in the <2μm clay size fraction, from Phillips (2011).

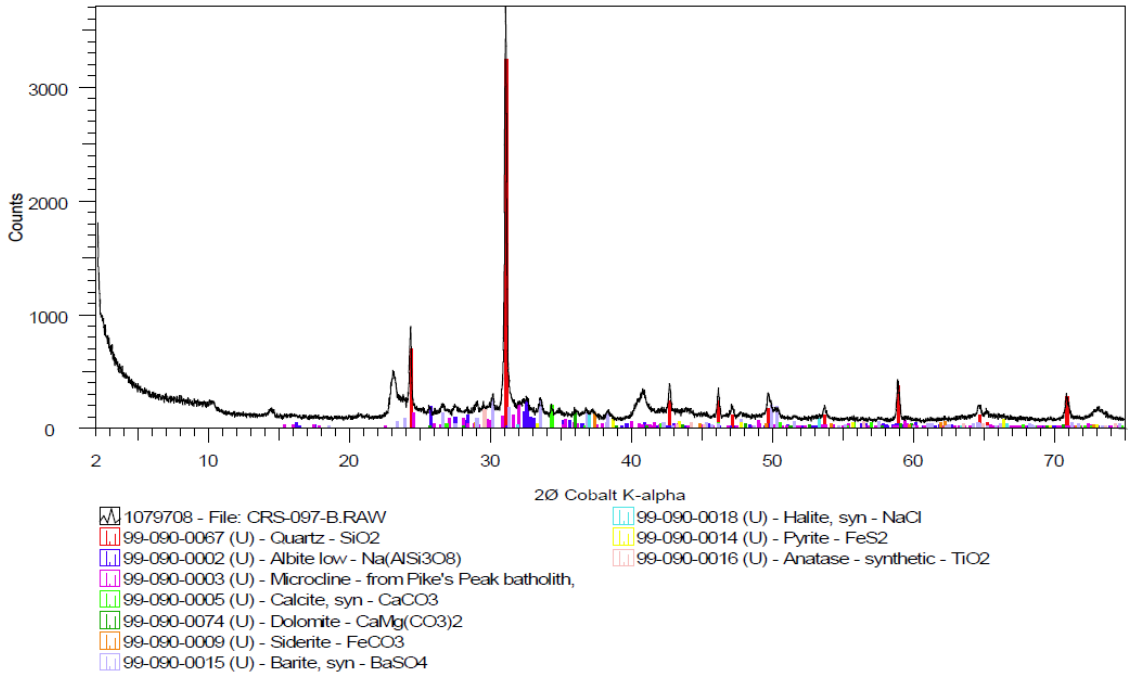

Figure A.1: Whole-sample XRPD pattern with the main phases identified by reference to patterns from the International Centre for Diffraction Database, from Phillips (2011).

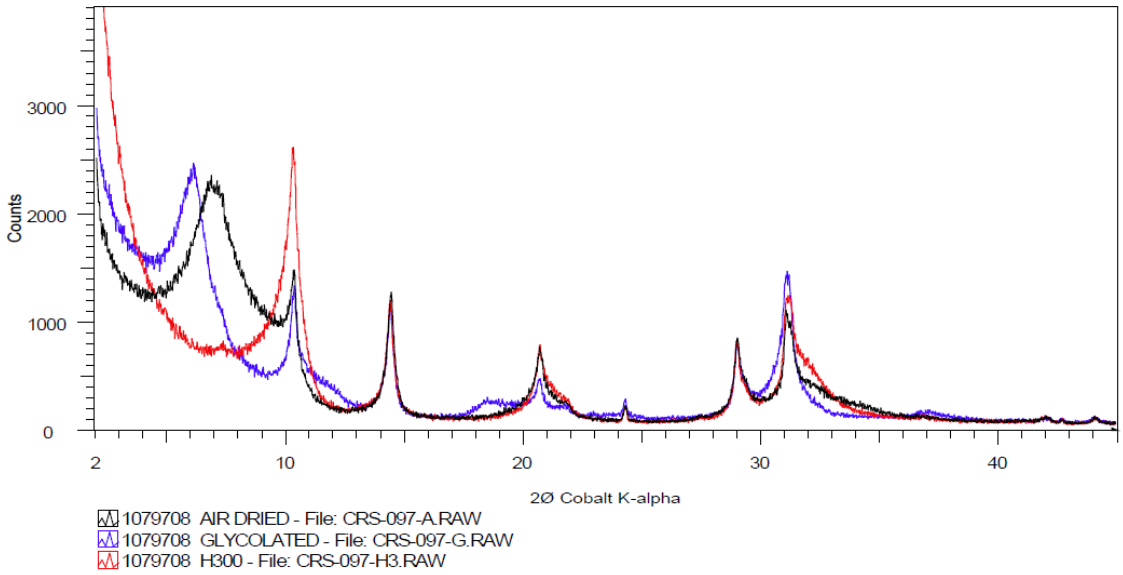

Figure A.2: Clay-size fraction XRPD pattern.

	Silt size (>2 μm)	Clay Size (<2 μm)
GS129	35.0	65.0
GS130	38.4	61.6
GS131	37.8	62.2
GS132	39.4	60.6
Average	37.6	62.4

Table A.3: Silt and clay-size fractions determined by four trials of grain size analysis.

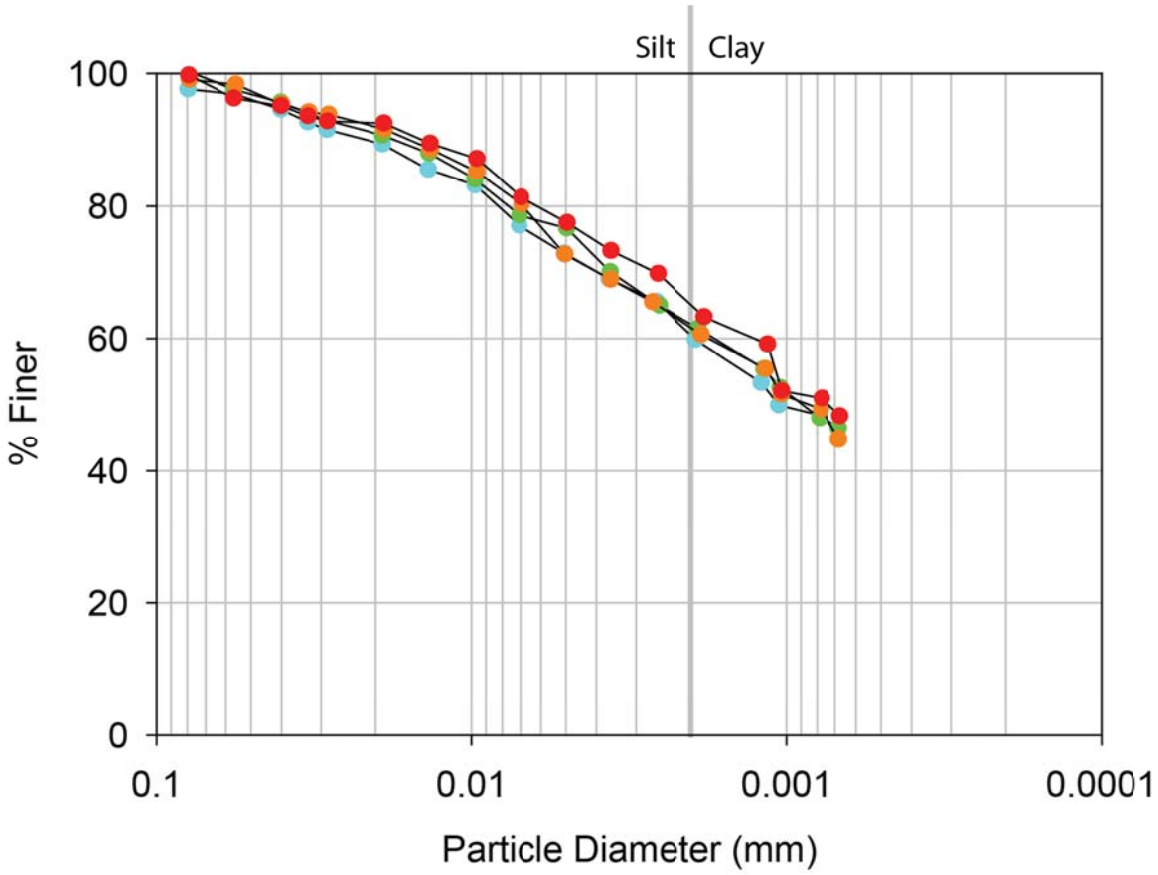

Figure A.3: Grain size distributions of RGoM-EI obtained from four sedimentation analyses.

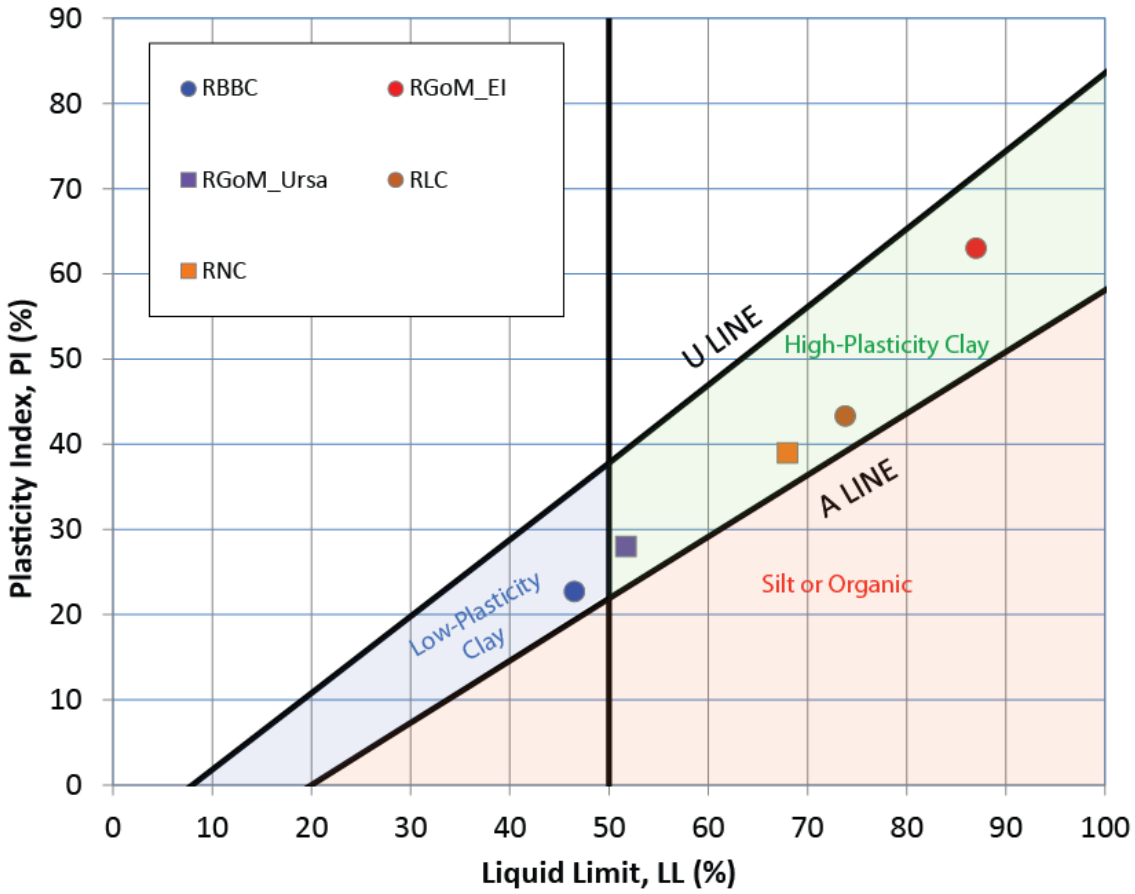

Figure A.4: Casagrande plasticity chart used in the Unified Soil Classification system. Based on its Atterberg limits, RGoM-EI plots as a high plasticity or "fat" clay, CH in the Unified Soil Classifications system. Also included for comparison are Boston Blue Clay (RBBC), Ursa Basin sediment (RGoM_Ursa), London Clay (RLC) and Nankai Clay (RNC). RGoM-EI has the highest liquid limit and the highest plasticity index of any of these.

Appendix B: Resedimentation of Gulf of Mexico mudrock from Eugene Island Block 330 oilfield, Offshore Louisiana (RGoM-EI)

INTRODUCTION

I used the resedimentation method to prepare samples of Gulf of Mexico Mudrock from the Eugene Island Block 330 oilfield for consolidation testing. Resedimentation is a process developed at MIT for preparing specimens with minimal spatial variability and a known uniaxial stress history (Sheahan, 1991).

During resedimentation, mechanically disaggregated mudrock specimens are mixed at a water content greater than the liquid limit, subjected to a vacuum to remove air bubbles, and then uniaxially consolidated. (Mazzei, 2008; Schneider, 2011; Sheahan, 1991). The resedimentation procedure and equipment have evolved over the years. The procedures used in this study most closely resemble those described by Mazzei (Mazzei, 2008) and Schneider (Schneider, 2011). The most-studied resedimented mudrock is resedimented Boston Blue Clay (Abdulhadi, 2009; Force, 1998; Gonzalez, 2000; House, 2012; Sheahan, 1991). In recent years, resedimentation has also been used to study other mudrocks from around the world, including kaolinite (Gao, 2013), Gulf of Mexico mudrock from the Ursa Basin (Mazzei, 2008), and mudrocks from offshore Japan (Schneider, 2011).

The preparation of resedimented mudrocks is similar, although not identical, to that of reconstituted mudrocks. Reconstituted, as defined by Burland (1990), refers to a state in which the material has been thoroughly mixed at a water content equal to or greater than the liquid limit. More specifically, clays reconstituted at a water content of between 1 and 1.5x the liquid limit, “without air drying or oven drying, and then consolidated, preferably under one-dimensional conditions.” are said to display the

intrinsic properties of the mudrock (Burland, 1990). Reconstituted mudrocks have also been studied by Karig and Hou (1992), and Mondol et al. (2007).

METHODS

Specimens were resedimented at a water content of 112%. For resedimentation to be successful, the slurry must have a sufficiently low viscosity to be effectively poured and flow through a relatively small diameter tube and then to evenly fill the consolidometer column. However, slurries containing too much water are unstable as particles may settle out and segregate according to grain size, resulting in a non-homogeneous specimen. Since RGoM-EI was a new material that had not been previously resedimented, the optimal water content was found experimentally by mixing small amounts of soil with saltwater in a series of test tubes encompassing a range of water contents. Test tubes were covered and allowed to sit for 24 hours, after which clear water had appeared above the slurry in all tests at a water content of above 112%. This separation of clear water indicates that settling and possibly particle segregation had occurred.

In order to simulate in-situ conditions, sea salt was added to all water used in the test tube tests and the resedimentation tests.

Appendix C: Data Report, Constant Rate of Strain Consolidation tests of resedimented Gulf of Mexico Mudrock from Eugene Island Block 330 Oil Field, offshore Louisiana.

TEST CONDITIONS

Strain rate, excess pore pressure, and pore pressure ratio.

Strain rates ranged from 0.35 to 0.075 %/hr and were chosen to maintain a pore pressure ratio below 0.15 (15%). Pore pressure ratio, defined as the ratio of excess pore pressure to total vertical stress, should be between 3 and 15% at the end of the loading phase (ASTM, 2006b). Pore pressure ratios generally increase monotonically during loading at a constant rate of strain. UT geomechanics lab procedure is to attempt to establish pore pressure ratios between 2 and 5% in the early stages of the testing. Previous unpublished tests of RGoM-EI conducted by the author at higher strain rates established a pore pressure ratio between 2 and 5 shortly after the start of consolidation, but the test results were affected by leaks which developed in the system and in some cases the extrusion of a portion of specimen. In order to reduce the risk of leak CRS107, 109, 110 and 111, starting strain rates of 0.3 to 0.35 were used and the strain rate was reduced during the test whenever the absolute pore pressure approached 140 PSI (965 kPa). These rate reductions, which are allowable under ASTM D 4186, also had the effect of temporarily reducing the pore pressure ratio. Pore pressure ratios throughout all tests are plotted in figures C.1-C.4, with the dips in pore pressure correspond to the strain rate reductions. During the creep phase of the test, pore pressure ratio gradually reduces at a constant effective stress, and negative pore pressure ratios occur during unloading.

Figures C.1-C.4 show test conditions and parameters for the four CRS tests of RGoM-EI. Compression curves are presented in terms of both void ratio and strain versus the logarithm of vertical effective stress. The strain energy method was used to determine preconsolidation pressure (Becker et al., 1987) and strain energy density (SED plots are also shown for all four tests. As expected, all tests had a preconsolidation pressure near 100 kPa. The coefficient of consolidation (c_v) and permeability data are also included in these figures.

Data Editing

According to procedure, all transducers were zeroed after the specimen was first placed in the chamber and the chamber placed in the load frame. Pore and cell pressure transducers then read zero at atmospheric pressure. After the chamber was pressurized to 56 PSI, in all tests the base and cell pressure transducers were found to give slightly different readings, even when the valve separating the base from the rest of the chamber was open. While barely noticeable in graphs of absolute pressure, this offset, likely due to nonlinearity of the calibration factor, resulted in erroneous effective stress readings and biased measurements in the initial phases of the test, resulting in apparent yield stresses (sometimes called "preconsolidation stresses") that were lower than the actual preconsolidation stresses of the resedimented specimens. This problem was solved by adjusting the zero values of one of the transducers by a small amount so that the pressure readings of the two transducers were equal in the backpressure stage of the test (occurring at 56 PSI with the valves open).

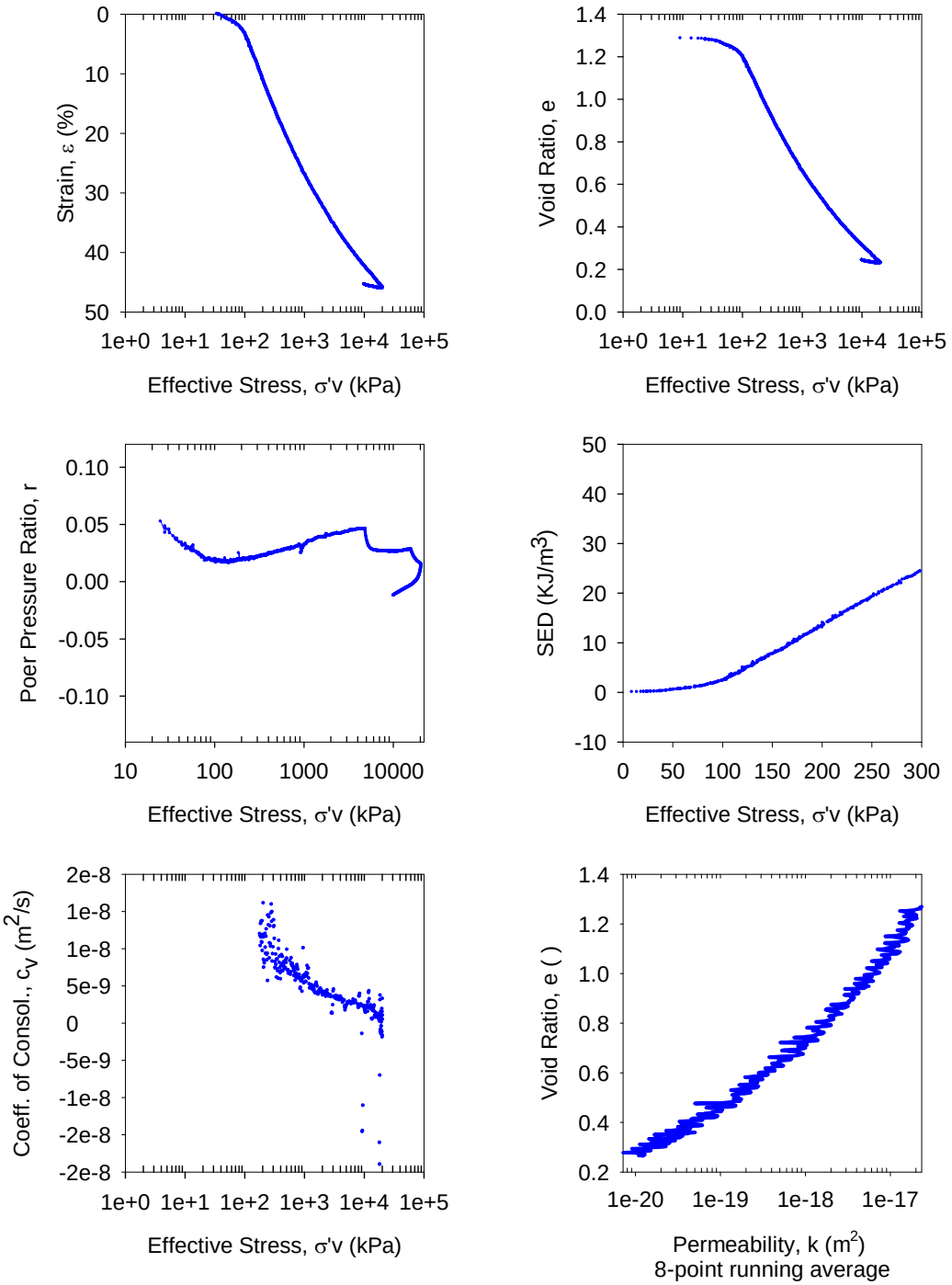

Figure C.1: CRS107 test results and conditions.

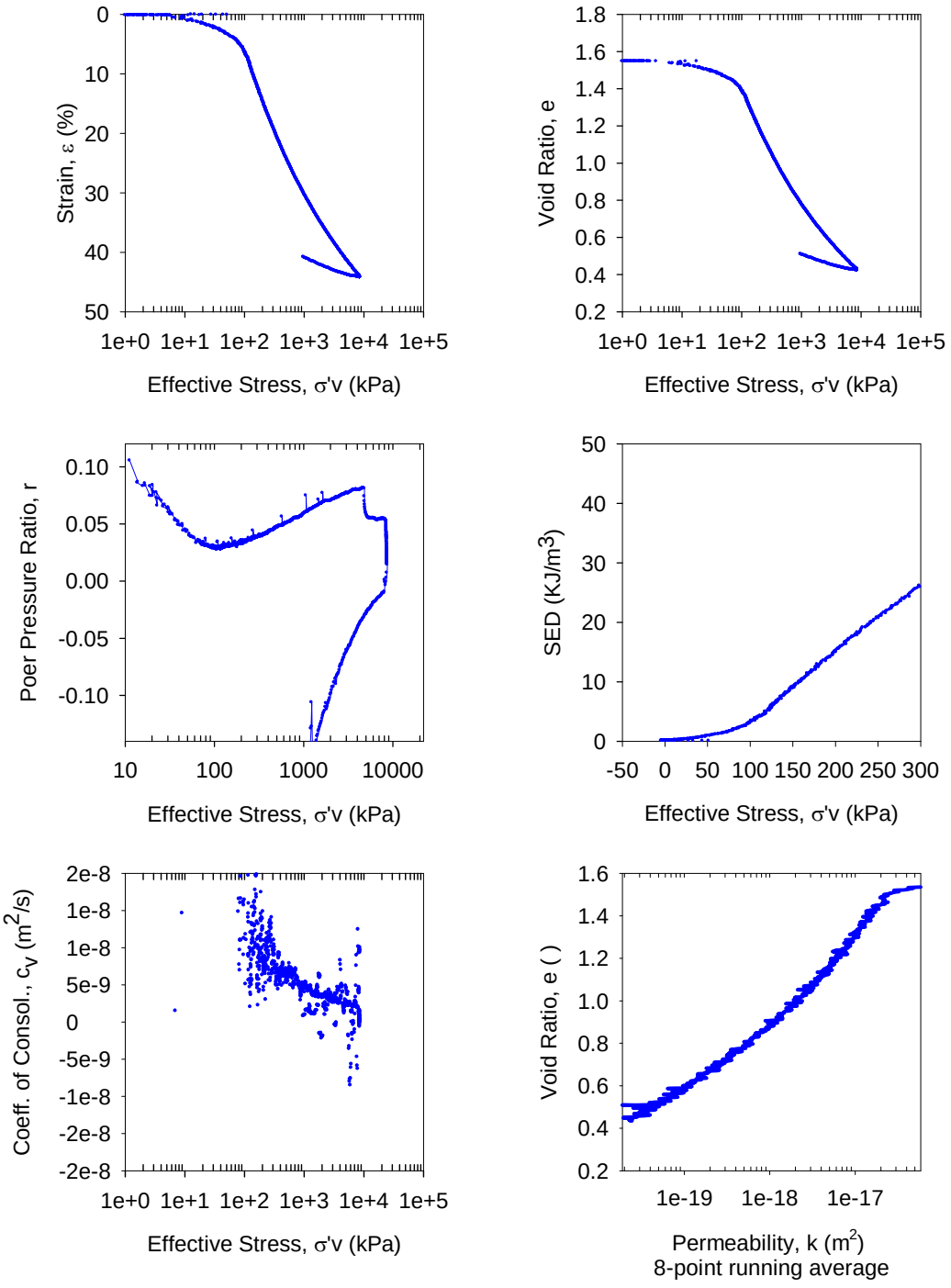

Figure C.2: CRS109 test results and conditions.

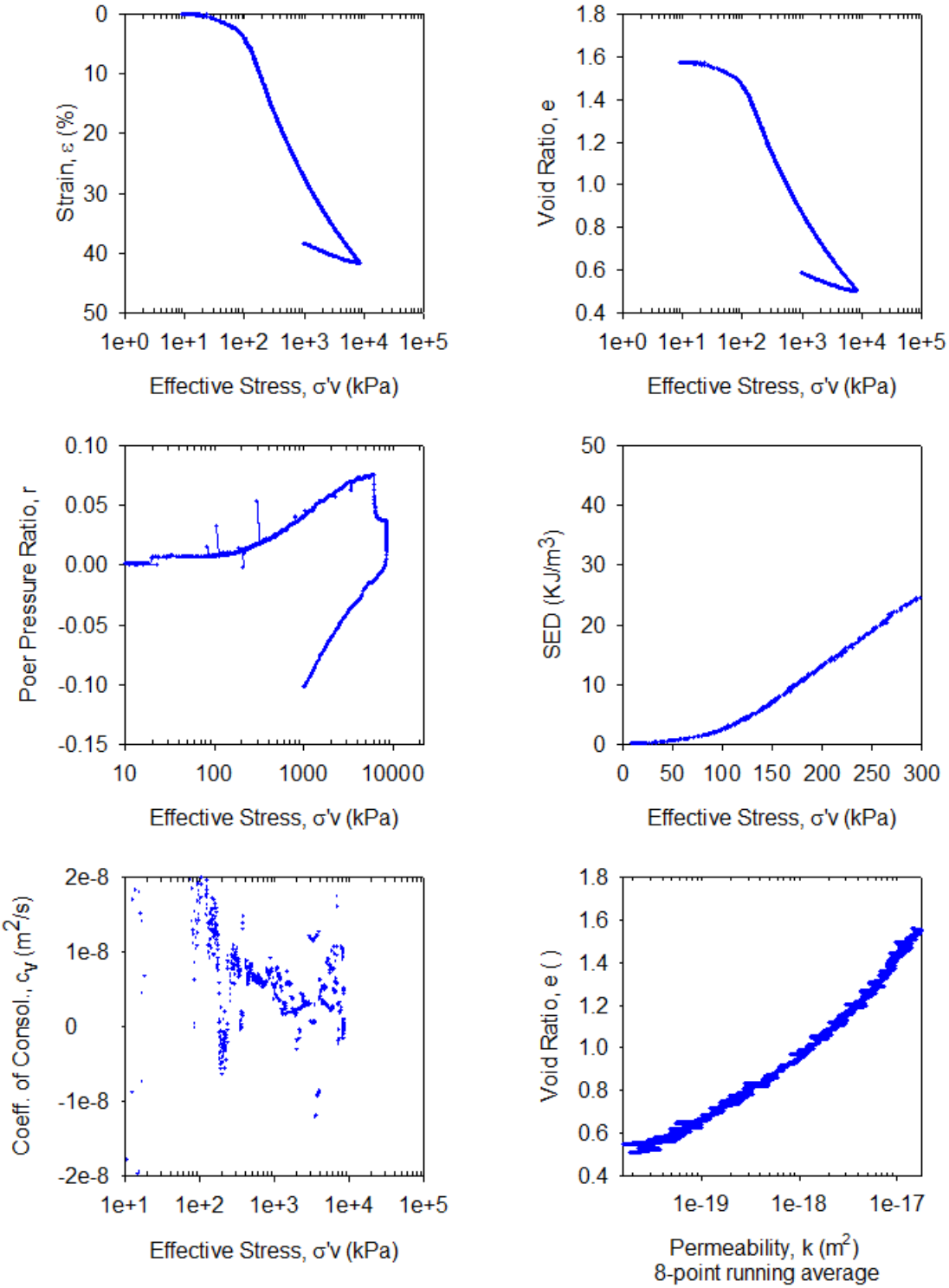

Figure C.3: CRS110 test results and conditions.

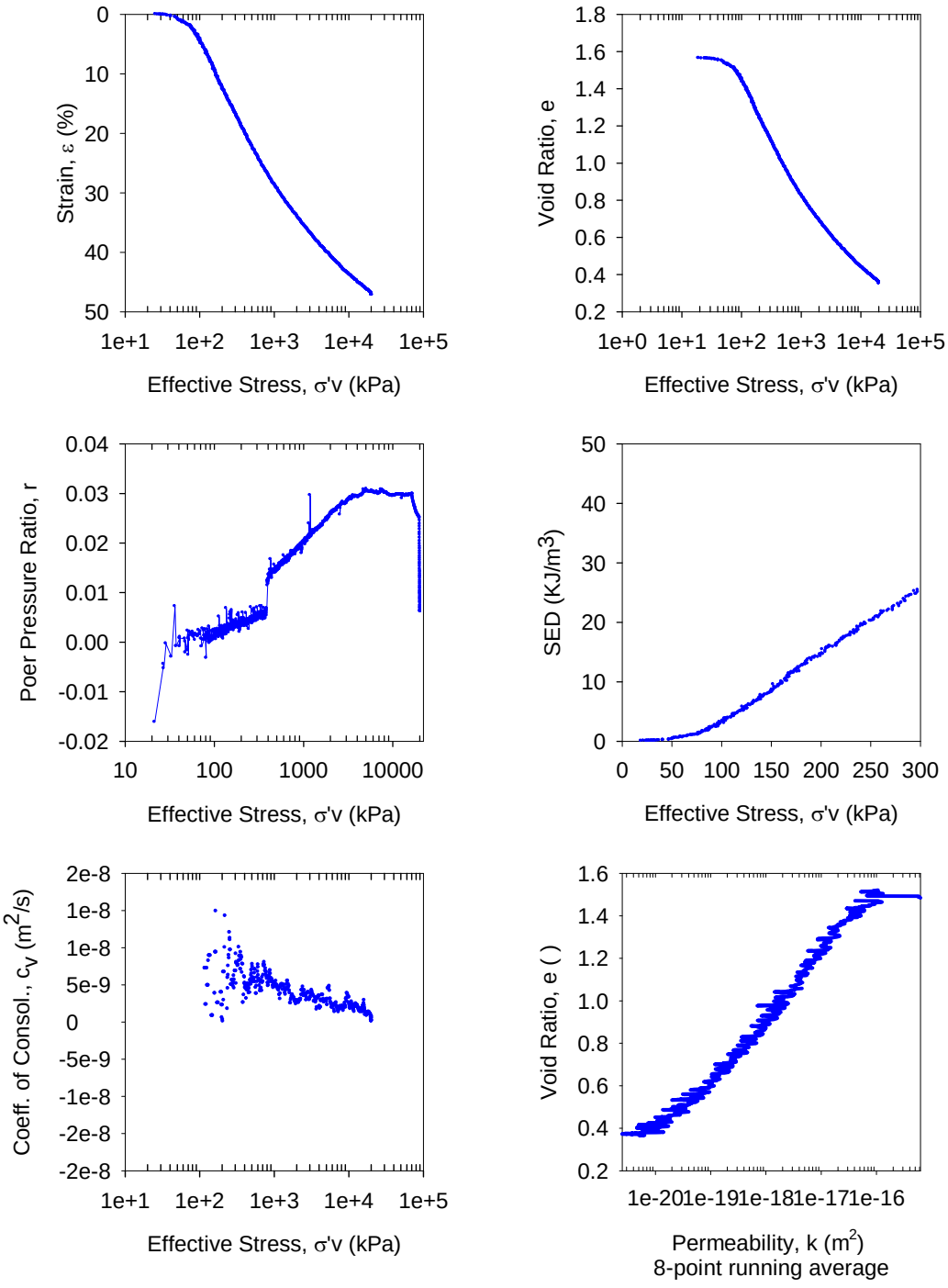

Figure C.4: CRS111 test results and conditions.

Appendix D: SEM Imaging of intact and resedimented mudrocks from the Eugene Island Block 330 Oilfield, Offshore Louisiana, Gulf of Mexico.

INTRODUCTION

We used scanning electron microscopy (SEM) to image specimens of resedimented mudrock from the Eugene Island block 330 oilfield, offshore Louisiana, in addition to a specimen taken from intact core from well 330 A-20. The intact specimen had experienced a maximum past effective stress of 7 to 8 MPa (Hart et al., 1995), while the resedimented specimens had been subjected to maximum stresses of 100 kPa, 8 MPa, and 20 MPa in the laboratory.

METHODS

Preparation

Specimens were prepared for imaging using the argon-ion milling technique (Loucks et al., 2009). Each specimen consisted of a cube of oven-dried material with dimensions of approximately 5x11x17 mm. Each cube was placed in a Leica EM TIC020 argon beam ion mill, which ablated a small area of a surface perpendicular to the bedding. The argon-milled surface cuts across grains and produces a topography that is not affected by grain hardness or grain plucking. (Day-Stirrat et al., 2012; Loucks et al., 2009) The specimens were then coated with carbon to prevent charging.

Imaging

Images were generated using a FEI Nova NanoSEM 430 field emission SEM, using an accelerating voltage of 10 kV, a spot size of 3.0, and working distances ranged from 4.5 to 10 mm. Imaging parameters are designated in the lower bar of each image. The Everhardt-Thornley Detector (ETD) was used for secondary electron imaging at low

resolutions. At higher resolutions, an in-lens secondary electron detector (TLD) was used. The in-lens detector provides greater detail for imaging nano-scale features (Loucks et al., 2009) Duplicate images were taken with a backscattered electron detector (BSED). Secondary electron images show the topography of the specimen surface, while backscattered electron images show compositional contrast, with regions of higher average atomic number appearing brighter (Pye and Krinsley, 1983). Some images, identified as "mix" were generated using the BSED and a secondary electron detector simultaneously. Images were taken at original magnifications ranging from 1000x to slightly in excess of 60,000x. The width of the field of vision is designated HFW and ranged from 298 μm to less than 5 μm, and a scale bar is included in each image.

SELECTED IMAGES

Intact Pathfinder Well Core.

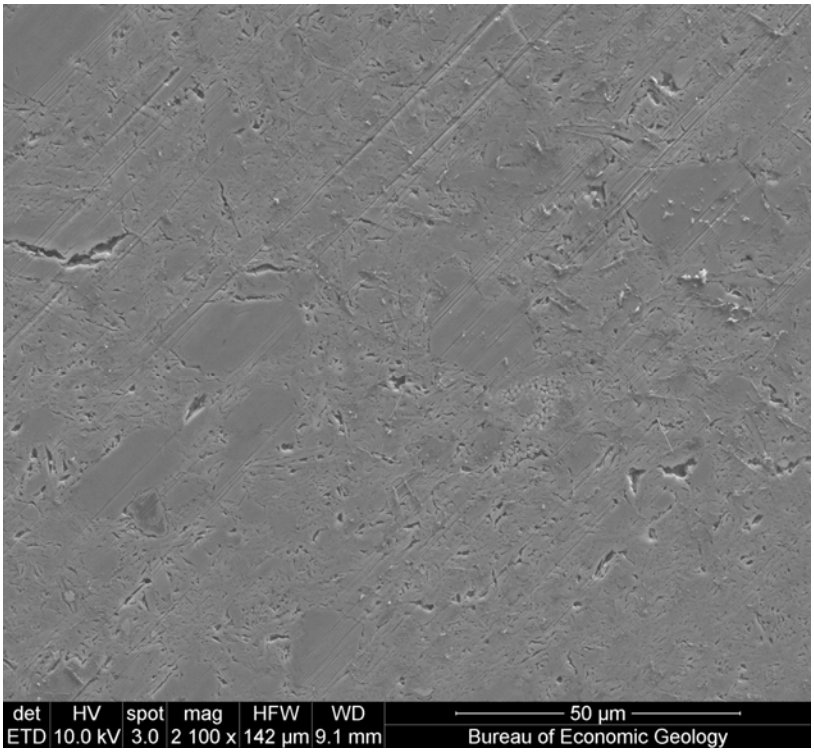

Figure D.1: Secondary electron image of intact pathfinder core.

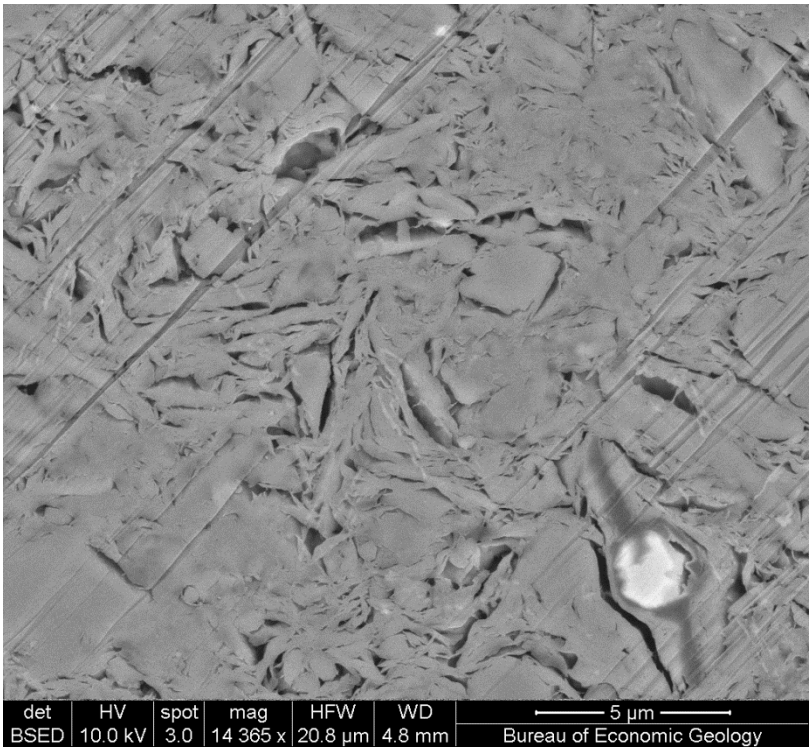

Figure D.2: Backscattered Electron image of intact pathfinder core.

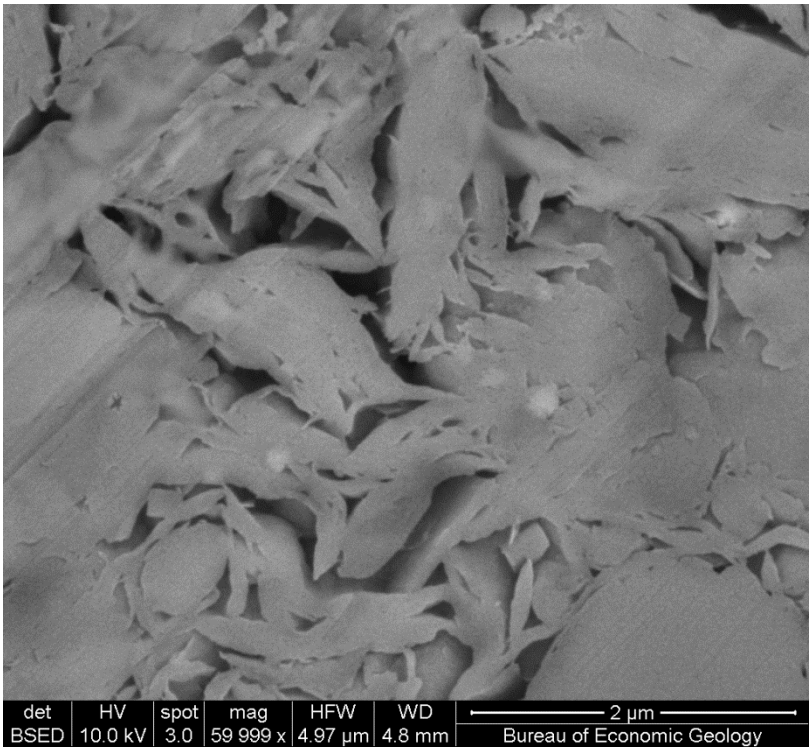

Figure D.3: Backscattered Electron image of intact pathfinder core.

RGoM-EI after resedimentation to 100 kPa.

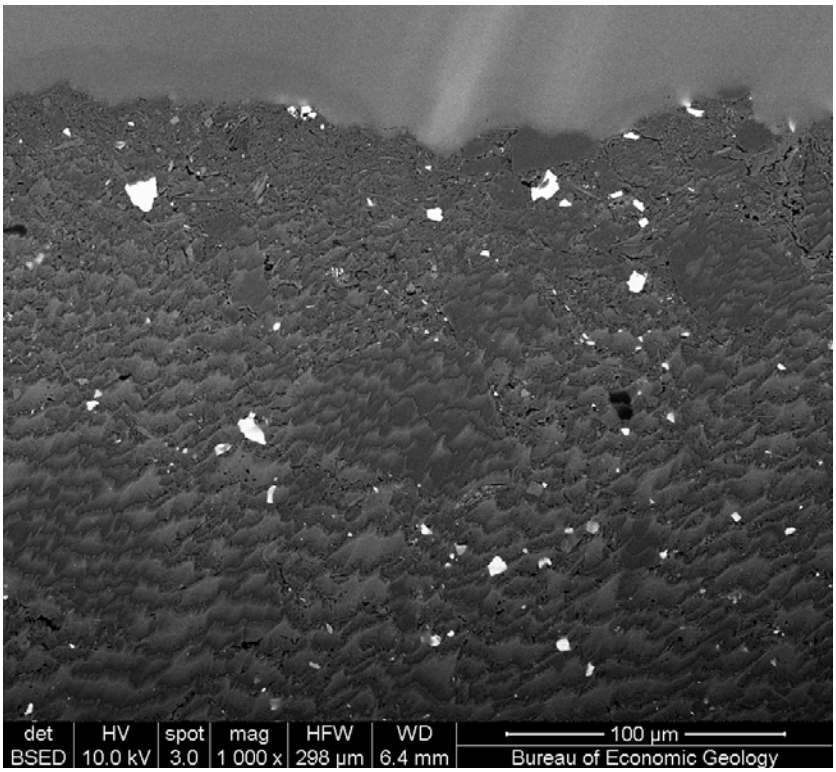

Figure D.4: Backscattered electron image of RGoM-EI with maximum past stress of 100 kPa.

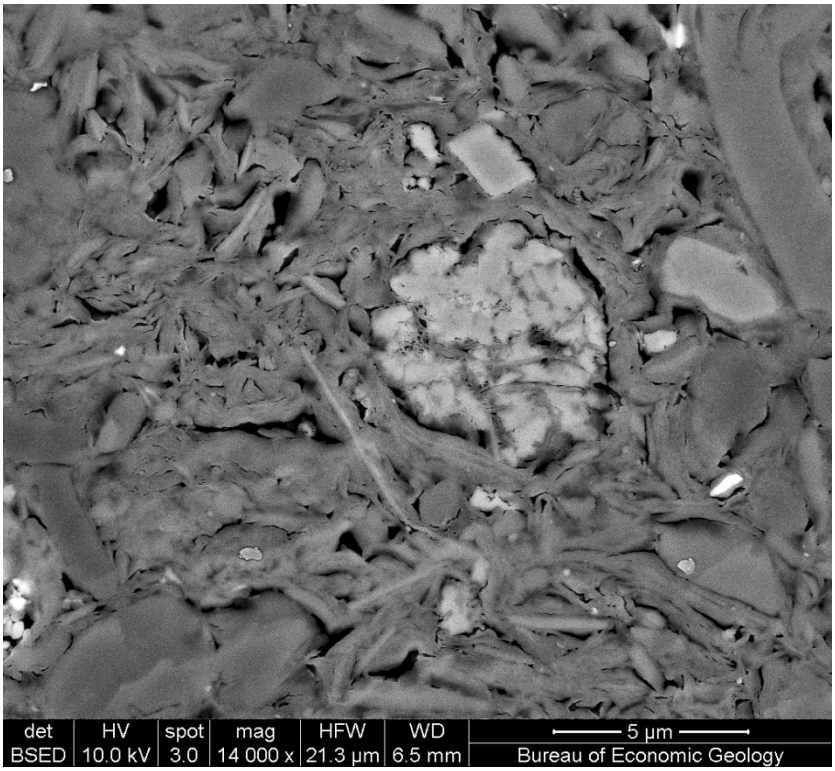

Figure D.5: Backscattered electron image of RGoM-EI with maximum past stress of 100 kPa.

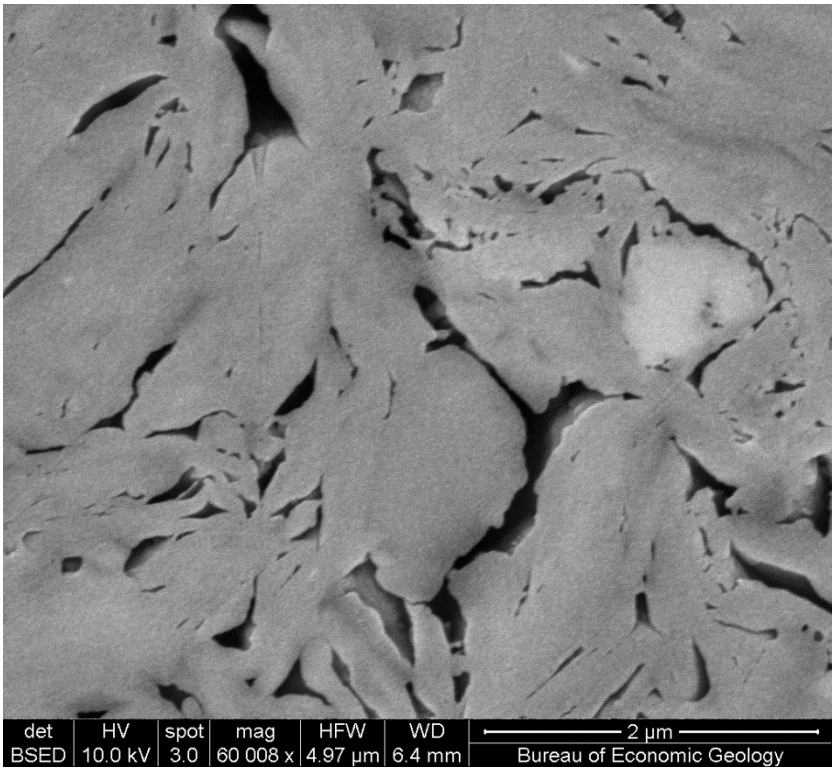

Figure D.6: Backscattered electron image of RGoM-EI with maximum past stress of 100 kPa.

RGoM-EI after CRS to 8 MPa.

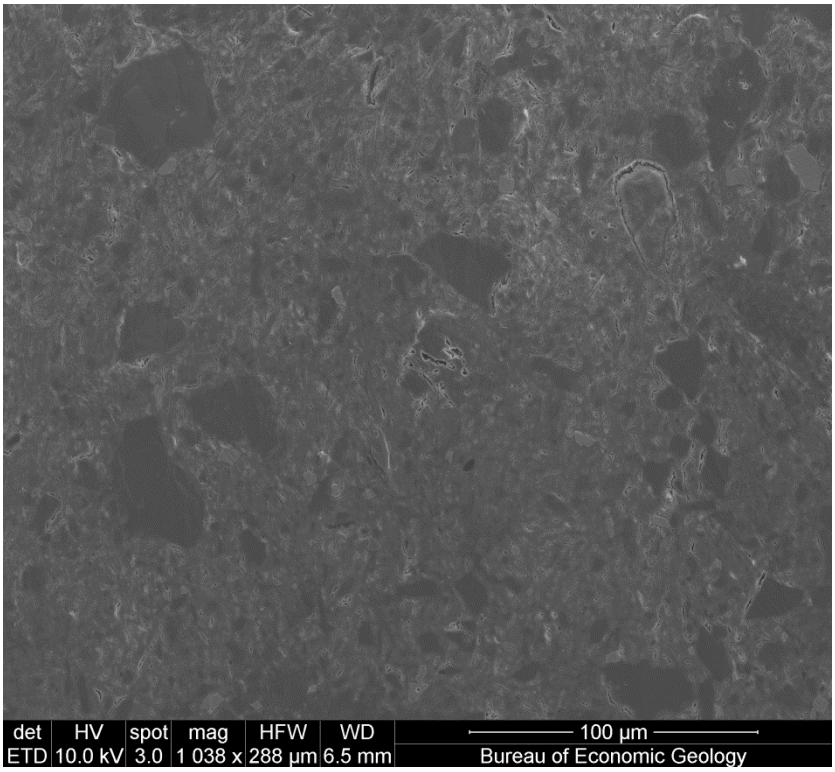

Figure D.7: Secondary electron image of RGoM-EI with maximum past stress of 8.7 MPa.

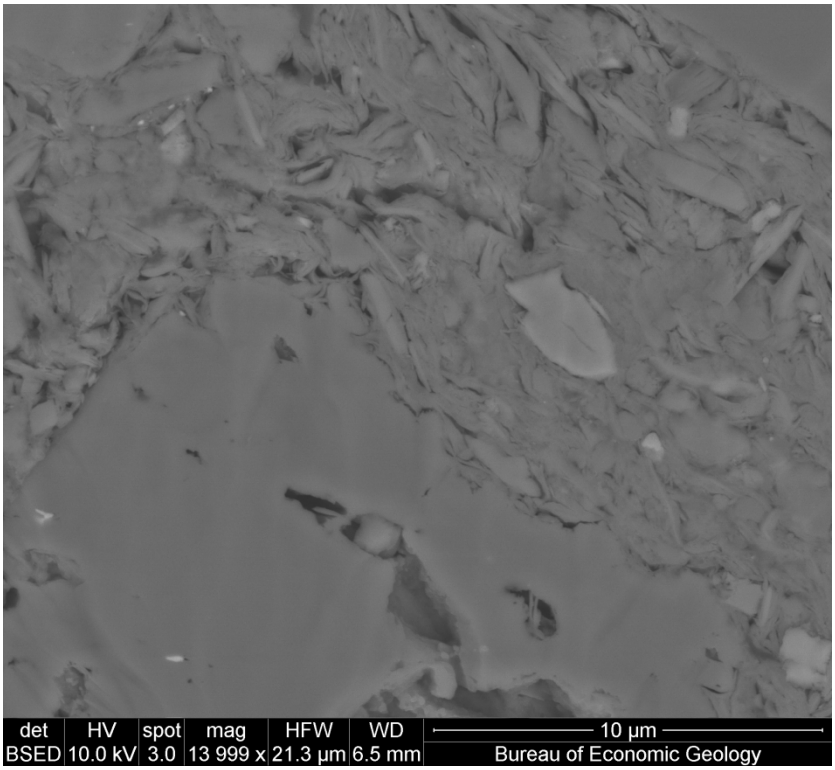

Figure D.8: Backscattered electron image of RGoM-EI with maximum past stress of 8.7 MPa.

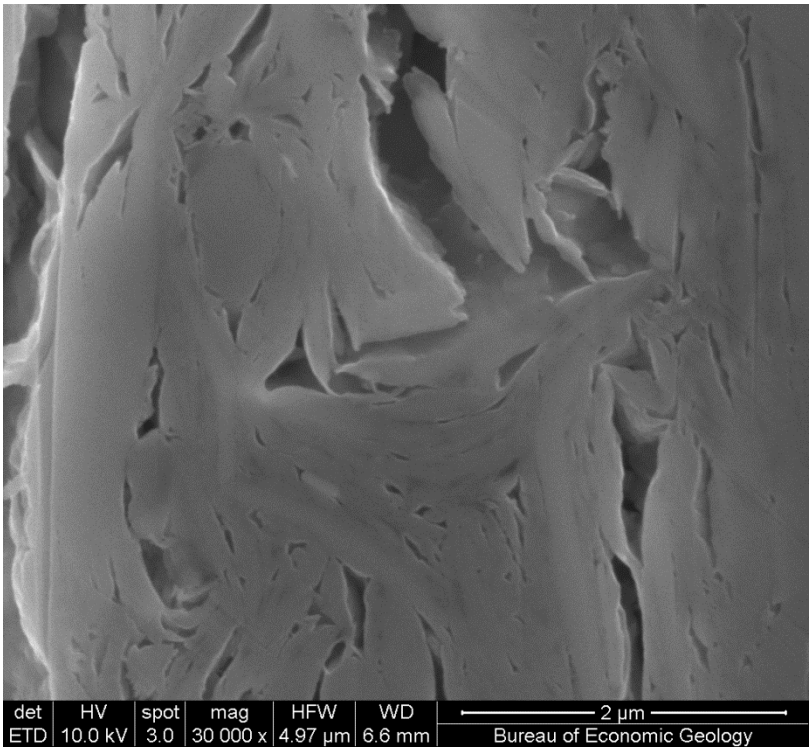

Figure D.9: Secondary electron image of RGoM-EI with maximum past stress of 8.7 MPa.

RGoM-EI at 20.4 MPa.

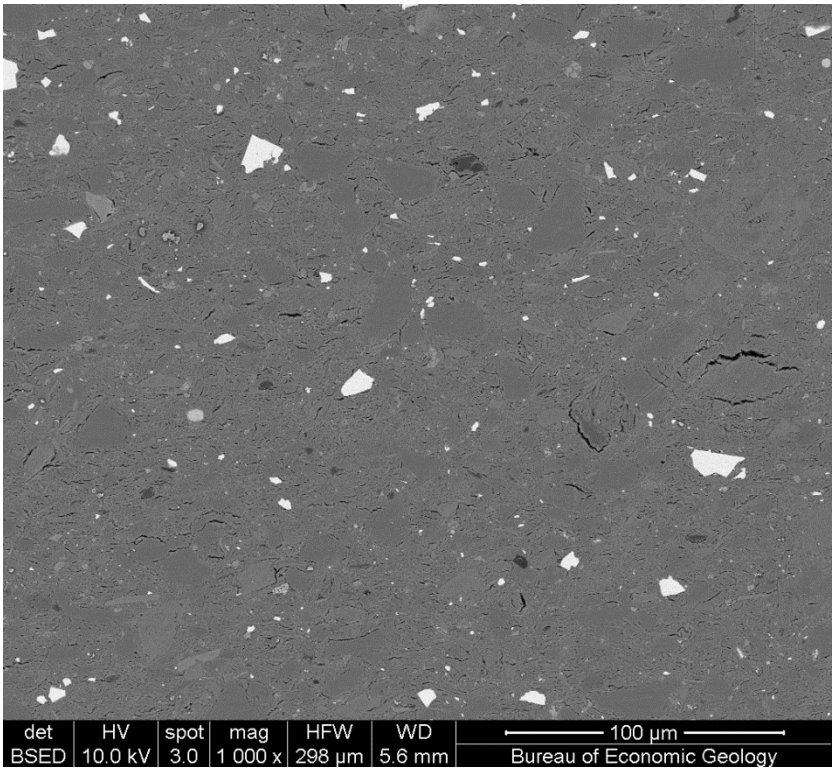

Figure D.10: Backscattered electron image of RGoM-EI with maximum past stress of 20.4 MPa.

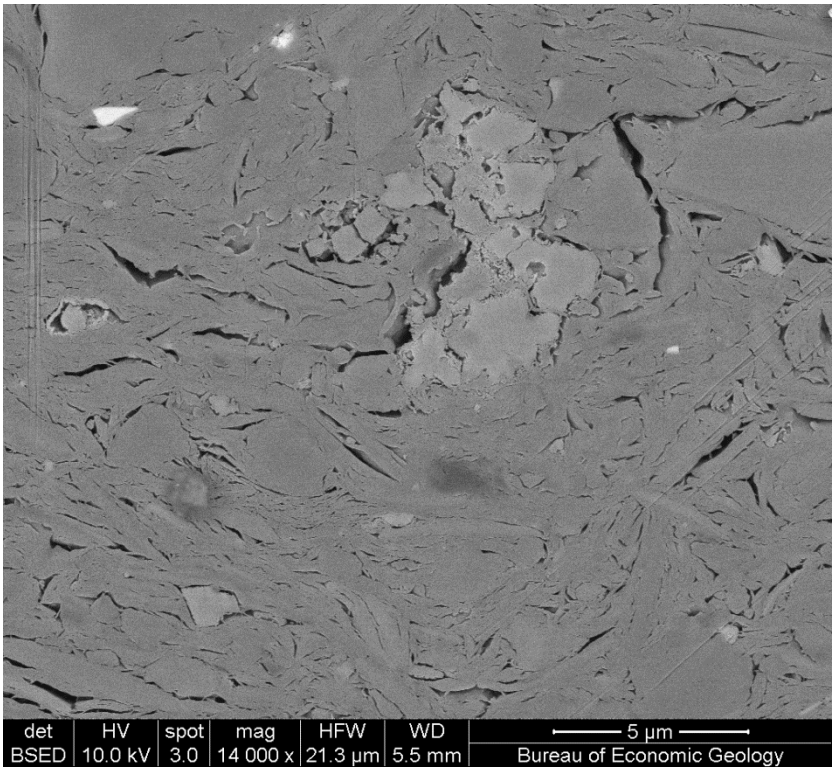

Figure D.11: Backscattered electron image of RGoM-EI with maximum past effective stress of 20.4 MPa.

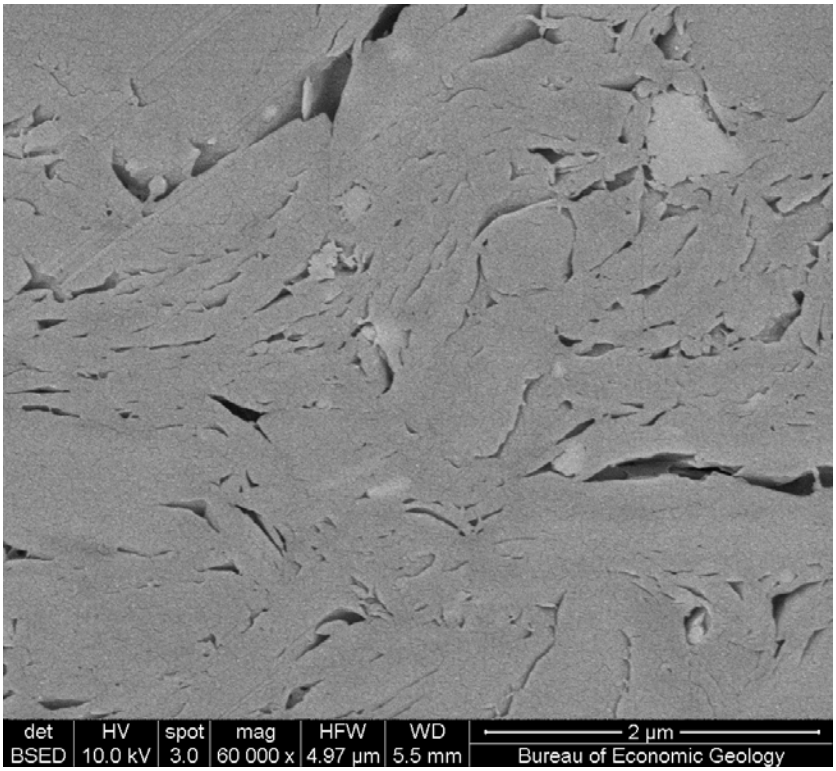

Figure D.12: Backscattered electron image of RGoM-EI with maximum past effective stress of 20.4 MPa.

Appendix E: Laboratory Procedures for Constant Rate of Strain (CRS) Testing.

INTRODUCTION

Consolidation tests in the UT Geofluids laboratory are conducted following a step-by-step procedure document, produced internally. This document combines the industry standard for the testing process (ASTM, 2006b) with specific instructions tailored to our laboratory equipment and its operating interface.

When I joined the UT GeoFluids team in 2010 I was trained using an existing procedure document, but it became necessary to update the procedures when the software which controlled the testing apparatus was upgraded. In addition, I felt that many of the steps in the original procedure were insufficiently explained and required more clarification in order for the instructions to be usable by inexperienced operators. I sought and obtained authorization to create a new procedure document for the laboratory reflecting the current practices, which is reproduced here.

Further adaptations were made to this test procedure in order to test RGoM-EI. These later adaptations are listed in Chapter 1.

NEW CRS PROCEDURES

Before you start.

We want to minimize the amount of time cores spend outside of the refrigerator and exposed to air, so it helps to have everything you'll need ready to go before you get the sample out.

Prepare Load Frame

[ ] Turn off load frame, pump(s), network module, external power supply, and computer.

[ ] Turn on power supply, load frame, pump(s), network module, and computer.

[ ] Start Sigma-1 CRS software.

[ ] Open Cell Pump Screen

[ ] Point pump valve to DI water carboy

[ ] Fill pump with water

[ ] Purge any air bubbles back into carboy

[ ] Point pump valve to the CRS system.

Prepare the CRS chamber

[ ] Select cutter ring (also called specimen ring), either 5.0 cm (1.96') or 6.35 cm (2.5") diameter, depending on the width and condition of your sample and the desired maximum stress.

[ ] Clean inside of CRS chamber and base if necessary

[ ] Clean inside of CRS chamber and base if necessary

[ ] Make sure that Platten in CRS chamber is same size as the chosen cutter ring

[ ] Get two clean porous stones and one filter paper of the proper size for your cutter ring and place them in a beaker filled with DI water. Set the beaker in the ultrasonic bath to clean and fully saturate the stones and filter paper.

[ ] Grease the rubber O-ring generously with a grease sealant such as Dow Corning compound 111 valve lubricant & sealant. (there is usually a tube of this in the drawer with the trimming tools).

[ ] Grease the outer edge of the circular structure on the CRS base that the cutter ring will rest on.

[ ] Grease the inner surface of the cutter ring. Be careful not to use too much grease. You should barely be able to leave a mark with your fingernail on the greased inner surface.

[ ] Weigh the greased cutter ring along with the moist (not dripping) piece of filter paper, and record the mass under "Mass of Ring + FP (g)" on the sample data form in the CRS binder. If there is no hardcopy available, you can find the sample data sheet on the server under the location:
\shannon\All_Access\GeoMechanics_Lab\Tests\Test_Worksheets\

[ ] Also, save a digital copy of the worksheet in a new folder with the test number as its name, for example,
\shannon\All_Access\GeoMechanics_Lab\Tests\CRS\CRS105\CRS105.pdf if this is CRS test # 105.

Round up supplies for sample preparation (See illustrations on the next page to identify)

In the GeoMechanics Lab we deal with two types of samples: intact cores still contained in a core tube and resedimented samples, which are stored in jars and do not require extrusion from a core tube. Preparation tools and preparation is slightly different for both. If you are using a sample that is not still in a core tube, you may skip the first two items. See figures E.1 and E.2 to identify items on this list.

[ ] Deburring tool (1)

[ ] Wire and guide tube (2)

[ ] Acrylic discs and cut pieces of wax paper (3)

[ ] Wire saw (4)

[ ] Trimming tools (5)

[ ] 50 mm cutting ring and acrylic recess tool (6) or 63.5 mm cutting ring and recess tool (7)

[ ] Straight razor blade (8)

[ ] Extruding jig (A) and disc (a')

[ ] Trimming jig (B)

[ ] Trimming block (C)

You may also find that C-clamps, pliers, and wooden blocks come in handy during the extruding and trimming process. The extruding jig can also be clamped to the table with blocks to make it easier to handle.

Initial measurements, data sheet and miscellaneous.

[ ] Fill out sample name, project, date, etc on CRS data sheet

[ ] Measure the diameter and height of cutter ring at 4 positions using a caliper and calculate an average number for both values. Make sure that for the height measurement you only measure the height down to the recess tool. Note both numbers on worksheet under "Height of Specimen (cm)" and "Diameter of Specimen (cm)".

[ ] Label and weigh four tares for trimmings and record their label numbers and masses in data sheet under "Tare Number" and "Tare Mass".

[ ] Label a plastic Ziploc bag for trimmings with CRS test number and contents (type of sample).

[ ] Get out and plug in vacuum sealer if you are taking your specimen from a longer piece of core and will need to return the remainder of the core to the freezer.

Sample Preparation

Extract sample from core

If you are using a sample which does not need to be extruded from its tube, you may skip to the next section (trimming the sample).

[ ] Retrieve core sample from refrigerator.

[ ] Open core packaging by cutting off the top, just below the seal, with scissors or razor blade. Save bag.

[ ] Determine which end of the core is up. Usually some indicator like an arrow or label will be on the tube. Be sure to keep track of this throughout the preparation process!

[ ] Using a large, black sharpie, write "up" arrows all along the length of the core tube so that any interval cut from the core will have an up indicator.

[ ] If necessary, remove end caps and tape from sample tube so you can inspect core.

[ ] If you are doing a CRS test on an intact core specimen, choose an interval of core, 5 cm in length for vertical samples, 7.5 cm for horizontal samples. The ideal interval will be as homogeneous as possible and without cracks.

[ ] Using band saw, cut the desired interval of core and tube.

[ ] Recap core tube and seal with black electrical tape.

[ ] Return core to its original bag (with label)

[ ] Put core bag within Vacuum seal bag with a wet paper towel, vacuum and seal.

[ ] Debur specimen tube (this means strip off splintered or jagged bits from the cut edge and inside of the tube using the deburring tool. To do so, lay the core tube on the table with the cut surface facing you. Hold it with your left hand. Debur only a quarter from about 3 o'clock to 6 o'clock. Then rotate the sample by a quarter of a rotation clockwise and repeat until the entire cut surface is deburred. (It may not be necessary to

do this if the tube is made of plastic, as ours usually are. It is crucial for metal tubes though.)

[ ] Place the sample up right on the table ("up" arrow pointing to the ceiling) with only a small portion of the sample protruding over the edge of the tabletop. At that point, slowly and carefully push the steel guide tube downward through the sample between specimen and tube. Pull the thread wire through the steel guide tube till both ends of the wire are sticking out of both ends of the sample. Then remove the steel tube while you keep the thread wire in place.

[ ] Use a C-clamp to fasten one end of the wire to the countertop. Pull the wire taut (with pliers, for example) and then rotate the tube in its own location around the long axis. This will loosen the sample from the tube.

[ ] Place the sample and tube into the extruding jig, making sure that the bottom of the sample is sitting on the base of the extruding jig. Do not flip the sample which would result in applying pressure opposite to the direction in which it is applied in-situ.

[ ] Put a round piece of wax paper and then the disc (a') on the top end of the sample.

[ ] Use the extruding jig and disc to push a few millimeters of sample out of the tube.

[ ] Use the wire saw to cut off the bottom edge of the sample where the saw blade may have strained or disturbed it.

[ ] Now use the extruding jig and disc to gently push the rest of the sample out of the tube and on to an acrylic disc with wax paper above it.

After the sample is out of the tube, be careful not to forget which end is the top and which end is the bottom. You may wish to mark the acrylic discs or round pieces of wax paper and keep them on or near the top or bottom as reminders.

Trimming the Sample.

Your goal here is to have the cutter ring completely filled with the sample, without cracks or voids, and smooth top and bottom surfaces.

[ ] If the top of the sample has been in contact with the band saw or otherwise strained, cut it off by laying the sample in the trimming block with the top few millimeters extended off the edge, and cutting down along the posts with the wire saw.

[ ] Using an ungreased cutter ring of the same diameter as your greased cutter ring (if available) , press down gently into the top of the sample to make a shallow circular impression which will be a guide to you in trimming the sample

[ ] Place the sample facing upward on the trimming block with one side overlapping the recessed edge.

[ ] Cut a strip off the side by sliding the wire saw down the guide posts on the trimming block. Use the circular impression on the top as a guide and leave a couple of millimeters around it.

[ ] Rotate the sample and repeat process until you have formed a solid with top and bottom surfaces that are at least octagonal, and with about 2-3 mm of excess material on the sides surrounding the circular impression on the top.

[ ] Turn the sample upside down on a wax-paper-covered acrylic disc, and place in the trimming jig with the top facing down.

[ ] Insert the cutter ring – tapered end facing downward - in the top of the trimming jig, lower the trimming jig with cutter ring till it reaches the sample and let it rest on the sample.

[ ] Push the ring slowly down into the sample (~1 mm).

[ ] With the trimming tools (#5), trim off the excess material around the edge of the ring that was produced by pushing the cutter ring into the sample.

[ ] While trimming rotate the specimen by turning the plastic spacer of trimming jig that holds cutter ring (do not turn cutter ring directly).

[ ] Material removed during trimming should be collected and placed in the labeled plastic bag.

[ ] Iterate the above three steps until the ring is filled, and a bit of trimmed core protrudes above the top. Be careful not to undercut the ring. If this happens, fill the gap with material you have previously scraped off. This is a delicate job. It can take up to an hour depending on the sample condition.

[ ] Lift the plastic spacer so it detaches from the cutter ring and specimen. Remove the specimen and ring from the trimming jig.

[ ] Using the wire saw or the straight blade knife, make a flat cut that removes any excess material beyond the cutting edge of the cutter ring.

[ ] Flip the sample over so that the top end faces up, setting it on a wax paper – covered acrylic disk. Use the straight razor blade, plane off the top surface of the specimen. Scraping gently with the blade inclined at about 45^{o} is likely to be easier than cutting. Make sure the entire razor blade resting on the specimen ring as you pull it across the top surface towards you. Don't put too much pressure on it or the razor blade will bend, causing an uneven top surface.

[ ] When you have a smooth surface, place the filter paper on top of it, making sure not to leave any bubbles underneath. Then overturn the sample and cutter ring (cutting edge down) onto the recess tool and push it down so that excess material comes out of the bottom end of specimen ring.

[ ] Now, using the straight razor blade and if necessary, the wire saw, remove excess material from the other side of the cutter ring and scrape the surface flat.

Setting up your test

[ ] Take mass of specimen, sample ring, and filter paper, and write the measurement down on the worksheet under "Mass of Ring + FP + Spec. (initial) (g)".

[ ] Remove the top of the CRS chamber.

[ ] Lock the piston in the upright position.

[ ] Put a 2.5" DI water saturated porous stone in the base of the CRS chamber

[ ] Make sure base water line is closed

[ ] Wipe off any excess water.

[ ] Add a little bit of grease along the bottom edge of the cutter ring; at the contact points with the CRS base.

[ ] Put the specimen into the CRS chamber, with the ring overlaying the raised circular area in the base which contains the porous stone, and with the cutting edge of the ring facing up.

[ ] Place a porous stone of the appropriate size and DI water saturated on top of the specimen and filter paper, partially recessed inside the cutting edge of the ring.

[ ] Slowly put on the top of the CRS chamber.

[ ] Lock down the top of the CRS chamber. Screw the three bolts in and make them more than hand-tight but don't over-tighten them.

[ ] Make sure the Base Valve is open on the chamber. [ ] Make sure the top drain valve is open on the chamber.

[ ] Unlock the piston and slowly lower it until the platen (the foot at the base of the piston) is resting atop the porous stone.

[ ] Make sure that the pump is full of water and that the pump valve is pointed in the direction of the CRS chamber.

[ ] Open the Cell Pump window in your Sigma-1 CRS software, if it is not already open.

[ ] Select the Volume Control tab, if it is not already selected in the main right-side area of the cell pump screen.

[ ] Set the pump to 10 ml/minute, 50 ml volume, and click the up arrow button (the second one, not the one that looks like this but the one that looks like this).

[ ] Now fill the chamber the rest of the way, still at 10 ml/min. Water will flow out the top drain valve when it's full (So the end of the drain tube should be in a bucket or something).

It is likely to be necessary to re-fill the pump at some point. Do this by stopping the pump, turning the valve towards the DI water carboy, and clicking the maximum rate down arrow in the volume control area of the screen. Then, turn the pump valve back towards the CRS system, reselect the controlled-rate up button, and return to filling the chamber at 10 ml/min.

[ ] Once water is flowing out the top drain line, the chamber is full. Stop the pump and close the top drain valve. If you can see large air bubbles trapped within the chamber, you may wish to try to drive them out by gently tilting the chamber (while holding it securely) to let them escape up the piston and into the top drain valve. This should be done after stopping the pump, but before closing the top drain valve.

[ ] Take the CRS chamber, and put it on the load frame platform, with the piston underneath the load cell. It may be necessary to lower the load frame in order to do this. Go to the "tools" menu in the Sigma-1 CRS window and select manual mode. Then use the up or down buttons to lower the platform.

[ ] The shear break, a short metal cylinder with a flat surface on the top and a concave surface on the bottom end, should now be placed over the top convex end of the piston, which it is machined to fit. Then slide the CRS chamber until the shear brake is underneath the corresponding metal cylinder at the bottom of the load cell.

Exception: the 50,000 lb load cell in its current configuration does not require a shear brake. The bottom surface of the load cell is concave and the chamber should be aligned so that the convex tip of the piston fits into this recess.

[ ] Make sure that the piston is locked.

[ ] Using the button in the manual mode box, and a very slow rate of displacement (such as 0.05 in/minute to close the last little gap of space), carefully move the load frame up until the shear brake top is just touching the bottom cylinder on the load cell. Be very careful not to let the load cell put significant force on the piston, you are just raising the chamber so that you can make a final alignment.

[ ] Make sure that the piston and shear brake are exactly lined up with the load cell.

[ ] Zero your DCDT sensor and your pressure transducers. Select the "setup" menu, then "sensors". In the sensors window, click on each sensor in turn and then "test" and "take zero".

[ ] Lower the load frame a few mm, and then zero the load cell using the same procedure as you did for the other sensors.

Test configurations

[ ] Go to the File menu and select Specimen Data. Fill out the form which pops up with enough information to identify the specimen (Figure E.3). Make sure that the

specimen diameter is correct. For the smaller rings it should be about 1.96, for the larger rings, 2.49.

[ ] Return to the File Menu and select Test Data. Fill out the form which pops up. Recommended Settings are shown in figure E.4.

[ ] in the test data window, select a loading schedule appropriate for your test specimen, testing plan, and apparatus configuration. IF an appropriate loading schedule is not already set up, you will need to create one yourself.

Starting your test.

[ ] Raise the platform slowly and carefully until the shear break (or top of the piston if you are using the 50k setup) is almost touching the bottom of the load cell.

[ ] Click the Make Contact button. This will slowly raise the platform and make contact between the shear break and the load cell. When contact is made, click the OK button in the dialog window. Note: The Dialog window says to unlock the piston here before clicking OK, but our procedure as it currently stands is to wait until after the backpressure phase starts to unlock the piston. So don't unlock the piston. After you've clicked OK in the dialog box, the Make Contact button will change into a Start Test button. Click it.

[ ] Go to your Cell Pump window. Select the Pressure Control tab. Set it to Ramp Pressure to 56 PSI over 180 Minutes. At this point, the

[ ] once the system reaches a couple of PSI, unlock the piston. (1/4 turn counterclockwise).

[ ] Now, you're pretty much done with this for today. Leave the chamber to pressure up, which will take three hours. Then, leave it to sit at backpressure overnight,

or for at least 8 hours. In this time, the high pressure should drive any remaining bubbles of air into solution and fully saturate your sample.

[ ] After leaving it at backpressure overnight, click Pause (at the bottom of the screen), then Done (lower right hand corner), then Yes (in the dialog box, when it asks if you want to start the consolidation portion of the test).

[ ] Start a manual data acquisition file here. In the Tools menu, click Data Acquisition then New Task. Type in a filename for it to save as. Then, select your reading schedule. From the drop-down menu. (The recommended reading schedule is one reading every 4 minutes. If there isn't an available 4 minute schedule, or you'd like to set up a custom schedule, then go to the File menu, then click on Reading Schedules, and Add Schedule, and set one up using the dialog box)

[ ] The program will move to the Consolidation tab. Check your loading schedule, which appears in the right-hand side of the screen. If you need to make any changes, right-click on the part you want to change and then select Edit from the menu which appears.

[ ] Click Start (bottom middle of screen), and let your test run.

[ ] Running the test will take days. Check periodically to make sure that no problems have developed. Extruded material escaping from the ring, changing chamber or pump pressures, and leaks in the chamber or tubing are indications that something is wrong. Make sure the pump does not run out of water and the displacement transducer and piston have room to move.

[ ] Periodically plot pore pressure ratio (ASTM, 2006b) against time or effective stress. Pore pressure ratio should rise slowly during loading and remain between 2 and 15%, with an ideal range of 3-5 percent (ASTM, 2006b; Germaine and Germaine, 2009).

Reduce strain rate if pore pressure ratio gets above 15%. Sudden changes in pore-pressure ratio can indicate a leak.

Ending your test.

[ ] Go to the Tools menu, and click on Data Acquisition and Close Task to end your manual data acquisition. Click Yes in the Dialog that appears asking for confirmation.

[ ] Lock the Piston

[ ] Hit the Pause button, and then Done (bottom right)

[ ] Program will exit. Relaunch the program.

[ ] open bottom valve on chamber.

[ ] Take the pressure off of the chamber, by going to Cell Pump window, Pressure Control tab, and selecting Ramp Pressure to 0 PSI over 10 minutes.

[ ] Mark and weigh a tare for final specimen measurement.

[ ] Stop pump when pressure = 0 PSI.

[ ] Turn off pump valve (point straight up).

[ ] Lower load frame (in manual mode, accessible from the tools menu) until there is a visible gap between the shear brake and the Load Cell.

[ ] Remove the chamber from the load frame.

[ ] Close the bottom valve.

[ ] Open the top drain valve.

[ ] Remove the top of the chamber (carefully).

[ ] Weigh the sample in the cutter ring, along with the porous stone and filter paper.

[ ] extrude the sample onto your recently labeled-and-weighed tare by pressing against the porous stone. Then, remove the filter paper from the top of the sample. If the sample is difficult to extrude, place the ring on top of two wooden blocks with the sample over a space in the middle and use a C-clamp to apply force down on the porous stone.

[ ] weigh the sample again, this time without the ring and filter paper and in a tare, and record the measurement in the CRS worksheet in the logbook.

[ ] put the tare with the sample in the oven (80^{o} C) and dry for at least 24 hours before weighing it again and recording the dry mass on the worksheet.

.

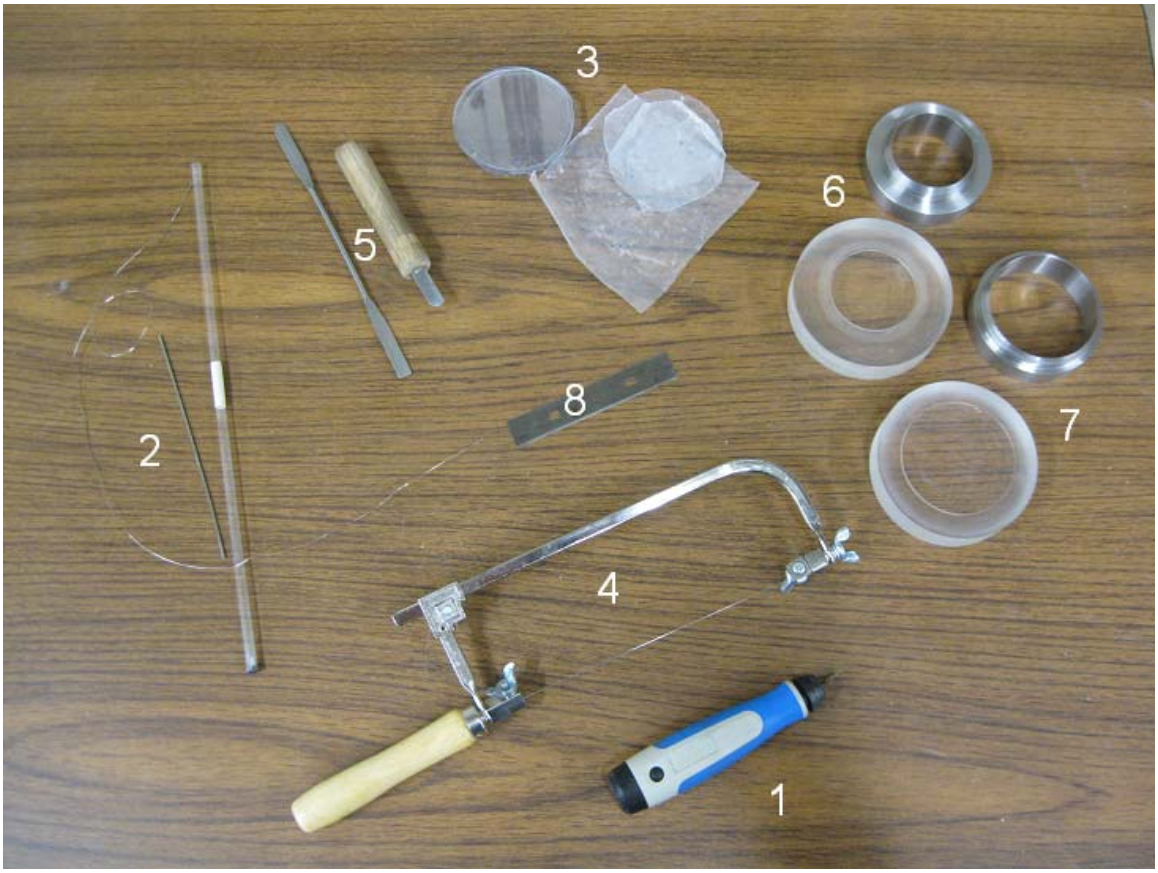

Figure E.1: Tools used in CRS sample preparation

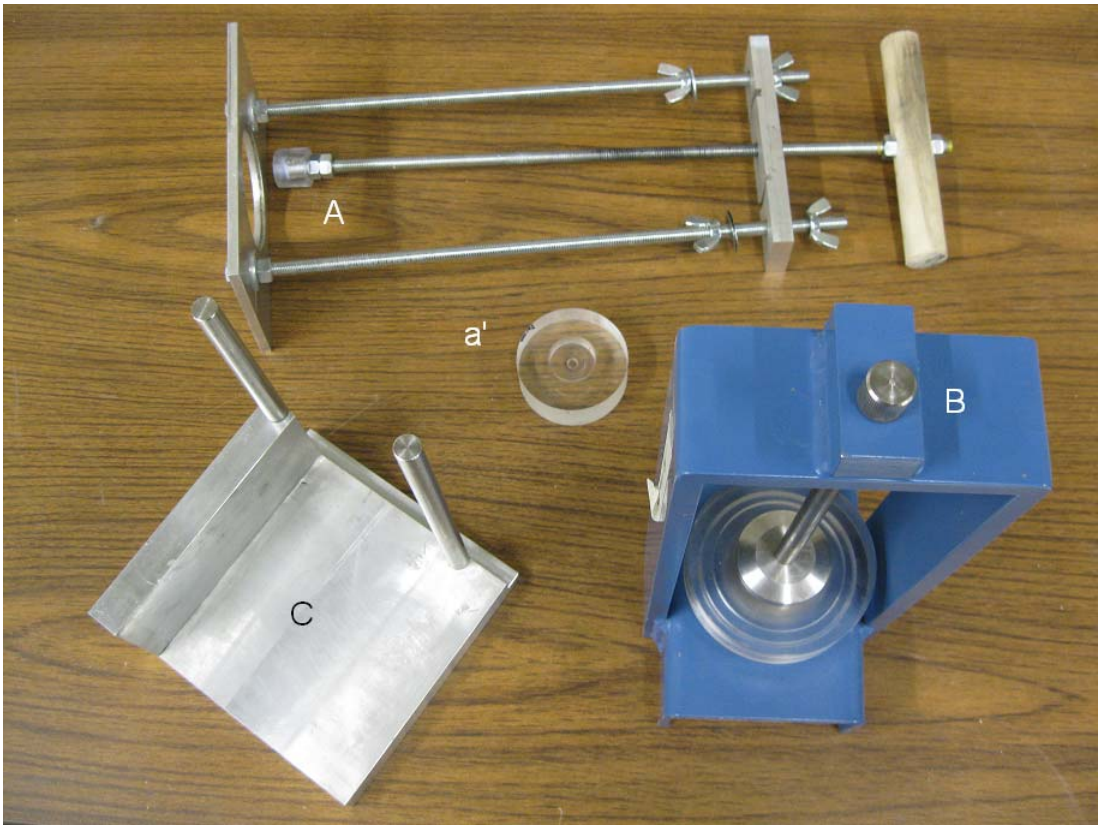

Figure E.2: CRS sample preparation equipment.

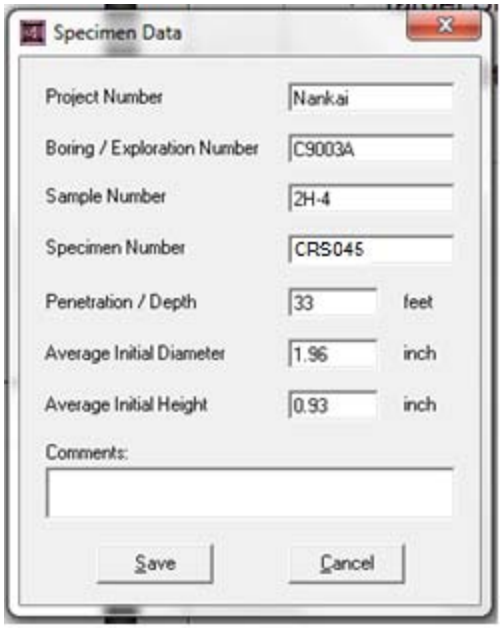

Figure E.3: Specimen Data menu in Sigma-1 CRS-SI software.

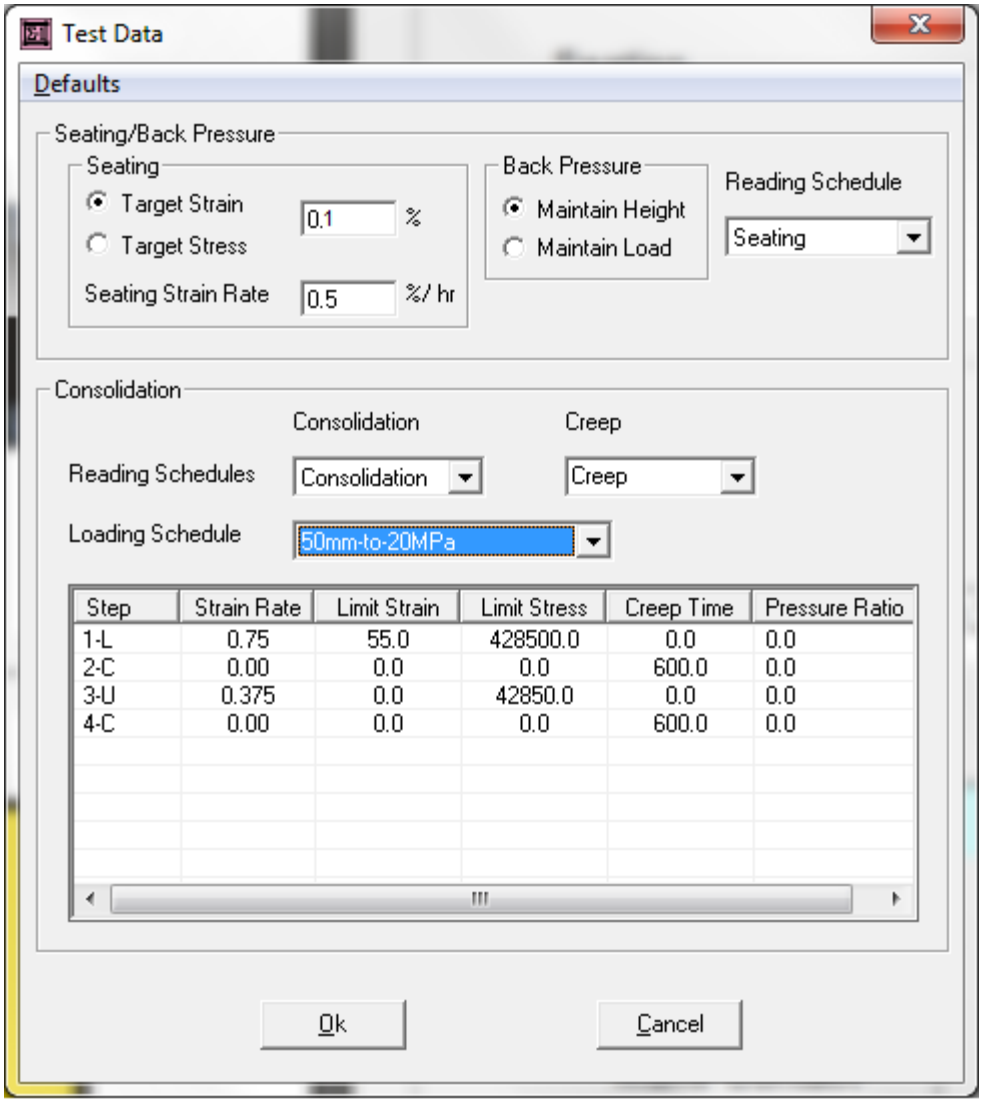

Figure E.4: Recommended settings for "Seating/Back Pressure) and sample consolidation loading schedule for Test Data menu in Sigma-1 CRS-SI software.

References

Abdulhadi, N.O., 2009, An experimental investigation into the stress-dependent mechanical behavior of cohesive soil with application to wellbore instability: Cambridge, MA, Massachusetts Institute of Technology.

Adams, A.L., 2011, Laboratory evaluation of the constant rate of strain and constant head techniques for measurement of the hydraulic conductivity of fine grained soils Cambridge, MA, Massachusetts Institute of Technology.

Adams, A.L., Germaine, J.T., Flemings, P.B., and Day, S.J., 2013, Stress Induced Permeability Anisotropy of Resedimented Boston Blue Clay: Water Resour. Res.

Ahmed, I., 1990, Investigation of normalized behavior of resedimented Boston Blue Clay using Geonor direct simple shear apparatus: Cambridge, Massachusetts Institute of Technology.

Alexander, L.L., and Flemings, P.B., 1995, Geologic Evolution of a Pliocene-Pleistocene Salt-Withdrawal Minibasin: Eugene Island Block 330, Offshore Louisiana: AAPG Bulletin, v. 79, p. 1737-1756.

Allen, D.F., Best, D.L., Evans, M., and Holenka, J.M., 1993, The effect ot wellbore condition on wireline and MWD neutron density logs. : SPE Formation Evaluation, v. 8, p. 50-56.

Aplin, A.C., Matenaar, I.F., McCarty, D.K., and van der Pluijm, B.A., 2006, Influence of mechanical compaction and clay mineral diagenesis on the microfabric and pore-scale properties of deep-water Gulf of Mexico mudstones: Clays and Clay Minerals, v. 54, p. 500-514.

Aplin, A.C., Yang, Y.L., and Hansen, S., 1995, Assessment of beta, the compression coefficient of mudstones and its relationship with detailed lithology: Marine and Petroleum Geology, v. 12, p. 955-963.

ASTM, 2005a, Standard Test Methods for Laboratory Determination of Water (Moisture) Content of Soil and Rock by Mass, *in* International, A., ed., D 2216-05: West Conshohocken, PA, p. 7.

ASTM, 2005b, Standard Test Methods for Liquid Limit, Plastic Limit, and Plasticity Index of Soils, *in* International, A., ed., D 4318-05: West Conshohocken, PA, p. 16.

ASTM, 2006a, Standard Practice for Classification of Soils for Engineering Purposes (Unified Soil Classification System), *in* International, A., ed., D 2487-06: West Conshohocken, PA, p. 11.

ASTM, 2006b, Standard test method for one-dimensional consolidation properties of saturated cohesive soils using controlled-strain loading (Standard D4186-06), *in* 04.08), A.B.o.A.S.V., ed., Soil and Rock (I): West Conshohocken, PA, American Society for Testing and Materials, p. 15.

ASTM, 2006c, Standard Test Methods for Specific Gravity of Soil Solids by Water Pycnometer, *in* International, A., ed., D 854-06: West Conshohocken, PA, p. 7.

ASTM, 2007, Standard D422, Standard Test Method for Particle-Size Analysis of Soils: West Conshohocken, PA.

Atterberg, A., 1911, Behavior of Clays with Water, Their Limits of Plasticity and Their Degrees of Plasticity: Kungliga Lantbruksakademiens Handlingar och Tidskrift, v. 50, p. 132-158.

Audet, D.M., 1996, Compaction and Overpressuring in Pleistocene Sediments on the Louisiana Shelf, Gulf of Mexico: Marine and Petroleum Geology, v. 13, p. 467-474.

Becker, D.E., Crooks, J.H.A., Been, K., and Jefferies, M.G., 1987, Work as a criterion for determining in situ and yield stresses in clays: Canadian Geotechnical Journal, v. 24, p. 549-564.

Bensari, J.E., 1984, Stress-strain characteristics from undrained and drained triaxial tests on resedimented Boston blue clay: Cambridge, Massachusetts Institute of Technology.

Braunsdorf, N., and Kittridge, M., 2003, Overburden pressure estimation in deepwater settings, PSU Geofluids consortium meeting,: Santa Cruz, CA.

Bryant, W.R., Hottman, W., and Trabant, P., 1975, Permeability of Unconsolidated and Consolidated Marine Sediments, Gulf of Mexico: Marine Geotechnology, v. 1, p. 1-14.

Bryant, W.R., Wetzel, A., and Sweet, W., 1986a, Geotechnical properties of intraslope basin sediments, Gulf of Mexico, Deep Sea Drilling Project leg 96, site 619, *in* Bouma, A.H., Coleman, J.M., and Meyer, A.W., eds., Init. Repts. DSDP, 96: Washington, U.S. Govt. Printing Office, p. 819-824.

Bryant, W.R., Wetzel, A., and Taylor, E., 1986b, Consolidation Characteristics and Permeability of Mississippi Fan Sediments, *in* Bouma, A.H., Coleman, J. M., Meyer, A. W., et al., , ed., Init. Repts. DSDP, 96: : Washington, DC

U.S. Govt. Printing Office, p. 797-809.

Burland, J.B., 1990, On the compressibility and shear strength of natural clays: Geotechnique, v. 40, p. 329-378.

Butterfield, R., 1979, A natural compression law for soils (an advance on e-logp'): Geotechnique, v. 29, p. 469-480.

Carman, P.C., 1937, Flow through a granular bed: Trans. Inst. Chem. Eng. London, v. 15, p. 150-156.

Casagrande, A., 1932, Research of the Atterberg Limits of Soils: Public Roads, v. 3, p. 121-130 & 136.

Casagrande, A., 1936, The determination of the pre-consolidation load and its practical significance, *in* Casagrande, A., Rutledge, P.C., and Watson, J.D., eds., Proceedings of the 1st International Conference on Soil Mechanics and Foundation Engineering, Volume 3, American Society of Civil Engineers, p. 60-64.

Casey, B., and Germaine, J.T., 2013, The stress-dependence of shear strength in fine-grained soils and correlations with liquid limit: Journal of Geotechnical and Geoenvironmental Engineering, v. 139, p. 1709-1717.

Cauble, D.F., 1993, The behavior of resedimented Boston blue clay at OCR4 in cyclic and post-cyclic undrained direct simple shear: Cambridge, Massachusetts Institute of Technology.

Day-Stirrat, R.J., Flemings, P.B., Yao, Y., Aplin, A.C., and Van der Pluijm, B., 2012, The fabric of consolidation in Gulf of Mexico mudstones: Marine Geology, p. 77-85.

Dewhurst, D.N., Aplin, A.C., and Sarda, J.P., 1999, Influence of clay fraction on pore-scale properties and hydraulic conductivity of experimentally compacted mudstones: Journal of Geophysical Research, v. 104, p. 29261-29274.

Dewhurst, D.N., Aplin, A.C., Sarda, J.P., and Yang, Y.L., 1998, Compaction-driven evolution of porosity and permeability in natural mudstones: An experimental study: Journal of Geophysical Research, v. 103, p. 651-661.

Dugan, B., and Flemings, P.B., 2000, Overpressure and Fluid Flow in the New Jersey Continental Slope: Implications for Slope Failure and Cold Seeps: Science, v. 289, p. 288-291.

Dugan, B., Flemings, P.B., Olgaard, D.L., and Gooch, M.J., 2003, Consolidation, effective stress, and fluid pressure of sediments from ODP Site 1073, US mid-Atlantic continental slope: Earth and Planetary Science Letters, v. 215, p. 13-26.

Fertl, W.H., 1976, Abnormal Formation Pressures: Implications to Exploration, Drilling, and Production of Oil and Gas Resources: Amsterdam, Elsevier, 382 p.

Flemings, P.B., Germaine, J., Long, H., Dugan, B., Sawyer, D., Behrmann, J.H., John, C., and Shipboard Scientific Party, I.E., 2006, Measuring Temperature and Pressure with the Temperature Two Pressure (T2P) Probe in the Ursa Basin, Gulf of Mexico: Development of a New Pressure and Temperature Probe for the IODP, Offshore Technology Conference, Volume OTC 17957: Houston, Texas, USA, p. 5.

Flemings, P.B., Stump, B.B., Finkbeiner, T., and Zoback, M., 2002, Flow focusing in overpressured sandstones: theory, observations, and applications: American Journal of Science, v. 302, p. 827-855.

Force, E.A., 1998, Factors controlling pore-pressure generation during K0-consolidation of laboratory tests.: Cambridge, MA, Mass. Inst. of Technology. .

Gao, B., 2013, Pore pressure within dipping reserviors in overpressure basins.: Austin, TX., The University of Texas.

Germaine, J.T., and Germaine, A.V., 2009, Geotechnical Laboratory Measurements For Engineers: Hoboken, NJ, John Wiley and Sons.

Gonzalez, J.H., 2000, Experimental and theoretical investigation of constant rate of strain consolidation: Cambridge, MA, Massachusetts Institute of Technology.

Gordon, D.S., and Flemings, P.B., 1998, Generation of overpressure and compaction-driven fluid flow in a Plio-Pleistocene growth-faulted basin, Eugene Island 330, offshore Louisiana: Basin Research, v. 10, p. 177-196.

Hart, B.S., Flemings, P.B., and Deshpande, A., 1995, Porosity and Pressure - Role of Compaction Disequilibrium in the Development of Geopressures in a Gulf-Coast Pleistocene Basin: Geology, v. 23, p. 45-48.

Hillier, S., 2000, Accurate quantitative analysis of clay and other minerals in sandstones by XRD: comparison of a Rietveld and a reference intensity ratio (RIR) method and the importance of sample preparation.: Clay Minerals, v. 35, p. 291-302.

Horan, A.J., 2012, The Mechanical Behavior of Normally Consolidated Soils as a Function of Pore Fluid Salinity: Cambridge, MA, MIT.

House, R.D., 2012, A comparison of the behavior of intact and resedimented Boston Blue Clay (BBC): Cambridge, MA, Mass. Inst. Technology.

Issler, D.R., 1992, A new approach to shale compaction and stratigraphic restoration, Beaufort-Mackenzie Basin and Mackenzie Corridor, northern Canada: American Association of Petroleum Geologist Bulletin, v. 76, p. 1170-1189.

Karig, D.E., and Ask, M.V.S., 2003, Geological perspectives on consolidation of clay-rich marine sediments: J. Geophs. Res., v. 108, p. 2197.

Karig, D.E., and Hou, G., 1992, High-Stress Consolidation Experiments and Their Geologic Implications: J. Geophys. Res, v. 97, p. 289-300.

Karig, D.E., and Morgan, J., 1994, Tectonic deformation: stress paths and strain histories, *in* Maltman, A., ed., The geological deformation of sediments: New York, Chapman and Hall, p. 167-204.

Leroueil, S., Tavenas, F., and Locat, J., 1985, Discussion: Corelations between index tests and the properties of remoulded clays: Geotechnique, v. 35, p. 223-226.

Long, H., Flemings, P.B., Germaine, J., Dugan, B., Sawyer, D., and Shipboard Scientific Party, I.E., 2007, In Situ Pore Pressure at IODP Site U1324, Ursa Basin, Gulf of Mexico: Proceedings of the Offshore Technology Conference, Houston, Texas.

Long, H., Flemings, P.B., Germaine, J.T., and Saffer, D.M., 2011, Consolidation and Overpressure near the seafloor in the Ursa Basin, Deepwater Gulf of Mexico: Earth and Planetary Science Letters, v. 305, p. 11-20.

Long, H., Flemings, P.B., Germaine, J.T., Saffer, D.M., and Dugan, B., 2008, Data report: consolidation characteristics of sediments from IODP Expedition 308, Ursa Basin, Gulf of Mexico, *in* Flemings, P.B., Behrmann, J.H., and John, C.M., eds., Proc. IODP, Volume 308: College Station, TX, Proc. IODP, Sci. Results, p. 47.

Losh, S., Eglinton, L., and Wood, J., 1994, Coring and Inorganic Geochemistry in the Pathfinder Well, Results of the Pathfinder drilling program into a major growth fault (CD-ROM): Palisades, NY, LDEO Press. Lamont Doherty Earth Observatory.

Losh, S., and Wood, J., 1995, Brine Chemistry, Blocks 330 and 316, Results of the Pathfinder drilling program into a major growth fault (CD-ROM): Palisades, NY, LDEO Press. Lamont Doherty Earth Observatory.

Loucks, R.G., Reed, R.M., Ruppel, S.C., and Jarvie, D.M., 2009, Morphology, genesis, and distribution of nanometer-scale pores in siliceous mudstones of the Mississippian Barnett Shale: Journal of Sedimentary Research, v. 79, p. 848-861.

Mazzei, D.P.C., 2008, Normalized Mechanical Properties of Resedimented Gulf of Mexico Clay from Integrated Ocean Drilling Program Expedition Leg 308: Cambridge, Massachusetts Institute of Technology.

Mitchell, J.K., 1976, Fundamentals of Soil Behavior: New York, Wiley.

Mondol, N.H., Bjørlykke, K., and Jahren, J., 2008, Experimental compaction of clays: relationship between permeability and petrophysical properties in mudstones: Petroleum Geoscience, v. 14, p. 319-337.

Mondol, N.H., Bjorlykke, K., Jahren, J., and Hoeg, K., 2007, Experimental mechanical compaction of clay mineral aggregates - Changes in physical properties of mudstones during burial: Marine and Petroleum Geology, v. 24, p. 289-311.

Nelson, P. H. 1994, Permeability-porosity relationships in sedimentary rocks, Log Anal., 38– 62

Neuzil, C.E., 1994, How permeable are clays and shales?: Water Resources Research, v. 30, p. 145-150.

Phillips, I.M., 2011, Report on the Whole Rock and <2 Micron Clay Fraction Mineralogy of a Single Sample by X-Ray Powder Diffraction (XRPD): Craigiebuckler, Aberdeen, Scotland, Macaulay Scientific Consulting Ltd. .

Prior, D.B., and Coleman, J.M., 1982, Active slides and flows in underconsolidated marine sediments on the slope of the Mississippi delta, *in* Saxov, S., and Nieuwenhuis, J.K., eds., Marine slides and other mass movements: New York, NY: Plenum Press, p. 21-49.

Pye, K., and Krinsley, D., 1983, Mudrocks examined by Backscattered Electron Microscopy: Nature, v. 301, p. 412-413.

Ransom, B., and Helgeson, H.C., 1989, On the correlation of expandability with mineralogy and layering in mixed-layer clays: Clays and Clay Minerals v. 37, p. 189-191.

Reece, J.S., Flemings, P.B., Dugan, B., Long, H., and Germaine, J.T., 2012, Permeability-porosity relationships of shallow mudstones in the Ursa Basin, northern deepwater Gulf of Mexico: J. Geophs. Res., v. 117.

Rubey, W.W., and Hubbert, M.K., 1959, Overthrust belt in geosynclinal area of western Wyoming in light of fluid-pressure hypothesis, 2: Role of fluid pressure in mechanics of overthrust faulting: GSA Bulletin, v. 70, p. 167-205.

Saffer, D.M., and Bekins, B.A., 2006, An evaluation of factors influencing pore pressure in accretionary complexes: Implications for taper angle and wedge mechanics: Journal of Geophysical Research, v. 111.

Santagata, M.C., and Kang, Y.I., 2007, Effects of geologic time on the initial stiffness of clays: Engineering Geology, v. 89, p. 98-111.

Sawyer, D.E., Jacoby, R., Flemings, P.B., and Germaine, J.T., 2008, Data report: particle size analysis of sediments in the Ursa Basin, IODP Expedition 308 Sites U1324 and U1322, northern Gulf of Mexico, *in* Flemings, P.B., Behrmann, J.H., John, C.M., and Scientists, t.E., eds., Proc. IODP, Volume 308: College Station, TX, p. 20.

Schneider, J., 2011, Compression and permeability behavior of natural mudstones: Thesis, The university of Texas at Austin, p. 302.

Schneider, J., Flemings, P.B., Day-Stirrat, R.J., and Germaine, J.T., 2011, Insights into pore-scale controls on mudstone permeability through resedimentation experiments: Geology, v. 39, p. 1011-1014.

Schowalter, T.T., 1979, Mechanics of secondary hydrocarbon migration and entrapment: AAPG Bulletin, v. 63, p. 723-760.

Seah, T.H., 1990, Anisotropy of resedimented Boston Blue Clay: Cambridge, Massachusetts Institute of Technology.

Sheahan, T.C., 1991, An experimental study of the time-dependent undrained shear behavior of resedimented clay using automated stress path triaxial equipment [Ph.D. thesis]: Cambridge, Massachusetts Institute of Technology.

Sheahan, T.C., and Watters, P.J., 1997, Experimental Verification of CRS Consolidation Theory: Journal of Geotechnical and Geoenvironmental Engineering, v. 123.

Shepard, F.P., 1954, Nomenclature based on sand-silt-clay ratios: Journal of Sedimentary Petrology, v. 24, p. 151-158.

Skempton, A.W., 1970, The Consolidation of Clays by Gravitational Compaction: Quarterly Journal of the Geological Society of London, v. 125, p. 373-411.

Skempton, A.W., and Jones, O.T., 1944, Notes on the compressibility of clays: Quarterly Journal of the Geological Society of London, v. 100, p. 119-135.

Stump, B., and Flemings, P.B., 2002a, Consolidation State, Permeability, and Stress Ratio as Determined from Uniaxial Strain Experiments on Mud Samples from the Eugene Island 330 Area, Offshore Louisiana,, *in* Huffman, A.R., Bowers, G.L. , ed., Pressure Regimes in Sedimentary Basins and Their Prediction, Volume AAPG Memoir 76, p. 131-144.

Stump, B.B., 1998, Illuminating basinal fluid flow in Eugene Island 330 (Gulf of Mexico) through in situ observations, deformation experiments, and hydrodynamic modeling [Masters Thesis thesis], The Pennsylvania State University.

Stump, B.B., and Flemings, P.B., 2002b, Consolidation State, Permeability, and Stress Ratio as Determined from Uniaxial Strain Experiments on Mudstone Samples from the Eugene Island 330 Area, Offshore Louisiana: AAPG Memoir, v. 76, p. 131-144.

Taylor, D.W., 1942, Research on Consolidation of Clays: Cambridge, MA, M.I.T. Department of Civil and Sanitary engineering, 143 p.

Terzaghi, K., 1941, Undisturbed clay samples and undisturbed clays: Journ. Boston Soc. C.E., v. 28, p. 211.

Van Paassen, L.A., and Gareau, L.F., 2004, Effect of Pore Fluid Salinity on Compressibility and Shear Strength Development of Clayey Soils Lecture Notes in Earth Sciences, v. 104, p. 327-340.

Wissa, A.E.Z., Christian, J.T., Davis, E.H., and Heiberg, S., 1971, Consolidation at constant rate of strain: Journal of the Soil Mechanics and Foundations Division, v. 97, p. 1393-1413.

Yang, Y.L., and Aplin, A.C., 2007, Permeability and petrophysical properties of 30 natural mudstones: Journal of Geophysical Research, v. 112.

Vita

William Betts graduated with a Bachelor of Science. in Geology from Brigham Young University in 2009, and joined the University of Texas at Austin in 2010. He has completed internships with NASA and Halliburton, and joined Halliburton full-time in 2014.

Permanent email: betts@utexas.edu

This thesis was typed by the author.